

THESIS ON CHEMISTRY AND CHEMICAL ENGINEERING G38

**Visible-light-sensitive Photocatalysts for  
Oxidation of Organic Pollutants and  
Hydrogen Generation**

OLGA BUDARNAJA

**TUT**  
PRESS

TALLINN UNIVERSITY OF TECHNOLOGY  
Faculty of Chemical and Materials Technology  
Department of Chemical Engineering

**This dissertation was accepted for the defence of the degree of Doctor of Philosophy in Engineering on March 11, 2014**

**Supervisor:** Senior Researcher Deniss Klauson, Department of Chemical Engineering, Tallinn University of Technology

**Opponents:** Prof. Miray Bekbölet, Bogazici University, Turkey

Dr. Artur Jõgi, OÜ Liprafarm, Estonia

Defence of the thesis: June 16, 2014

Lecture Hall VII-226

Tallinn University of Technology, Ehitajate tee 5, Tallinn

**Declaration:**

*Hereby I declare that this doctoral thesis, my original investigation and achievement, submitted for the doctoral degree at Tallinn University of Technology has not been submitted for any academic degree.*

Olga Budarnaja



European Union  
European Social Fund



Investing in your future

Copyright: Olga Budarnaja, 2014

ISSN 1406-4774

ISBN 978-9949-23-623-7 (publication)

ISBN 978-9949-23-624-4 (PDF)

**Fotokatalüsaatorid orgaaniliste  
saasteainete fotokatalüütiliseks oksüdatsiooniks  
ja vesiniku tootmiseks nähtavas valguses**

OLGA BUDARNAJA



# TABLE OF CONTENTS

List of publications.....	6
The author's contribution to the publications.....	7
List of abbreviations and symbols in alphabetical order.....	8
List of chemical formulae in alphabetical order.....	9
<b>INTRODUCTION.....</b>	<b>10</b>
<b>1. LITERATURE REVIEW.....</b>	<b>11</b>
1.1. Basis of Photocatalysis.....	11
1.2. Semiconductor photocatalytic water splitting for hydrogen production.....	13
1.3. Visible light-active TiO <sub>2</sub> photocatalysts.....	14
1.4. Pollutants: an overview.....	14
Humic substances.....	14
Aromatic substances: <i>p</i> -toluidine and phenol.....	15
Aliphatic substances: methyl- <i>tert</i> -butyl ether.....	15
Prednisolone.....	15
<b>2. MATERIALS AND METHODS.....</b>	<b>17</b>
Experimental setup.....	17
Experimental and analytical procedures.....	18
Photocatalyst synthesis and characterisation.....	19
PCO efficiency.....	20
<b>3. OBJECTIVES.....</b>	<b>21</b>
<b>4. RESULTS AND DISCUSSION.....</b>	<b>22</b>
4.1. Photocatalytic oxidation of organic pollutants.....	22
Sulphur-doped TiO <sub>2</sub> .....	22
Boron-doped TiO <sub>2</sub> .....	23
P25 Evonik TiO <sub>2</sub> .....	24
Carbon-doped TiO <sub>2</sub> .....	24
TiO <sub>2</sub> coatings obtained by spray deposition.....	25
Photocatalytic oxidation: summary.....	25
4.2. Photocatalytic production of hydrogen.....	26
<b>5. CONCLUSIONS.....</b>	<b>28</b>
<b>6. REFERENCES.....</b>	<b>29</b>
Acknowledgements.....	35
<b>KOKKUVÕTE.....</b>	<b>36</b>
<b>ABSTRACT.....</b>	<b>38</b>
<b>APPENDIX I: PUBLICATIONS.....</b>	<b>41</b>
<b>APPENDIX II: CURRICULUM VITAE.....</b>	<b>109</b>

## LIST OF PUBLICATIONS

### **Article I:**

Klauson, D., Portjanskaya, E., Budarnaja, O., Krichevskaya, M., Preis, S. The synthesis of sulphur and boron-containing titania photocatalysts and the evaluation of their photocatalytic activity. - *Catalysis Communications*, 2010, 11 (8), 715-720.

### **Article II:**

Klauson, D.; Pilnik-Sudareva, J.; Pronina, N.; Budarnaja, O.; Krichevskaya, M.; Käkinen, A.; Juganson, K.; Preis, S. Aqueous photocatalytic oxidation of prednisolone. - *Central European Journal of Chemistry*, 2013, 11 (10), 1620 - 1633.

### **Article III:**

Klauson, D., Budarnaja, O., Stepanova, K., Krichevskaya, M., Dedova, T., Käkinen, A., Preis, S. Selective performance of sol-gel synthesized titanium dioxide photocatalysts in aqueous oxidation of various-type organic pollutants. - *Kinetics and Catalysis*, 2014, 55 (1), 47-55.

### **Article IV:**

Budarnaja, O.; Klauson, D.; Dedova, T.; Kärber, E.; Viljus, M.; Preis, S. Template synthesis of titanium dioxide coatings and determination of their photocatalytic activity by aqueous oxidation of humic acid. - *Kinetics and Catalysis*, 2014, in press.

### **Article V:**

Klauson, D., Budarnaja, O., Beltran, I.C, Krichevskaya, M., Preis, S. Photocatalytic decomposition of humic acids in anoxic aqueous solutions producing hydrogen, oxygen and light hydrocarbons. – *Environmental Technology*, 2014, in press.

## **THE AUTHOR'S CONTRIBUTION TO THE PUBLICATIONS**

Article I: The author fulfilled part of the experiments (MTBE, *p*-toluidine, phenol) and respective analyses, obtained and analysed part of the experimental results and participated in manuscript writing.

Article II: The author fulfilled part of the experiments (prednisolone degradation with doped photocatalysts, the influence of wastewater matrix) and respective analyses, synthesised the doped photocatalysts used in the study, obtained and analysed the experimental results and wrote part of the manuscript.

Article III: The author fulfilled part of the experiments and respective analyses, obtained and analysed the experimental results and wrote the paper.

Article IV: The author fulfilled part of the experiments and respective analyses, obtained and analysed the experimental results, wrote the paper, and presented the results at the 7<sup>th</sup> European Meeting on Solar Chemistry and Photocatalysis: Environmental Applications (SPEA7).

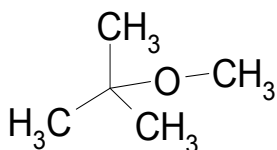
Article V: The author fulfilled major part of the experiments and respective analyses, obtained and analysed the experimental results and wrote the main part of the manuscript.

## LIST OF ABBREVIATIONS AND SYMBOLS IN ALPHABETICAL ORDER

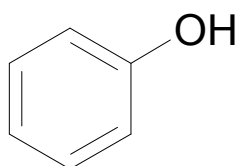
CB	Conduction band
COD	Chemical oxygen demand
CTAB	Cetyltrimethylammonium bromide
$e^-$	Electron
EDS	Energy-dispersive spectroscopy
GC-TCD-FID	Gas chromatograph equipped with thermal conductivity and flame ionisation detector
$h^+$	Positively charged hole
HA	Humic acid
HS	Humic substances
ICP-OES	Inductively coupled plasma optical emission spectrometry
IEP	Isoelectric point
IR	Infrared radiation
L-H	Langmuir-Hinshelwood
MTBE	Methyl <i>tert</i> -butyl ether
PCO	Photocatalytic oxidation
PNL	Prednisolone
ppm	parts per million
SEM	Scanning electronic microscope
THMs	Trihalomethanes
TTB	Titanium tetrabutoxide
UV	Ultraviolet
VB	Valence band
VIS	Visible light
XRD	X-ray diffraction



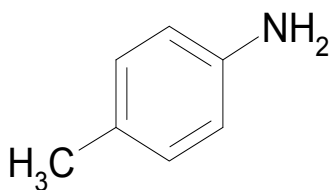
# LIST OF CHEMICAL FORMULAE IN ALPHABETICAL ORDER



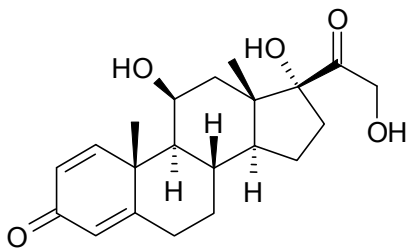
MTBE



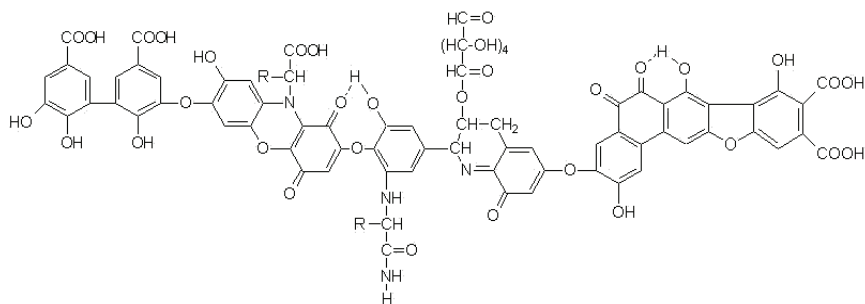
Phenol



*p*-Toluidine



PNL



HS

## INTRODUCTION

Nowadays, the questions of water and energy are perhaps the most immediate problems facing mankind. The increase in population, urbanisation and industrialisation, combined with intensified agricultural activities, are the main causes for increased water pollution, being at the same time the main reasons behind constantly increasing water and energy demands.

On one hand, not only water shortage is the main issue in the global water crisis, but also its quality tends to be a major issue. Many pollutants present in the contaminated water, including those studied in this work, are not effectively removed by the conventional and even some advanced water treatment methods, putting forward the need for alternative treatment technologies, both efficient and cost-effective.

On the other hand, the ever growing need for energy coupled with the likely shortage of fossil fuels, reported in the literature, raises the question of new, sustainable energy sources, e.g. hydrogen. Needless to say, such fuels must be produced in a sustainable way without secondary pollution.

Photocatalytic oxidation (PCO) is a technology that can provide solutions for both recalcitrant pollutant degradation, giving clean water, and hydrogen (i.e. clean fuel) production by water splitting. While the rate of water splitting is quite low, the process can be accelerated by orders of magnitude with the addition of sacrificial electron donors (hole scavengers) which, reacting with semiconductor photocatalyst valence band (VB) holes, obstruct the recombination of the mentioned holes with conduction band (CB) electrons. The latter are, in turn, responsible for hydrogen production. In the process, electron donors are oxidised. Using waste organic compounds as sacrificial electron donors can accomplish the tasks of hydrogen production and waste treatment simultaneously.

Pure semiconductor photocatalysts, like titanium dioxide, need UV-irradiation to drive PCO process; however, doping them with various elements can result in pronounced photocatalytic activity under visible light (VIS), which significantly increases the perspectives of PCO and solar-driven PCO applications in terms of both energy efficiency, and geographical range.

Consequently, the following objectives of the study can be declared:

- The determination of PCO applicability range when using visible light-sensitive photocatalysts
- Synthesis and characterisation of photocatalysts and photocatalytic coatings
- Testing their performance under various conditions in the degradation of pollutants with various chemical structure and properties
- Testing the performance of various doped photocatalyst in hydrogen-producing photocatalysis
- The investigation of photocatalytic reactions' mechanism

# LITERATURE REVIEW

## 1.1. Basis of photocatalysis

Heterogeneous photocatalysis can be defined as a catalytic process taking place due to photogeneration of electron-hole pairs on the surface of semiconducting materials illuminated by electromagnetic irradiation possessing energy equal to or higher than that of the material's band gap energy (Palmisano and Sclafani, 1997). The process can be carried out in various media: gaseous phase, aqueous solutions, and pure organic liquids (Herrmann, 1999). Various catalysts have been used in PCO: TiO<sub>2</sub>, ZnO, CeO<sub>2</sub>, CdS, ZnS, etc. As generally observed, the best photocatalytic performances with maximum quantum yields are usually obtained with titania, coupled with titania's high chemical stability in a wide range of conditions. Anatase is the most active allotropic form in comparison with two others, rutile and brookite. Anatase is thermodynamically less stable than rutile, but its formation is kinetically favoured at lower temperatures (< 600 °C) (Herrmann, 1999). Titanium dioxide (anatase) is a semiconductor photocatalyst with an energy band gap of 3.2 eV thus being activated by UV illumination with wavelength up to 387.5 nm, which comprises around 4 % of the solar irradiation reaching the Earth's surface (Zhang et al., 1994).

The major difference between conventional heterogeneous catalysis and photocatalysis is the mode of activation of the catalyst in which the thermal activation is replaced by a photonic activation. The semiconductor absorbs radiation quanta that promote electrons from the valence band to the conduction band of the metal oxide (Eq. 1). The electron-hole pair migrates to the solid-fluid interface where they can react with species in fluid phase. Transfer of electrons across the interface is dependent on the relative energy levels of electron donors and acceptors (Carey, 1992). When the photocatalyst is in contact with fluid phase, adsorption of the fluid matter takes place; according to the adsorbate redox potential, either conduction band electron transfer may proceed towards electron acceptor (A) molecules (Eq. 2), reducing them, or the electron donor (D) molecules have their electrons transferred to positively charged holes on the semiconductor surface (Eq. 3), oxidising the donor molecules (Herrmann, 1999). Alternatively, electron and hole may recombine; this is a fast process taking place in up to 40 ns (Kolen'ko et al., 2004), and it limits the overall PCO process efficiency.



These steps are followed by subsequent transformation of the reduced electron acceptor and oxidised electron donor. The photocatalytic oxidation (PCO) process investigation mainly involves the fate of electron donor transformations, as this is the role taken by the pollutants.

In the aqueous phase, which is the situation examined in the present work, both pollutant molecules and water molecules act as electron donors. Depending on the applied conditions, either dissolved oxygen (Eq. 4), or protons act as electron acceptors, with the latter situation, taking place under anoxic conditions, yields gaseous hydrogen (Eq. 5). Water molecules, reacting with positively charged holes, decompose, producing highly reactive hydroxyl radicals (Eq. 6); there is experimental evidence (Carey, 1992) indicating that at its formation it remains absorbed at the interface. While hydroxyl radicals can subsequently desorb into the solution, due to their relatively short lifetime of  $10^{-7}$  s (Buxton et al., 1988), they cannot migrate into the bulk of the solution, instead remaining a region in the vicinity of the photocatalyst surface. Thus in order for the organic compounds to be photocatalytically degraded, these probably have to be either adsorbed or be present in the vicinity of the surface at the time of excitation. As a consequence, it can be seen that mass transfer is of great importance, especially in case of dilute solutions where it becomes the limiting factor of photocatalytic process. Dissolved oxygen, being reduced by the CB electrons to superoxide ion-radical, serves as a source of additional radical species.



At this point it can be seen that photocatalytic oxidation process has two basic mechanisms: one initiated by the direct reaction of the substrate and hole on the semiconductor surface (hole mechanism), and another one initiated directly by the radical attack (Turci and Ollis, 1990). The latter is done not only by the hydroxyl radicals, but also by the numerous radical species originating from superoxide ion-radicals formation (Eq. 7-13).



The main advantages of PCO is that as a treatment method for water and air purification it utilises simultaneously two oxidants with the highest available redox potential, i.e. hole and hydroxyl radical, with the potential values of 3.5 and 2.8 V, respectively (Sun et al., 1997, Bahneman, 2004), and the ability of using direct solar radiation for the catalyst excitation, which makes photocatalytic treatment cost-effective. The major disadvantages of PCO are the relatively low reaction rate and quantum yield. Another PCO-connected challenge is the process's selective performance towards different substrates, which inevitably requires testing the activity of any novel photocatalytic material with a range of substrates having

different structure, composition and properties. However, such investigations increase the amount of available knowledge on PCO, bringing this technology closer to practical applications either as a standalone process, or integrated as a stage into a more complex combined technology.

## **1.2. Semiconductor photocatalytic water splitting for hydrogen production**

Hydrogen is considered as an ideal fuel for the future. Hydrogen fuel can be produced from renewable and/or clean sources and, thus, it can be clean and renewable throughout the whole of its life cycle. However, presently the majority of commercially available hydrogen (95 %) is produced from fossil fuels (Ni et al., 2004). Renewable hydrogen production, using e.g. solar or wind energy for water electrolysis, is not popular due to high production costs. Alternatively, hydrogen can be produced photocatalytically by water splitting; this allows the use of an abundant, clean and renewable resource, i.e. water, which is also the product of hydrogen fuel combustion.

With water subjected to photocatalytic treatment by unmodified titania, the aforementioned recombination severely limits the results of water splitting, with the reaction quantum yields being at the level of a centime fraction of per cent. However, with certain photocatalyst modifications (introduction of crystal lattice defects and other charge carrier traps, e.g. noble metal nanoparticles), and the addition of sacrificial electron donors can greatly improve the process performance: the latter has been reported to increase hydrogen yields by several orders of magnitude (Ni et al., 2007; Kim and Choi. 2010). As mentioned, in order to obtain hydrogen, oxygen needs to be eliminated from the treated solution.

In terms of photocatalyst modifications, the literature data from the last years shows a significant growth in the quantity and the complexity of the photocatalytic systems for water decomposition. The examples of dopants applied can be nitrogen- (In et al., 2006), gold- (Sreethawong and Yoshikawa, 2005), palladium- (Bahruji et al., 2010) or platinum- doped titanium dioxide (Matsuoka et al., 2007). Also, a number of systems based on the In, Sn, Sb and Ge compounds doped with ions of various metals (e.g. strontium, niobium, tantalum, etc.) exhibited certain activity in UV-induced photocatalytic water decomposition (Sato et al., 2001, Ikarashi et al., 2002, Sato et al., 2001, Sato et al., 2002, Sato et al., 2003a, Sato et al., 2003b, Kadowaki et al., 2005).

As for the sacrificial electron donor addition, a wide range of inorganic and organic substances can be put into that role. Utilising non-biodegradable recalcitrant water pollutants this way allows simultaneous solution to two problems, waste decomposition and clean fuel production; also, part of the organics can directly degrade producing hydrogen and low molecular weight (LMW) hydrocarbons, as observed both in the literature (Bahruji et al., 2010), and by the author (Article V).

### 1.3. Visible light-active TiO<sub>2</sub> photocatalysts

To improve the photocatalytic properties of TiO<sub>2</sub>-based materials, many studies have been performed to enhance the light absorption and delay recombination of photogenerated electron-hole pairs by adjusting its microstructure, processing routes and compositions (Chang et al., 2005). To increase visible light absorption of TiO<sub>2</sub> materials these can be doped with metals, like Al, Ag, Li, Cd, Co, Fe, Pd, Pt, Zn, Cr, Ni, and Zr or non-metals, like S, B, N, C, or F to reduce energy band-gap of the photocatalyst (Asahi et al., 2001, Yu et al., 2002, Umebayashi et al., 2003, Irie et al., 2003, Lettmann et al., 2001, Ihara et al., 2003, Bessekhoud et al., 2004, Ohno et al., 2004, Wang et al., 2005, Sharma et al., 2006, Arpac et al., 2007). Doping titanium dioxide results in the formation of an additional energy level inside the semiconductor band gap, whether donor level (*n*-type semiconductors), or acceptor level (*p*-type semiconductors). In both scenarios, the electrons are displaced to CB from an additional level inside the band gap, thus decreasing the energy required for the creation of electron-hole pairs. Other options allowing the utilisation of visible light by titanium dioxide include coupling TiO<sub>2</sub> with narrow band-gap semiconductors, preparing oxygen-deficient TiO<sub>2</sub> (e.g. by hydrogen treatment of photocatalyst, as in Article V).

### 1.4 Pollutants: an overview

#### *Humic substances*

The name “humic substances” (HS) is applied to a wide range of water-soluble plant tissue decomposition products with the molecular weight ranging from several hundreds to a few hundred thousand Daltons. Structurally, the HS are believed to possess a branched polyaromatic carbon skeleton with a large number of carboxylic and phenolic groups, although the exact structure is not clearly established; moreover, it may vary significantly depending on the HS source and geographical location. While the HS are not toxic, the intensive yellow-to-black colour given by their presence in water may irritate end-users and make water inappropriate for food industry, laundering, paper, and textile making (Manahan, 1994). However, a real threat that the HS pose is their ability to bond heavy metals, and organic toxics (e.g. pesticides, insecticides, herbicides etc.), consequently making them difficult to remove by simple methods, as the HS are resistant towards biological oxidation and conventional physical and chemical removal methods are not efficient in their removal as well, as the HS have radical scavenging properties (Manahan, 1994). This is especially well-pronounced in the landfill leachate, where the HS are abundantly formed due to natural decomposition processes. Also, the HS are known as precursors of carcinogenic trihalomethanes (THMs) upon chlorination (Eggins et al., 1997, Wang et al., 2001).

### *Aromatic substances: p-toluidine and phenol*

*p*-Toluidine is used mostly as an intermediate in chemical processes, such as in production of pigments, dyestuff, pesticides, rubber chemicals, antioxidants and pharmaceuticals (Bowers, 2002; Srour, 2002), being also a major component of jet and rocket fuels (Hingst et al., 1994). Non-biodegradable *p*-toluidine may accumulate in groundwater aquifers in toxic amounts. Phenol is a renowned environment pollutant strongly associated with e.g. oil shale industry (Kahru et al., 2002) and a variety of chemical productions such as coal refineries, manufacturing of pharmaceuticals, resins, plastics, paints, dyes, textile wood and petrochemicals (Howard, 1989; Jaromir et al., 2005); while it has a reputation of a standard model contaminant for the activity comparison of various oxidation methods and catalysts, the findings of Article III demonstrate that such an approach may often be somewhat misleading.

The most common methods for the removal of the amines and phenols from effluents are biological wastewater treatment technologies, both aerobic and combined aerobic/anaerobic. Chemical oxidation and several membrane technologies were suitable to recover and reuse aromatic amines from the wastewater cycle cost-effectively (Ferreira et al., 2002; Sarasa et al., 2002). But still these water treatment methods have been shown to be inadequate against aromatic amino compounds pollution (Rozkov et al., 1999). Adsorption on activated carbon is an effective method for phenol removal from wastewater. This method is simple, economical, fast and requires no chemical treatment (Qadeer and Rehan, 2002). Phenol-containment water can effectively be treated by ozonation. However this method showed to be a costly process (Busca et al., 2008).

### *Aliphatic substances: methyl-tert-butyl ether*

Methyl *tert*-butyl ether (MTBE) is a widely used motor fuel oxygenate and octane booster, although currently banned in the USA. Biodegradability of MTBE is low, and as a consequence it accumulates in groundwater aquifers (Yeh and Novak, 1994). Moreover, MTBE is readily miscible in water and does not adsorb to soil very well; consequently, unlike main fuel compounds, it migrates faster and farther from the original spill site, making it more likely to reach and contaminate water supply sources (US Environmental Protection Agency, 2009). At the same time, MTBE is not readily removed by conventional physical removal and chemical oxidation (Johnson, 1998, Xu et al., 2004; Safarzadeh-Amiri, 2001).

### *Prednisolone*

Prednisolone (PNL) is an extremely widely used anti-inflammatory agent, representative of corticosteroid class, and, in environmental terms, an emerging micropollutant with a polycyclic structure. Like other micropollutants in general, and corticosteroids in particular, they exhibit a range of effectson aquatic organisms even at very low concentrations (Li et al., 2009; Chang et al., 2007). Conventional treatment methods have not shown high efficiency in micropollutant

abatement, thus, the need for new efficient technologies is an important matter in this field as well. While PNL concentrations used in Article II are higher than those found in the natural water samples (Ikehata et al., 2006; Liu et al., 2011), this was an inevitable measure allowing the investigation of PNL PCO regularities and degradation mechanism; the observations can be then extrapolated to lower concentrations, where kinetic control of the reaction is pronounced (Klauson et al., 2010), similarly to the studied concentrations range.



## 2. MATERIALS AND METHODS

### *Experimental setup*

In the research described in Articles I to III, PCO experiments were undertaken in two thermostatted ( $20 \pm 1$  °C) 200-mL simple batch reactors, agitated with magnetic stirrers, having the inner diameter of 100 mm (evaporation dishes) and the irradiated contact surface  $40 \text{ m}^2 \text{ m}^{-3}$ . Each experiment involved the use of a two-reactor set: the first one used for the PCO (“active”) while the second one (“reference” or “blank”), containing no photocatalyst and not exposed irradiation. This was done in order to compensate the concentration changes due to water evaporation taking place during the experimental run. The photocatalysts were used as a  $1 \text{ g L}^{-1}$  slurry (Articles I-III, V), or attached to Pyrex glass plates of 8 to  $12 \text{ cm}^2$  (Article IV) during the catalyst synthesis (see below). The photocatalyst-coated plates were submerged into the solution to the depth of ca 10 mm.

Two sorts of light sources were used in the research, UV-A and daylight fluorescent lamps. A Philips Actinic 15 W 365-nm low pressure luminescent lamp was used as UV-A source. Artificial daylight was provided by Philips TL-D 15W/33-640 fluorescent lamp. The lamps were positioned horizontally over the active reactor, providing the irradiance of about  $1 \text{ mW cm}^{-2}$  measured at a distance corresponding to the level of the free surface of the reactor. With UV-A, the irradiance was measured by Micropulse MP100 optical radiometer (Micropulse Technology, UK) in Articles I to III, and with Ocean Optics USB 2000+ radiometer in Article IV. In case of artificial daylight fluorescent lamp (Articles I to III), the irradiance was determined indirectly, being calculated from the illuminance, measured by TES luxmeter (TES, Taiwan), using lumen to watt ratio of 684 (Kirkpatrick, 2005); the amount of UV-light emitted by the mentioned lamp type was determined by the USB 2000+ spectrometer to be negligible, in accordance to the data from the lamp manufacturer. Thus, any noticeable action of the photocatalyst when using Philips TLD visible light lamp may not be attributed to the emitted UV fraction but is clearly due to the activity of the catalysts in visible light.

Adsorption experiments with the pollutants on the photocatalyst surface were carried out at respective pH in closed flasks thermostatted at  $20 \pm 1$ °C and equipped with magnetic stirrers. The adsorbed amount of substances was derived from the batch mass balance: the concentration of the dissolved substance was determined before and after adsorption.

All the experiments were carried out for at least three times under identical experimental conditions. The average deviation of data in parallel experiments did not exceed 5 %.

The experimental setup for Article V, used to photocatalytically produce hydrogen and LMW hydrocarbons, needs a separate description. The photocatalytic reaction vessel used was a glass vial equipped with magnet stirrer; the vial contained 5 mL of the treated solution, and was placed in a hermetically sealed metal reactor (interior volume 48.2 mL), having a window on top for the solution illumination. Solar simulator (Abet Technologies) with the irradiance of 1

SUN ( $\approx 100 \text{ mW cm}^{-2}$ ) was used as the radiation source; in order to cut off IR in the radiation spectrum and thus avoid treated solution overheating, a Petri dish containing water was placed between the reactor and solar simulator. The solution to be treated was first purged with nitrogen ( $0.15 \text{ L min}^{-1}$ ) for 0.5 h before the experiment to eliminate oxygen, and then the reaction system was purged for another 0.5 h with argon ( $0.1 \text{ L min}^{-1}$ ), which was used as the carrier for the gas chromatography (GC) system in subsequent reaction gaseous products analysis. The treatment time 4 h was chosen to provide reasonable HA decomposition and enable comparison of the photocatalysts' potentials in water splitting in terms of gaseous products amounts.

### *Experimental and analytical procedures*

In Articles I and III, the experiments were carried out with  $100 \text{ mg L}^{-1}$  of *p*-toluidine and phenol in acidic (pH 3), natural (pH 6.5) and alkaline (pH 11) media, adjusted either by 4 N sulphuric acid or 15% sodium hydroxide (Article I). In Article III, natural pH values of the solutions were used (pH ca. 6.5); the pH was monitored, but not adjusted. With the mentioned substances, the treatment time was 24 h. Concentrations of MTBE (Articles I, III) were  $100 \text{ mg L}^{-1}$  likewise, with the treatment time chosen to be 2 h and 4 h, respectively. Concentrations of PNL varied between 10 and  $100 \text{ mg L}^{-1}$  (Article II); the experiments were conducted at natural pH values (ca. 6.5), unadjusted during the experimental runs. Treatment time for PNL was 2 h. Humic acid sodium salt (HA), taken as a representative of HS (Articles IV and V), had initial concentration of  $100 \text{ mg L}^{-1}$ ; treatment time was chosen to be 24 h in Article IV, and 4 h in Article V, where radiation source with much higher irradiance was applied.

Concentrations of *p*-toluidine (Articles I, III) were measured photometrically after diazotation and reaction with phenol at 490 nm, and those of phenol were determined photometrically after reaction with *p*-nitroaniline at 570 nm using Helios  $\beta$  spectrophotometer together with the COD. In case of *p*-toluidine, the evolution of nitrite and nitrate ions was also determined using Metrohm 761 Compact ion chromatograph (IC).

The decrease in the MTBE concentration was determined by gas chromatography using Finnigan Focus GC chromatograph (Article III); MTBE was extracted from pre-salinated aqueous samples by benzyl alcohol using IKA Vortex Genius 3 extractor. As expected, complete MTBE removal was observed during the treatment time, unlike the mineralisation. Consequently, the performance of MTBE PCO was determined from the decrease in chemical oxygen demand (COD), measured by a standard method, as applied previously (Article I).

Prednisolone concentrations were determined by Shimadzu 2020 HPLC-PDA-MS, using Gemini-NX 5u  $\text{C}_{18}$  reverse-phase column, operating in gradient mode with the total flow of eluents (acetonitrile and acetic acid-containing water) of  $0.3 \text{ mL min}^{-1}$  (Article II).

For the HA concentration measurement, the analytical procedure used by Portjanskaja et al. (2009) was applied: colour at 455 nm was determined with the Thermo Scientific Evaluation 300 UV-VIS dual-wavelength spectrophotometer

(Article V) with the results interpreted using VisionPro software, or with HACH Lange DR2800 spectrophotometer (Article IV).

In hydrogen-producing photocatalytic experiments (Article V), in the end of each experimental run, the gaseous products in 1-mL sample were analysed using the Hewlet Packard GC, model #61540A with the thermal conductive and the flame ionizer detectors (GC-TCD-FID), with the concentrations expressed as parts per million (ppm).

### *Photocatalyst synthesis and characterisation*

Sulphur-containing photocatalysts were prepared by titanium tetrabutoxide (TTB) hydrolysis with addition of a pre-calculated amount sulphur source (0.1 N sodium thiosulphate); this was followed by calcination at 400 °C for 4 h. This was followed by washing the catalyst with hot distilled water applied in a sequence of 10–15 rinsing rounds (ca. 1 L per 1 g of catalyst) in order to clean the catalyst surface from water-soluble compounds, with the obtained leachate analysed by Metrohm 761 Compact IC. In case of boron-containing photocatalysts, sodium tetraborate was used as boron source. An additional catalyst was synthesised using the same pattern, although without the addition of sulphur or boron sources.

Carbon-containing photocatalysts were prepared by the near-instant hydrolysis of pure TTB, followed by calcinations at temperatures from 200 to 950 °C for 4 h. Subsequently, the abovementioned washing procedure was undertaken in order to clean the catalyst surface from water-soluble compounds.

Iron-containing titanium dioxide samples were prepared by a variation of sol-gel method: 75 mL of TTB (25 % solution in tert-butyl alcohol) were sprayed into 1 L of pre-sonicated Fe<sub>2</sub>O<sub>3</sub> suspension (0.5 g L<sup>-1</sup>). Hydrolysis was followed by sonication, drying at room temperature and calcination at 200 °C. These steps were followed by the washing procedure.

Copper-containing hydrogen treated titanium dioxide sample was synthesised by sol-gel method, as described by (Chen et al., 2011), loaded with pre-calculated amount of copper (I) acetate to achieve 0.5 % of copper in the catalyst, dried under vacuum, and then calcinated at 400 °C for three hours. This was followed by the drying period at 200 °C with gaseous hydrogen introduced to the pressurized compartment at 200° C and 25 bar. The sample was left in the reactor for three days and then cooled down to ambient temperature. Platinum-containing photocatalyst was produced by Vorontsov et al. (1999), referred in their publication as the specimen C. Cobalt- and tungsten-containing photocatalysts were obtained by the hydrolysis of TiCl<sub>3</sub> (15 % solution in 10 % HCl, Merck) in presence of cetyl trimethylammonium bromide (0.005 µg mL<sup>-1</sup>, Merck) as template with dopant sources, Co(OOCCH<sub>3</sub>)<sub>2</sub> (9.4 µg mL<sup>-1</sup> solution) and Na<sub>2</sub>WO<sub>4</sub> (1.17 µg mL<sup>-1</sup> solution) respectively added to the solution. The precipitate was dried at room temperature and calcinated at 400 °C in order to remove template.

The crystallinity, crystal structure and phase composition of carbon-doped photocatalysts were analysed using D 5000 Kristalloflex X-ray diffractometer (XRD), Siemens, with the phase composition calculated by Topas R Software. The crystal structure of copper-containing catalyst was determined with XRD

measurements using Scintag XDS 2000 diffractometer. With other samples, Scintag Pad V Siemens (Cu-K $\alpha$  irradiation source) diffractometer was used. Titanium dioxide coatings were analysed by Rigaku Ultima IV diffractometer using Cu K $\alpha$  radiation.

Surface morphology of doped photocatalysts was examined by scanning electronic spectroscopy (SEM) JEOL JSM-6480 LV equipped with energy-dispersive spectroscopy (EDS), while in case of titanium dioxide coatings, Zeiss EVO MA-15 SEM was used.

The specific surface area (BET and Langmuir adsorption) and the pore volume of the sulphur, boron and iron-containing catalysts were measured by the adsorption of nitrogen using KELVIN 1042 sorptometer.

Quantitative measurements of the photocatalysts' composition in Article V were performed with an ARL 3410+ inductively coupled optical emission spectrometer (ICP-OES).

The isoelectric points (IEP) of pure and sulphur-, carbon and iron-doped titanium dioxide suspensions (Article II) were determined by potentiometric titration using a Zetasizer Nano-ZS equipped with an MPT-2 autotitrator and vacuum degasser (Malvern Instruments, UK). Toxicity issues (Article II) were addressed by the analyses performed with Protozoan culture (*Tetrahymena thermophila* strain BIII).

### *PCO efficiency*

The performance of PCO with artificial radiation sources was characterised by the process efficiency  $E$  (Eq. 14), defined as the pollutants degradation relative to the energy reaching the surface of the treated sample calculated for the treatment time. This makes the PCO efficiency the universal term to compare the results achieved with different catalysts (Preis et al., 2002):

$$E = \frac{\Delta c \times V \times 1000}{I \times s \times t} \quad (14)$$

where  $E$  – PCO efficiency,  $\text{mg W}^{-1} \text{h}^{-1}$ ;  $\Delta c$  – the decrease in the pollutant's concentration or COD,  $\text{mg L}^{-1}$  or  $\text{mg O L}^{-1}$ ;  $V$  – the volume of the sample to be treated, L;  $I$  – irradiance,  $\text{mW cm}^{-2}$ ;  $s$  – irradiated area,  $\text{cm}^2$ ;  $t$  – treatment time, h.

### 3. OBJECTIVES

Based on its performance and relatively low operating costs, PCO can be promising treatment method for the removal of pollutants from contaminated water, together with the possibility of simultaneously producing green fuel, i.e. hydrogen.

The main objectives of the present research were as follows:

1. To clarify the PCO potential in degradation of a fairly wide range of model pollutants, and investigate the process mechanism;
2. To compare different modifications of synthesised titanium dioxide-based photocatalysts;
3. Combine pollutant photocatalytic decomposition with hydrogen production.

In order to fulfil the objectives, the following questions were examined:

1. The efficiency of PCO in degradations of pollutants;
2. Synthesis and examination of visible-light-sensitive modified photocatalysts with both non-metal and metal dopants.
3. Establishment of maximal hydrogen, oxygen and low molecular weight hydrocarbons photocatalytic production using non-biodegradable pollutant as sacrificial electron donor.

## 4. RESULTS AND DISCUSSION

The obtained results show that the performance of doped titania photocatalysts, although relatively efficient, can be selective dependent on the substrate applied. The noted performance selectivity in the PCO of various water pollutants with different chemical structure and composition is studied in Articles I-III; these observations allow drawing some general conclusions on PCO process mechanism and influencing factors. The reaction pathway of an emerging micropollutant, prednisolone, was also investigated (Article II). Article IV provides an insight on the role of titanium dioxide surface features on the PCO process performance. Article V examines hydrogen-producing photocatalysis, comparing different materials in terms of gaseous products yield and also differentiating two mechanism of hydrogen production: water splitting with organic pollutant acting as sacrificial electron donor *versus* direct organic pollutant photocatalytic splitting.

### 4.1. Photocatalytic oxidation of organic pollutants

#### *Sulphur-doped TiO<sub>2</sub>*

The photocatalytical decomposition of a several pollutants, namely, MTBE, *p*-toluidine and phenol, was investigated under both UV and VIS irradiation (Article I). Composition and surface properties of S-TiO<sub>2</sub> can be seen in Table 1 (Article I). According to the XRD investigation results, S-TiO<sub>2</sub> photocatalysts were of anatase phase.

The experiments with aliphatic MTBE have shown that its PCO efficiency under VIS-irradiation with S-doped titanium dioxide catalysts were to up twice as high as that achieved with P25 Evonik, and comparable to that under UV. The best results were obtained in acidic media (Article I, Fig. 2a). In terms of dopant content influence on the PCO process, it can be seen (Article I, Fig. 3a) that the PCO efficiency under both UV and VIS increased at smaller sulphur concentration with the increase of S content up to 1.5 at. %, followed by a steady decreased. The MTBE degradation under the solar light with Degussa P25 and S-doped catalysts proceeded quite similarly.

When PCO by S-TiO<sub>2</sub> was applied to aromatic substances, the results obtained with phenol were inefficient. In case of *p*-toluidine, the best performance was observed in alkaline media; in general, the results observed were comparable to that of P25 Evonik TiO<sub>2</sub> (Article I, Fig. 4a).

Consequently, it can be seen that the performance of S-TiO<sub>2</sub> towards three substrates of different structure – aliphatic MTBE, aromatic phenol, and aromatic heteroatom-containing *p*-toluidine – is highly selective. As no adsorption of substances under scope was experimentally determined on the surface of the catalysts within the limits of analytical precision, the PCO is assumed to proceed here mainly as a nucleophilic attacks of hydroxyl radicals, and the observed differences thus arise from the substances' properties, PCO regularities and nucleophilic reaction mechanism. According to the latter, the attack of hydroxyl radical should proceed upon the carbon atom having the highest partial positive

charge: tertiary carbon atom in MTBE, and carbon atoms connecting with –OH and –NH<sub>2</sub> groups in phenol and *p*-toluidine. While in case of MTBE, the nucleophilic attack on the mentioned atom effectively destroys the molecule, the rupture of stable aromatic cycle is a much harder task. Consequently, phenol PCO with S-TiO<sub>2</sub> was poor, while in case of *p*-toluidine the amine group is oxidised as the step preceding the immediate aromatic cycle rupture, effectively producing the observed substrate concentration decrease. The growth of the PCO efficiency of sulphur-doped catalysts with the growth of sulphur content, as observed in case of MTBE, and the subsequent decrease may be explained by the overpowering of the positive effect obtained from the band-gap decrease by the decrease of the catalysts' redox potential.

In PCO of PNL (Article II), S-TiO<sub>2</sub> performance was inferior to that of P25 Evonik (PCO efficiency 1.5-2 times lower, depending on the sulphur content), although superior to other doped catalyst species used (Fe-TiO<sub>2</sub> and C-TiO<sub>2</sub>). This can be attributed to the electrostatic repulsion between PNL molecules and S-TiO<sub>2</sub> surface, as no adsorption of PNL was observed indeed. Under natural solar irradiation, the acceleration of PNL degradation in comparison to artificial radiation increased to greater extent than that of P25, although being still inferior to the latter. While the PNL oxidative ability of sulphur-containing titania was lower, it was shown, unlike P25, to be non-toxic towards *Tetrahymena thermophila*, activated sludge ciliate protozoa, both in the dark or under irradiation, indicate the potential of using such materials for selective removal of micropollutants when combined with activated sludge process, as photocatalysis has been shown (Article II) to selectively remove these from wastewater matrix.

### *Boron-doped TiO<sub>2</sub>*

The action of B-TiO<sub>2</sub> in the PCO of MTBE and *p*-toluidine was also investigated in Article I. The dependence of MTBE PCO efficiency on pH was similar to that of S-TiO<sub>2</sub> (Article I, Fig. 2b). Under visible radiation in acidic media an increasing trend in PCO efficiency was observed with the boron content increasing to 2 atomic % (at. %); above that content, the efficiency remained at a constant level (Article I, Fig. 3b), with the MTBE PCO efficiency significantly exceeding the one observed with P25 Evonik under UV, however, somewhat inferior to the results of S-TiO<sub>2</sub>.

With *p*-toluidine, contrary to the S-TiO<sub>2</sub> catalysts, the highest PCO efficiency of B-TiO<sub>2</sub> was observed in acidic media followed by neutral and basic ones (Article I, Fig. 4b). In acidic media, the PCO efficiency values obtained under VIS-irradiation exceeded the one of P25 under UV by 1.5 times for *p*-toluidine and two times for COD removal. Remarkably, the dependence of the PCO efficiency on dopant content with B-TiO<sub>2</sub> has different trends dependent on the values of pH: in neutral and alkaline media the PCO efficiency decreases slightly with the increase in the boron content in the catalysts, however, in acidic media, where a certain increase is observed. This can be explained by the different behaviour in acidic media of the blank catalyst containing only carbon as opposed to those containing both boron and carbon.

### *P25 Evonik TiO<sub>2</sub>*

The results of PNL PCO investigation (Article II) show efficient removal of a widely-used micropollutant by photocatalytic oxidation. The PCO of PNL was shown to follow well Langmuir-Hinshelwood (L-H) kinetics. A high degree of mineralisation was obtained: indeed, at PNL concentrations up to 25 mg L<sup>-1</sup>, the removal rate was around 90-96 % with simultaneous COD decrease over 80 %. To compare, at 100 mg L<sup>-1</sup> PNL, the target pollutant and COD removal rates decreased to 57 and 30 %, respectively, although the absolute oxidation rates increased. Thus, photocatalytic oxidation is able to degrade both target compound and its degradation by-products reasonably well. The effect of wastewater matrix, modelled by carbamide and sucrose, was shown to possess only some inhibitive effect on PNL PCO. The LC-MS investigation of PNL PCO by-products allowed the proposition of four degradation pathways, dependent on pH.

### *Carbon-doped TiO<sub>2</sub>*

The experiments with carbon-containing photocatalysts were undertaken with MTBE, *p*-toluidine and phenol (Article III). Crystallographically, photocatalysts calcinated at 200 to 600 °C were a mixture of anatase and brookite, while at higher temperatures (700 to 1000 °C) they were pure rutile (Article III, Fig. 1). Crystallographic composition and surface properties of C-TiO<sub>2</sub> photocatalysts can be seen in Table 1 (Article III). The investigation of the photocatalysts' optical properties, especially band gap energy (Table 2) provides evidence of carbon incorporation into titanium dioxide crystal lattice, i.e. actual doping; this is also supported by slight shifts observed in XRD peak positions.

As no adsorption of the mentioned substances was detected on the surface of the carbon-containing photocatalysts above the limits of analytical precision, it can be stated that radical reactions should be responsible for PCO at C-TiO<sub>2</sub> catalysts, as opposed to surface hole reactions.

The values of PCO efficiency observed with carbon-doped catalysts irradiated with VIS were higher than that with UV-irradiated P25 under similar conditions (Article III, Fig. 3), with photocatalyst calcinated at 600 °C exhibiting the highest performance. Under VIS, MTBE was totally degraded within 1 h with all tested C-TiO<sub>2</sub> samples, including the less photocatalytically active rutile. With *p*-toluidine the PCO efficiency values observed with the catalysts under artificial daylight was close to that of P25 under UV at lower calcination temperatures, steadily decreasing with the growth of calcination temperature, i.e. with the decrease in carbon content and contact surface area (Article III, Fig.4). With phenol, the PCO efficiency was lower than in case of P25 TiO<sub>2</sub> and declined with the growing catalyst calcination temperature as well (Article III, Fig. 5).

The observed differences in the PCO activity of the substances under scope can be explained by their different interactions with the surface of the catalysts due to their electrostatic properties. Under the experimental conditions (pH slightly lower than neutral) both TiO<sub>2</sub> surface and aromatic substances (phenol and *p*-toluidine) are partially positively charged, and the aromatics are repelled from the catalyst



surface. While C-TiO<sub>2</sub> catalysts have a lower point zero charge, and forces of electrostatic attraction may come into effect, this still does not inevitably result in increased adsorption, dependent on surface features; the stability of aromatic cycle discussed earlier is another matter responsible for the PCO results observed. On the other hand, MTBE is electrically neutral and can thus get closer to the vicinity of the photocatalyst surface, where larger supply of hydroxyl radicals is available for efficient PCO. Photocatalytic oxidation of MTBE does not depend on the calcinations temperature even at calcination temperature exceeding 600 °C when all anatase and brookite turned to rutile; photonic efficiency calculations suggest that during PCO MTBE can partially undergo auto-catalysis. The latter supports the use of its relatively recalcitrant degradation by-products' mineralisation as a meter of MTBE-related contamination removal.

In general, the decrease of carbon-doped photocatalysts' performance with the increase of calcination temperature is attributed to both loss of carbon and transformation of anatase and brookite phases into less active rutile. C-TiO<sub>2</sub> photocatalysts showed stable activity even after repeated applications.

#### *TiO<sub>2</sub> coatings obtained by spray deposition*

Immobilisation of photocatalysts on various surfaces allows numerous operating benefits and ease of the material's applications. Consequently, in Article IV the author investigated the performance of spray-deposition synthesised titanium dioxide coatings with varying amount of template substance, cetyltrimethylammonium bromide (CTAB), used (0 to 3 µg mL<sup>-1</sup>). Humic acid sodium salt (HA), a representative of the HS class, was taken as the test substrate.

Examination of the coatings' surface, performed by SEM, revealed the availability of the following surface features: cracks, pores, collapsed bubbles and unbroken bubbles. The changes in HA PCO efficiency dependent on the template amount in the coating's synthesis (showing performance comparable with or superior to P25 titanium dioxide) were observed to clearly correlate to the surface concentration of unbroken bubbles (amount of surface features per surface unit of the coatings): their sharp edges protruding into the treated solutions, where the surface defects localisation can be significantly higher in comparison to the remaining coating surface, can act as "radical volcanoes" producing the oxidants responsible for HA oxidation. In the sample showing the best performance, the combination of highest surface concentration of collapsed bubbles and the smallest crystallites is able to produce the highest amount of sharp spiked catalyst edges with larger area possessing greater defect concentration, which results in enhanced radical production.

#### *Photocatalytic oxidation: summary*

The observed selective performance of doped titania species clearly demonstrates that contrary to the well-established practice, an objective view of the materials' capabilities can be obtained only through testing their photocatalytic performance by the examination of PCO of several substrates possessing different

chemical structure; choosing recalcitrant pollutants as degradation substrates, as opposed to photolysis-prone dyes, allows the evaluation of the photocatalysts' applicability to the solution of actual environmental problems. Also, the established use of phenol as a "standard" pollutant for the comparison of various oxidative technologies can be questioned.

Photocatalyst surface features and defects possess significant influence on the material's activity. Contrary to what might be expected from surface-related phenomenon such as photocatalysis, the increase in photocatalyst specific surface area does not necessary result in increased photocatalytic activity of the materials, or even increased adsorption. On the other hand, electrostatic interactions between the photocatalyst surface and the pollutants to be degraded are of high importance: they influence the ease of the pollutant molecules' adsorption on the photocatalyst, resulting in direct hole oxidation, or their movement into the close vicinity of photocatalyst surface where hydroxyl radicals exist during their lifetime.

## 4.2. Photocatalytic production of hydrogen

Titanium dioxide catalysts doped with platinum, cobalt, tungsten, copper and iron were experimentally tested for production of hydrogen, oxygen, and low molecular weight (LMW) hydrocarbons from aqueous solutions of HA (Article V). The crystallographic data and the composition of the photocatalysts used in the study can be seen in Fig. 2 and Table 1 (Article V).

The experimental results of the HA aqueous solution photocatalytic treatment can be found in Table 2 (Article V). Remarkably, HA removal rate and the yields of gaseous products seem not to be directly correlated. While the highest oxygen yield (ca. 310 ppm O<sub>2</sub> in gas, or 0.45 μmol O<sub>2</sub> produced per 1 μmol of HA degraded) was observed simultaneously with highest (over 50 %) HA removal (P25), this did not result in any noticeable hydrogen yield. On the contrary, Pt-TiO<sub>2</sub> photocatalyst removed 29 % of HA, producing 94 ppm of hydrogen (0.25 μmol H<sub>2</sub> produced per 1 μmol HA degraded), together with small amounts of LMW hydrocarbons (C1-C2), and some amounts of oxygen as well. Cu<sub>x</sub>O-H<sub>2</sub>-TiO<sub>2</sub> degraded around 6 % of HA, producing 15 ppm of hydrogen, and 280 ppm of oxygen (2 μmol O<sub>2</sub> per 1 μmol of HA).

The investigation of the gas composition obtained with different samples allows suggesting two principal mechanisms for gaseous product yields in the anoxic photocatalytic treatment of HA solutions: water splitting with HA acting as electron donor, and direct HA splitting. Hydrogen production appears to be directly tied to LMW hydrocarbons production (Article V, Table 2): both seem to proceed simultaneously and they appear to be interdependent. The majority of hydrogen thus originates not from water splitting, but from HA molecule cleavage, where the shortest pathway for hydrogen production is hydroxyl groups' dissociation on platinum particles, which also serve as electron traps. Oxygen production, on the other hand, in the amounts actually observed is more likely the result of water splitting: indeed, in case of oxygen-producing photocatalysts, the amount of HA degraded by them differed by an order of magnitude, whereas their results in oxygen production were comparable. As a result, it can be seen that under anoxic

conditions, HA can successfully undergo photocatalytic splitting, producing hydrogen. Direct HA photocatalytic splitting seems to result in a higher hydrogen yields than water splitting with HA as sacrificial electron donor.

## 5. CONCLUSIONS

A number of photocatalytic systems, namely visible-light sensitive photocatalysts containing both metallic and non-metallic admixtures (C, S, B, Pt, CuO, Co, Fe, W), and photocatalytic TiO<sub>2</sub> coatings were synthesized and their activity successfully tested for the degradation of several environmental pollutants having different structure and properties, namely methyl-*tert*-butyl ether (MTBE), *p*-toluidine, prednisolone (PNL), phenol and humic acid sodium salt (HA), taken as a representative of humic substances (HS). A renowned commercial photocatalyst, P25 Evonik titanium dioxide was used as a reference.

The performance of doped titania species was shown to be selective in photocatalytic oxidation (PCO) of different pollutants. While S-, B- and C-doped catalyst species showed superb performance in MTBE PCO, surpassing P25, being comparable to the latter with *p*-toluidine PCO, they performed poorly with phenol. Similarly, while the performance of S-TiO<sub>2</sub> was somewhat inferior, but still comparable to that of P25 with PNL PCO, the performance of C- and Fe-TiO<sub>2</sub> were significantly inferior. The purpose of the observed selective performance was found mainly in different interactions of the pollutant molecules and the surface of the photocatalysts due to their electrostatic properties. Another aspect of PCO selective performance was exhibited in case of PNL degradation: the availability of wastewater matrix (represented by carbamide and sucrose) did not have significant effect on PNL degradation. At the same time, the doped photocatalysts were shown to be non-toxic in comparison to P25 TiO<sub>2</sub> both in the dark and under illumination, providing a possibility of their future applications as a stage of combined processes including biological degradation. Surface morphology was shown to be another important factor influencing PCO, specifically, the availability of active sites, serving as radical species sources.

The performance of Pt-, Co-, W-, Cu<sub>x</sub>O- and Fe-TiO<sub>2</sub> in hydrogen, oxygen, and low molecular weight (LMW) hydrocarbons production from anoxic aqueous solutions of HA allowed differentiating two principal sources of gaseous products: HA serving as a sacrificial electron donor *versus* direct HA photocatalytic splitting. The relative prevalence of one mechanism over another depends on the catalysts' composition. The direct HA splitting results in higher hydrogen yield than the water splitting, and also gives LMW hydrocarbons. Oxygen production, on the other hand, could be attributed to water splitting reactions.

## 6. REFERENCES

- Arpac, E., Sayilkan, F., Asiltürk, M., Tatar, P., Kiraz, N., Sayilkan, H. *Photocatalytic performance of Sn-doped and undoped TiO<sub>2</sub> nanostructured thin films under UV and vis-lights*. – Journal of Hazardous Materials, 2007, 140, 69–74.
- Asahi, R., Morikawa, T., Ohwaki, T., Aoki, T., Taga Y. *Visible-light photocatalysis in nitrogen-doped titanium oxides*. - Science, 2001, 223, 269 – 271.
- Bahruji, H., Bowker, M., Davies, P.R., Al-Mazroai, L.S., Dickinson, A., Greaves, J., James, D., Millard, L., Pedrono, F. *Sustainable H<sub>2</sub> gas production by photocatalysis*. - Journal of Photochemistry and Photobiology A: Chemistry, 2010, 216, 115-118.
- Bessekhouad, Y., Robert, D., Weber, J.-V., Chaoui, N. *Effect of alkaline-doped TiO<sub>2</sub> on photocatalytic efficiency*. – Journal of Photochemistry and Photobiology A, 2004, 167, 1, 49-57.
- Bowers, J.S. *Toluidines*. *Ullmann's encyclopedia of industrial chemistry* (2002 electronic release). Wiley-VCH Verlag GmbH & Co. KGaA, 2002.
- Busca, G., Berardinelli, S., Resini, C., Arrighi, L. *Technologies for the removal of phenol from fluid streams: A short review of recent developments*. – Journal of Hazardous Materials, 2008, 160, 265-288.
- Buxton, G.V., Greenstock, C.L., Helman W.P., Ross, A.B., *Critical review of rate constants for reactions of hydrated electrons, hydrogen atoms and hydroxyl radicals (•OH/•O) in aqueous solution*. – Journal of Physical and Chemical Reference Data, 1988, 17 (2), 513-886.
- Chang H., Hu, J.Y., Shao, B. *Occurrence of natural and synthetic glucocorticoids in sewage treatment plants and receiving river waters*. - Environmental Science & Technology, 2007, 41, 3462-3468.
- Chang, J.T., Lai, Y.F., He, J.L. *Photocatalytic performance of chromium or nitrogen doped arc ion plated-TiO<sub>2</sub> films*. - Surface and Coating Technology, 2005, 200, 1640-1644.
- Chen, X.B., Liu, L., Yu, P.Y., Mao, S.S. *Increasing solar absorption for photocatalysis with black hydrogenated titanium dioxide nanocrystals* – Science, 2011, 331, 746-750.
- Eggins, B. R., Palmer, F. L., Byrne, J. A. *Photocatalytic treatment of humic substances in drinking water*. - Water Research, 1997, 31, 1223-1226.

Ferreira, F.C., Han, S., Boam, A., Zhang, S., Livingston A.G. *Membrane aromatic recovery system (MARS): lab bench to industrial pilot scale.* - Desalination, 2002, 148, 267–273.

Herrmann, J. M. *Heterogeneous photocatalysis: fundamentals and applications for removal of various types of aqueous pollutants.* - Catalysis Today, 1999, 53, 1, 115-129.

Hingst, G., Ahrens, H., Otsa, E., Mueller, S. *Gefährdungsabschätzung für die Liegenschaft Raketenbasis Keila Joa (Estland).* Industriebetriebe Betriebsdesellschaft mbH, Niederlassung Berlin, Estnisches Umweltuntersuchungslabor, Tallinn, Estland, 1994, 118.

Howard, P.H. Handbook of environmental fate and exposure data for organic chemicals, vol. I, Large production and priority pollutants. Lewis Publishers, Chelsea, MI, USA, 1989.

Ihara, T., Miyoshi, M., Iriyama, Y., Matsumoto, O., Sugihara, S. *Visible-light active titanium dioxide realized by an oxygen-deficient structure and by nitrogen doping.* - Applied Catalysis B, 42, 2003, 403-409.

Ikarashi, K., Sato, J., Kobayashi, H., Saito, N., Nishiyama, H., Inoue, Y. *Photocatalysis for water decomposition by RuO<sub>2</sub>-dispersed ZnGa<sub>2</sub>O<sub>4</sub> with d(10) configuration.* - Journal of Physical Chemistry B, 2002, 106, 9048-9053.

Ikehata, K., Naghashkar, N.J., Ei-Din, M.G. Degradation of aqueous pharmaceuticals by ozonation and advanced ozonation processes: A review. - Ozone: Science & Engineering. 2006, 28, 353.

In, S., Orlov, A., Garcia, F., Tikhov, M., Wright, D.S., Lambert, R.M. *Efficient visible light active N-doped TiO<sub>2</sub> photocatalysts by a reproducible and controllable synthetic route.* - Chemical Communications, 2006, 236-238.

Irie, H., Watanabe, Y., Hashimoto, K. *Carbon-doped anatase TiO<sub>2</sub> powders as a visible-light sensitive photocatalyst.* - Chemistry Letters, 2003, 32, 772-773.

Jaromir, M., Ozadowicz, R., Duda, W. *Analysis of chlorophenols, chlorocatechols, chlorinated methoxyphenols and monoterpenes in communal sewage of łódź and in the Ner river in 1999-2000.* - Water, Air and Soil Pollution, 2005, 16, 205.

Johnson, P. *Assesment of the contribution of volatilization and biodegradation to in situ air sparging performance.* – Environmental Science and Technology, 1998, 32, 276-281.

Kadowaki, H., Sato, J., Kobayashi, H., Saito, N., Nishiyama, H., Simodaira, Y., Inoue, Y. *Photocatalytic activity of the RuO<sub>2</sub>-dispersed composite p-block metal oxide LiInGeO<sub>4</sub> with d(10)-d(10) configuration for water decomposition.* - Journal of Physical Chemistry B, 2005, 109, 22995-30000.

Kahru, A., Maloverjan, A., Sillak, H., Pollumaa, L. *The toxicity and fate of phenolic pollutants in the contaminated soils associated with the oil-shale industry.* – Environmental Science and Pollution Research, 2002, 1, 27- 33.

Kim, J., Choi, W. *Hydrogen producing water treatment through solar photocatalysis.*- Energy and Environmental Science, 2010, 3, 1042-1045.

Kirkpatrick, S. *A primer on radiometry.* - Dental Materials, 2005, 21, 21-26.

Klauson, D., Babkina, J., Stepanova, K., Krichevskaya, M., Preis, S. *Aqueous photocatalytic oxidation of amoxicillin.* - Catalysis Today, 2010, 151, 39-45.

Lettmann, C., Hildenbrand, K., Kisch, H., Macyk, W., Maier, W.H. *Visible light Photodegradation of 4-chlorophenol with a coke-containing titanium dioxide photocatalyst.* – Applied Catalysis B, 2001, 32, 215–227.

Lin, A.Y.C., Yu, T.H., Lateef, S.K. *Removal of pharmaceuticals in secondary wastewater treatment processes in Taiwan.* - Journal of Hazardous Materials, 2009, 167, 1163.

Liu, S., Ying, G.G., Zhao, J.L., Chen, F., Yang, B., Zhou, L.J., Lai, H.J. *Trace analysis of 28 steroids in surface water, wastewater and sludge samples by rapid resolution liquid chromatography-electrospray ionization tandem mass spectrometry.* - Journal of Chromatography A, 2011, 1218, 1367–1378.

Manahan, S.E. *Environmental Chemistry.* 6th ed. Lewis Publishers, 1994, USA, 80-259.

Matsuoka, M., Kitano, M., Takeuchi, M., Tsujimaru, K., Anpo, M., Thomas, J.M. *Photocatalysis for new energy production: Recent advances in photocatalytic water splitting reactions for hydrogen production.* - Catalysis Today, 2007, 122, 51-61.

Ni, M., Leung, M.K.H., Leung, D.Y.C., Sumathy, K. *A review and recent developments in photocatalytic water-splitting using for hydrogen production.* - Renewable and Sustainable Energy Reviews, 2007, 11, 401-425.

Ni, M., Leung, M.K.H., Sumathy, K., Leung, D.Y.C. *Water electrolysis—a bridge between renewable resources and hydrogen.* - Proceedings of the International Hydrogen Energy forum, 2004, 1, 475–480.

Ohno, T., Akiyoshi, M., Umebayashi, T., Asai, K., Mitsu, T., Matsumura, M. *Preparation of S-doped TiO<sub>2</sub> photocatalysts and their photocatalytic activities under visible light.* – Applied Catalysis A, 2004, 265, 115-121.

Palmisano, L., Sclafani, A. *Thermodynamics and kinetics for heterogeneous photocatalytic processes.* In: Schiavello, M. (ed.), Heterogeneous photocatalysis. Chichester: Wiley & Sons, 1997, 109–132.

Preis, S., Krichevskaya, M., Terentyeva, Y., Moiseev, A., Kallas, J. *Treatment of phenolic and aromatic amino compounds in polluted waters by photocatalytic oxidation.* – Journal of Advanced Oxidation Technologies, 2002, 5, 77-84.

Qadeer, R., Reham, A. H. A. *Study of the adsorption of phenol by activated carbon from aqueous solution.* – Turkish Journal of Chemistry, 2002, 26, 357-361.

Rozkov, A., Vassiljeva, I., Kurvet, M., Kahru, A., Preis, S., Kharchenko, A., Krichevskaya, M., Liiv, M., Käär, A., Vilu, R. *Laboratory study of bioremediation of rocket fuel-polluted groundwater.* – Water Research, 1999, 33, 1303-1313.

Safarzadeh-Amiri A. *O<sub>3</sub>/H<sub>2</sub>O<sub>2</sub> treatment of methyl-tert-butyl ether (MTBE) in contaminated waters.* – Water Research, 2001, 35, 3706-3714.

Sarasa, J., Cortes, S., Ormad, P., Gracia, R., Ovelleiro, J.L. *Study of aromatic by-products formed from ozonation of anilines in aqueous solution.* - Water Resources, 2002, 36, 3035-3044.

Sato, J., Saito, N., Nishiyama, H., Inoue, Y. *New photocatalyst group for water decomposition of RuO<sub>2</sub>-loaded p-block metal (In, Sn, and Sb) oxides with d(10) configuration.* - Journal of Physical Chemistry B, 2001, 105, 6061-6063.

Sato, J., Saito, N., Nishiyama, H., Inoue, Y. *Photocatalytic activity for water decomposition of RuO<sub>2</sub>-loaded SrIn<sub>2</sub>O<sub>4</sub> with d(10) configuration.* - Chemistry Letters, 2001, 868-869.

Sato, J., Saito, N., Nishiyama, H., Inoue, Y. *Photocatalytic water decomposition by RuO<sub>2</sub>-loaded antimonates, M<sub>2</sub>Sb<sub>2</sub>O<sub>7</sub> (M=Ca, Sr), CaSb<sub>2</sub>O<sub>6</sub> and NaSbO<sub>3</sub>, with d10 configuration.* - Journal of Photochemistry and Photobiology A: Chemistry, 2002, 148, 85-89.

Sato<sup>a</sup>, J., Kobayashi, H., Saito, N., Nishiyama, H., Inoue, Y. *Photocatalytic activities for water decomposition of RuO<sub>2</sub>-loaded AInO<sub>2</sub> (A=Li, Na) with d10 configuration.* - Journal of Photochemistry and Photobiology A: Chemistry, 2003, 158, 139-144.



Sato<sup>b</sup>, J., Saito, N., Nishiyama, H., Inoue, Y. *Photocatalytic activity for water decomposition of indates with octahedrally coordinated d(10) configuration. I. Influences of preparation conditions on activity.* - Journal of Physical Chemistry B, 2003, 107, 7965-7959.

Sharma, S.D., Singh, D., Saini, K.K., Kant, C., Sharma, V., Jain, S.C., Sharma, C.P. *Sol-gel derived super-hydrophilic nickel doped TiO<sub>2</sub> film as active photocatalyst.* - Applied Catalysis A, 2006, 314, 40-46.

Sreethawong, T., Yoshikawa, S. *Comparative investigation on photocatalytic hydrogen evolution over Cu-, Pd-, and Au-loaded mesoporous TiO<sub>2</sub> photocatalysts.* - Catalysis Communications, 2005, 6, 661-668.

Srour, R. *Mononitrotoluenes and derivatives.* Chapter A. VII.I and A. VII.PNT, Paris, 2002.

Sun, B., Seto, M., Clements, J.S. *Optical study of active species produced by a pulsed corona discharge in water.* - Journal of Electrostatics, 1997, 39, 3, 189-202.

Zhang, Y., Crittenden, J.C., Hand, D.W., Perram, D.L. *Fixed-bed photocatalysts for solar decontamination of water.* - Environmental Science and Technology, 1994, 28, 435-442.

Turci, C.S., Ollis, D.F. *Photocatalytic degradation of organic water contaminants: mechanisms involving hydroxyl radical attack.* - Journal of Catalysis, 1990, 122, 178-192.

U.S. Environmental Protection Agency, Methyl Tertiary Butyl Ether (MTBE) - <http://www.epa.gov/mtbe/water.htm>, 2009 (10.2009)

Umebayashi, T., Yamaki, T., Tanaka, S., Asai, K. *Visible light-induced degradation of methylene blue on S-doped TiO<sub>2</sub>.* - Chemistry Letters, 2003, 32, 4, 330-331.

Wang, G., Liao, C., Wu, F. *Photodegradation of humic acids in the presence of hydrogen peroxide.* -Chemosphere, 2001, 42, 379-387.

Wang, Z., Cai, W., Hong X., Zhao, X., Xu, F., Cai, C. *Photocatalytic degradation of phenol in aqueous nitrogen-doped TiO<sub>2</sub> suspensions with various light sources.* - Applied Catalysis B, 2005, 57, 223-231.

Vorontsov, A.V., Savinov, E.N., Jin, Z.S. *Influence of the form of photodeposited platinum on titania upon its photocatalytic activity in CO and acetone oxidation.* - Journal of Photochemistry and Photobiology A: Chemistry, 1999, 125, 113-117.

Xu, X.R., Zhao, Z.X., Li, X.Y., Gu, J.P. *Chemical oxidative degradation of methyl-tert-butyl ether in aqueous solution by Fenton's reagent*. - *Chemosphere*, 2004, 55, 73-79.

Yeh, C.K., Novak, J.T. *Anaerobic biodegradation of gasoline oxygenates in soils*. - *Water Environmental Research*, 1994, 66, 744-752.

Yu, J.C., Yu, J.G., Ho, W.K., Jiang, Z.T., Zhang, L.Z. *Effects of F- doping on the photocatalytic activity and microstructures of nanocrystalline TiO<sub>2</sub> powders*. - *Chemistry of Materials*, 2002, 14, 3808-3816.

## **Acknowledgements**

I would like to express my very great appreciation to my supervisor, Dr. Deniss Klauson, for his valuable and constructive assistance during the planning and development of this research work. His willingness to give his time so generously has been very much appreciated.

Special thanks should be given to Dr. Marina Krichevskaya, for her professional guidance on practical work. I would also like to thank Dr. P. Boni, Mr. I. Castellanos Beltran, Dr. T. Dedova, Ms. K. Stepanova, Dr. Mart Viljus, Mr. E. Kärber, Dr. Anne Kahru, Dr. R. Geiss, Ms. K. Juganson and Mr. A. Käkinen for assistance and contribution to this work.

Finally, I wish to thank my family and friends for their understanding, patience, support and encouragement throughout my study.

Financial support of the research from Estonian Scientific Foundation, Estonian Research Council, United States Civilian Research and Development Foundation, Doctoral School of Functional Materials and Technologies is also very much appreciated.

## KOKKUVÕTE

Käesolevas töös uuriti mitme erineva struktuuriga bioloogiliselt lagundamatu orgaanilise saasteaine traditsioonilist fotokatalüütilist oksüdatsiooni vees, kasutades katalüsaatorina legeeritud titaandioksiidi. Samuti võrreldi erinevate fotokatalüsaatorite toimet fotokatalüüsis, mille käigus toimub vesiniku genereerimine.

Vee ja õhu puhastamisel on fotokatalüütilisel oksüdatsioonil võrreldes teiste meetoditega teatud eelised – selles kasutatakse kõige kõrgema redokspotentsiaaliga oksüdanti, positiivselt laetud auku ja suhteliselt odavast materjalist fotokatalüsaatorit, samuti ei mõjuta protsessi reovee põhikomponendid ning on võimalus kasutada päikesevalgust katalüsaatorite fotoergastamiseks. Seega võib fotokatalüüs osutada perspektiivseks meetodiks sihtreainete selektiivsel lagundamisel reovees, kusjuures samaaegselt on võimalik toota rohelist kütust – vesinikku.

Käesoleva töö põhieesmärgid olid järgmised:

1. Uurida legeeritud katalüsaatorite fotokatalüütilise oksüdatsiooni potentsiaali erineva struktuuriga saasteainete lagundamisel ning protsessi mehhanismi.
2. Võrrelda erinevaid titaandioksiidi baasil sünteesitud fotokatalüsaatoreid.
3. Kombineerida saasteaine fotokatalüütilist lagundamist vesiniku genereerimisega.

Töös uuriti eksperimentaalselt:

1. erinevate saasteainete fotokatalüütilise oksüdatsiooni efektiivsust;
2. nähtavas valguses aktiivsete mittemetalliliste ja metalliliste lisanditega legeeritud titaandioksiidfotokatalüsaatorite sünteesi ja toimet ning titaandioksiidkatete aktiivsust;
3. fotokatalüütilise oksüdatsiooni mehhanismi ja reovee põhikomponentide mõju protsessi efektiivsusele;
4. vesiniku, hapniku ja madalmolekulaarete süsivesinike fotokatalüütilist genereerimist, kasutades bioloogiliselt lagundamatut saasteainet elektronide doonorina.

Käesoleva töö peamine uudsus seisneb järgmises:

1. Saadud tulemused näitavad, et erinevalt laialt levinud praktikale kasutada uuringutes värvaineid, tuleb fotokatalüsaatorite töö uurimisel kasutada mitut erineva keemilise struktuuriga saasteainet, et objektiivselt hinnata uute fotokatalüsaatorite materjalide efektiivsust. Erinevalt värvainetest, mis

võivad fotolüüsil laguneda, võimaldab rasketilagundatavate saasteainete kasutamine uuringutes hinnata fotokatalüsaatorite rakendatavust reaalsete keskkonnaprobleemide lahendamisel.

2. Leiti, et fotokatalüütilise oksüdatsiooni selektiivse toime tõttu erinevate saasteainete suhtes pole fenooli kasutamine standardsaasteainena erinevate oksüdatsioonimeetodite võrdlemiseks õigustatud.
3. Tehti kindlaks, et fotokatalüütilise oksüdatsiooniga hästi lagundatav metüül-*tert*-butüüleeter (MTBE) võib protsessi käigus osaliselt laguneda autokatalüütiliselt. Seetõttu on sobiv kasutada MTBE suhteliselt rasketilagundatavate vaheproduktide mineraliseerumist MTBE-reostuse kõrvaldamise uurimiseks.
4. Selgitati, et fotokatalüsaatorite pinna morfoloogia ja defektid omavad olulist mõju fotokatalüütiliste materjalide aktiivsusele. Fotokatalüsaatori eripinna suurendamine ei too tingimata endaga kaasa fotokatalüütilise aktiivsuse või adsorptsioonivõime kasvu. Samas, fotokatalüsaatori pinna ja lagundatavate ainete molekulide elektrostaatilisest vastasmõjudest omavad suurt tähtsust: nad võimaldavad saasteainete molekulide levi fotokatalüsaatori pinna lähedusse, tsooni, milles saavad eksisteerida oma lühikese eluea jooksul hüdroksüülradikaalid. Samuti mõjutavad elektrostaatilisest vastasmõjudest saasteainete adsorptsiooni fotokatalüsaatori pinnale, kus nad saavad laguneda vahetult positiivselt laetud aukude peal.
5. Fotokatalüüs hapnikuvabas keskkonnas võimaldab peale saasteainete lagundamise genereerida ka vesinikku, hapnikku ja madalmolekulaarseid süsivesinikke märgatavates kogustes, kusjuures on võimalik eristada kaht mehhanismi.

Antud töö tulemused on avaldatud viies artiklis eelretsenseeritavates rahvusvahelistes ajakirjades (kategooria 1.1) ning on esitatud ühel rahvusvahelisel teaduskonverentsil.

## ABSTRACT

The present research considers conventional aqueous photocatalytic oxidation (PCO) of a range of non-biodegradable water pollutants having different chemical structure by doped photocatalysts, and also compares the performance of various doped photocatalysts in hydrogen-producing photocatalysis.

As a method for water and air treatment PCO is in a somewhat advantageous position due to a combination of its high oxidation potential, relative inexpensiveness of photocatalysts, noted little interference from the main wastewater matrix, and the ability of using direct solar radiation for the catalyst excitation. Photocatalysis can be a promising treatment method for the selective removal of target pollutants from contaminated water, together with the possibility of simultaneously producing green fuel, i.e. hydrogen.

The main objectives of the present research were:

1. To clarify the doped catalysts' PCO potential in degradation of a fairly wide range of model pollutants, and investigate the process mechanism;
2. To compare different modifications of synthesised titanium dioxide-based photocatalysts;
3. Combine pollutant photocatalytic decomposition with hydrogen production.

The following points were addressed:

1. The efficiency of PCO in degradations of pollutants;
2. Synthesis and examination of visible-light-sensitive modified photocatalysts with both non-metal and metal dopants, and that of titania coatings;
3. The investigation of PCO mechanism and the role of wastewater matrix on the process performance
4. Establishment of maximal hydrogen, oxygen and low molecular weight hydrocarbons photocatalytic production using non-biodegradable pollutant as sacrificial electron donor.

The novelty of the present research includes:

1. The results obtained show that contrary to the practice well established in the literature, an objective view of the materials' abilities can be obtained only through testing their photocatalytic performance by the degradation of several substrates with different chemical structure; choosing recalcitrant pollutants as degradation substrates, as opposed to photolysis-prone dyes, allows the evaluation of the photocatalysts' applicability to the solution of actual environmental problems.

2. Due to the observed selective character of photocatalysis towards substrates with different chemical structure, the established use of phenol as a “standard” pollutant for the comparison of various oxidative technologies can be questioned.
3. Methyl-*tert*-butyl ether (MTBE), yielding well to photocatalysis, can be partly prone to autocatalysis during the process. This supports the use of its relatively recalcitrant degradation by-products’ mineralisation as a meter of MTBE-related contamination removal.
4. Photocatalyst surface features and defects possess significant influence on the material’s activity. However, the increase in specific surface area does not necessary result in either increased adsorption capability or photocatalytic activity of the materials. On the other hand, electrostatic interactions between the photocatalyst surface and the substrates to be degraded are of high importance: they govern the ease of the pollutant molecules’ movement into the close vicinity of photocatalyst surface where hydroxyl radicals exist during their lifetime, or to the surface where the pollutants can undergo direct hole oxidation.
5. Photocatalysis carried out under anoxic conditions is capable not only of degrading the pollutant, but also shows noticeable results in hydrogen, oxygen and low molecular weight hydrocarbons production, with two separate mechanisms clearly differentiated.

The issues of this work were published in five articles in international peer-reviewed journals and presented at one international scientific conference.





**APPENDIX I**  
**PUBLICATIONS**



### **Article I:**

Klauson D., Portjanskaja E., Budarnaja O., Krichevskaya M., Preis S., The synthesis of sulphur and boron-containing titania photocatalysts and the evaluation of their photocatalytic activity. *Catalysis Communications*, 2010, 11 (8), pp. 715-720, doi: 10.1016/j.catcom.2010.02.001





## The synthesis of sulphur and boron-containing titania photocatalysts and the evaluation of their photocatalytic activity

Deniss Klauson<sup>a,\*</sup>, Elina Portjanskaya<sup>a</sup>, Olga Budarnaja<sup>a</sup>, Marina Krichevskaya<sup>a</sup>, Sergei Preis<sup>b</sup>

<sup>a</sup> Department of Chemical Engineering, Tallinn University of Technology, Ehitajate Tee 5, 19086 Tallinn, Estonia

<sup>b</sup> Department of Chemical Engineering, Lappeenranta University of Technology, P.O. Box 20, 53851 Lappeenranta, Finland

### ARTICLE INFO

#### Article history:

Received 30 December 2009

Received in revised form 28 January 2010

Accepted 1 February 2010

Available online 6 February 2010

#### Keywords:

Photocatalytic oxidation

Sulphur-containing titania

Boron-containing titania

Methyl-*tert*-butyl ether

*tert*-Butyl alcohol

*i*-Propanol

2-Ethoxy ethanol

*p*-Toluidine

Phenol

### ABSTRACT

Aqueous photocatalytic oxidation of methyl-*tert*-butyl ether, *p*-toluidine, *tert*-butyl alcohol, *i*-propanol, 2-ethoxy ethanol and phenol, was studied using sulphur and boron-containing titania photocatalysts, active in visible light. The activity of the catalysts, compared to commercial Degussa P25, was tested in PCO of the pollutants dependent on the admixture content. The performance of S- and B-TiO<sub>2</sub> under visible light in PCO of MTBE, TBA and *i*-propanol was surpassing that of P25 under UV. However, in respect of *p*-toluidine and phenol both S- and B-containing titania showed an inferior, although comparable, performance, to that of P25. Experiments were carried out under artificial and solar light.

© 2010 Elsevier B.V. All rights reserved.

### 1. Introduction

Aqueous photocatalytic oxidation (PCO) of organic groundwater pollutants, methyl-*tert*-butyl ether (MTBE, CH<sub>3</sub>-O-C(CH<sub>3</sub>)<sub>3</sub>), *tert*-butyl alcohol ((H<sub>3</sub>C)<sub>2</sub>C-OH, TBA), *i*-propanol (H<sub>3</sub>C-CH(OH)-CH<sub>3</sub>), 2-ethoxy ethanol, *p*-toluidine, and phenol, was studied using two series of titania photocatalysts, synthesised by sol-gel method, doped with sulphur and boron active in visible light.

Methyl-*tert*-butyl ether, banned for its use in the USA, is still widely used as an oxygenated component of motor fuels by the rest of the world. Water pollution with MTBE may occur due to traffic accidents, fuel leaks or inappropriate fuel disposal. This substance is of particular concern because of its accumulation in groundwater due to its low biodegradability [1]. Physical removal and chemical oxidation methods, such as air stripping, activated carbon adsorption, ozonation and treatment with Fenton's reagent have been proven to be ineffective against MTBE [2–4].

*p*-Toluidine is a widely used industrial chemical, with its use ranging from a component of several jet and rocket fuels to applications in paint and pharmaceutical industries [5]. Also, at former munitions sites *p*-toluidine is a degradation intermediate of *p*-nitrotoluene, and occurs in tobacco smoke [6]. Thus, the pollution

of soil and groundwater with *p*-toluidine occurs at the military sites; industrial emissions are also possible. Non-biodegradable *p*-toluidine may accumulate in groundwater aquifers in toxic amounts. Conventional water treatment methods have been shown to be inadequate against *p*-toluidine pollution [7].

Phenol, being a substantial environment pollutant of, for example, oil shale industry [8], has a reputation of a standard model contaminant used to test the activity of various oxidation methods and catalysts. *tert*-Butyl alcohol (TBA) can be primarily found in the groundwater as a result of MTBE hydrolysis; it may also enter groundwater as an impurity of MTBE-blended motor fuels [9]. 2-Ethoxy ethanol is used in multiple applications in industry and transport and also may accumulate in subsurface aquifers. The main interest in *i*-propanol, however, was to study the PCO of secondary carbon atom when compared to primary carbon of 2-EE, tertiary carbon atom of MTBE and TBA and aromatic structures of phenol and *p*-toluidine. Thus the choice of model pollutants was serving the systematic study of the catalysts' performance on pollutant substances of different molecular structure found simultaneously in polluted groundwater. Although dyes are often used as test objects for novel photocatalysts, the authors believe that the performance of the latter would better be checked by real and chemically stable pollutants, unlike dyes that can spontaneously decompose under visible irradiation. Also, often the modified catalysts exhibit dramatically different performance with different

\* Corresponding author.

E-mail address: [dklauson@hotmail.com](mailto:dklauson@hotmail.com) (D. Klauson).

substances [10]. In case when various pollutants can be found simultaneously in, for example, fuel-polluted groundwaters, the knowledge of photocatalytic activity against multiple targets is necessary.

Subjected to electromagnetic irradiation of appropriate energy, the excited semiconductor's valence band electrons are displaced to the conduction band, forming positively charged holes oxidizing the water molecules into hydroxyl radicals reacting with the pollutant. Also, the direct oxidation of organic pollutant adsorbed on the photocatalyst surface by the positively charged holes takes place.

Most commonly used titanium dioxide photocatalysts can be excited only by ultraviolet irradiation, as the band-gap energy of  $\text{TiO}_2$  is 3.2 eV. This way, only 4% of the solar radiation reaching the Earth surface can be used. However, the semiconductor band-gap can be reduced by doping, i.e. introducing additive atoms into titanium dioxide structure, thus forming a crystalline structure with a misbalance in charge carriers. These charge carriers, either electrons or holes, have enough energy to create a new energetic level inside the band-gap (named either donor or acceptor level, depending on whether it is formed by electrons or holes respectively), which is occupied at room temperature by electrons. When subjected to electromagnetic irradiation, the electrons of donor or acceptor level can be excited and displaced to the conduction band from an energetic level inside the band-gap with less energy required for electron excitation, i.e. light with greater wavelength may be utilised.

Sulphur- and boron-containing titania visible light-sensitive photocatalysts were synthesised using sol-gel method and tested in PCO of the abovementioned pollutants. An undoped titania sample synthesised by the same pattern was used as a reference. The performance of the modified catalysts, dependent on the admixture content, was compared to one another and to that of Degussa P25 titanium dioxide.

## 2. Experimental

Two thermostatted at  $20 \pm 1$  °C 200-mL simple batch reactors with inner diameter 100 mm (evaporation dishes), aperture  $40 \text{ m}^2 \text{ m}^{-3}$ , mechanically agitated with magnetic stirrers, were used in PCO experiments: the one used for the PCO was called "active" and the other containing no photocatalyst was called "reference". Both reactors were exposed to identical experimental conditions. The samples from the active reactor were compared to the reference samples to avoid complications caused by water evaporation. A UV-light source, Philips 365-nm low pressure luminescent mercury UV-lamp (Sylvania Blacklight F 15 W 350 BL-T8), was positioned horizontally over the reactors, providing the irradiance of about  $0.7 \text{ mW cm}^{-2}$  measured at a distance of 25 cm, corresponding to the level of the free surface of the reactor by the optical radiometer Micropulse MP100 (Micropulse Technology, UK). With daylight fluorescent lamp (Philips TLD 15 W/33–640), the irradiance was measured indirectly, being calculated from the illuminance, measured by TES luxmeter (TES Inc., Taiwan), using lumen to watt ratio of 684, as the response of human eye to light with the illuminance of 684 lumens (lm) equals to that to the irradiance of  $1 \text{ W}$  [11]. With Philips TLD lamp, the amount of UV-irradiation was also specifically measured using the above-mentioned Micropulse radiometer for 254 and 365 nm and total amount of UV by using Ocean Optics USB2000 + UV-VIS spectrometer. Only negligibly small fraction of UV around 365–400 nm was observed. These measurements are also confirmed by the publicly available data from the lamp manufacturer [12]. Thus, any noticeable action of the photocatalyst when using Philips TLD lamp as the irradiation source may not be attributed to the UV fraction emitted by the lamp but is clearly due to the activity of the catalysts in

visible light region. There were also some experiments conducted outdoors, using natural solar irradiation. A schematic representation of the experimental setup can be seen in Fig. 1.

The experiments were carried out using aqueous solutions of the chemicals supplied by Aldrich. With all chemicals except 2-EE, the experiments were conducted with synthetic solutions (i.e. the pollutants dissolved in distilled water) at  $100 \text{ mg L}^{-1}$ ; with 2-EE the concentration was higher, being  $300 \text{ mg L}^{-1}$ . The concentrations were chosen with reference to those that may be found in real contaminated aquifers used in previously conducted experiments [7,13]. The experiments were carried out in acidic (pH 3), natural (pH 6.5) and alkaline (pH 11) media, adjusted either by 4 N sulphuric acid or 15% sodium hydroxide. The treatment time for MTBE was 2 h under artificial light and 30 min under solar radiation. With *i*-propanol, treatment time was also 2 h. For *p*-toluidine and phenol, treatment time was 24 h. TBA solutions were treated for 4 h. Treatment time for 2-EE was chosen to be 24 h under artificial and 5 h under solar light. The treatment time in every case was chosen to reduce the concentration of pollutants below 50% of the residual concentration and was used in calculations of the process efficiency  $E$  (see Eq. (1)). All the experiments were carried out for at least three times under identical experimental conditions to derive the average value of the process efficiency. The average deviation of data in parallel experiments did not exceed 5%.

Adsorption experiments with the pollutants on the photocatalyst surface were carried out at respective pH in closed flasks thermostatted at  $20 \pm 1$  °C and equipped with magnetic stirrers. The adsorbed amount of substances was derived from the batch mass balance: the concentration of the dissolved substance was determined before and after adsorption.

Titanium dioxide Degussa P25, eight sulphur-containing and five boron-containing synthetic catalysts were used. Sulphur-containing photocatalysts were prepared by the hydrolysis of titanium tetrabutoxide with addition of a pre-calculated amount of 0.1 N sodium thiosulphate as sulphur source, followed by calcination at 400 °C for 4 h. After this, the catalyst was washed with hot distilled water applied in a sequence of 10–15 rinsing rounds (ca. 1 L per 1 g of catalyst) in order to clean the catalyst surface from water-soluble compounds. In case of boron-containing photocatalysts, sodium tetraborate was used as boron source. An additional catalyst was synthesised using the same pattern, although without the addition of sulphur or boron sources. The experiments were performed in photocatalyst suspensions of  $1 \text{ g L}^{-1}$ .

Many authors indicate complete transformation of sulphide to sulphate at calcination temperature in air from 300 to 500 °C [14]. For verification of the catalysts stability, the S-modified catalyst was suspended in distilled water in amount of  $1 \text{ g L}^{-1}$  under the UV light for 24 h. The sulphate determination was carried out with the IC (Dionex DX-120) with no corresponding peaks observed at the sensitivity of 10 ppb. As for carbon, the available

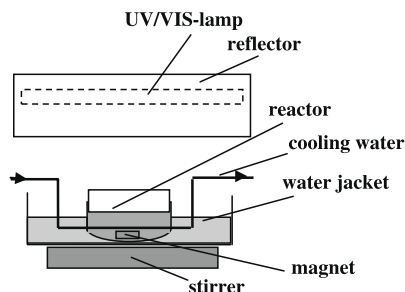


Fig. 1. Experimental setup.

**Table 1**

Main characteristics of sulphur- and carbon-doped photocatalysts.

Composition (at.%)					$S_{\text{BET}}$	$S_{\text{Langmuir}}$	$S_{\text{millipores}}$	$V_{\text{millipores}}$
S	Ti	O	C	Impurities	$\text{m}^2 \text{g}^{-1}$	$\text{m}^2 \text{g}^{-1}$	$\text{m}^2 \text{g}^{-1}$	$\text{mm}^3 \text{g}^{-1}$
0	18.1	46.6	33.9	0	105.7	144.7	4.1	5.1
0.8	17.9	47.5	32.8	1.0	93.8	126.7	1.7	0.6
1.1	17.5	46.2	34.1	1.1	129.0	176.0	0	0
1.4	18.1	47.1	33.4	0	170.7	234.0	0	0
1.7	16.6	46.1	34.3	1.4	164.5	219.2	10.5	3.4
1.7	18.5	50.5	28.0	1.3	132.0	178.4	4.7	1.7
2.5	17.7	49.9	28.7	1.6	141.9	149.3	58.3	20.6
2.8	18.7	48.1	28.9	1.6	163.6	222.7	6.1	2.1
B	Ti	O	C	Impurities				
1.1	17.3	47.1	34.0	0.6	150.7	206.1	10.3	3.6
1.5	12.3	34.2	51.1	0.8	112.6	156.6	0	0
2.0	9.9	35.0	53.1	0	272.4	380.1	0	0
3.2	9.7	33.7	53.4	0.06	242.5	337.8	0	0
3.8	12.1	37.5	46.5	0	78.2	107.8	0	0

knowledge shows that when preparing titania photocatalysts by sol-gel method, it is impossible to completely eliminate carbon originating from tetrabutyl orthotitanate even when calcining the catalysts at high temperatures, where free and organic carbon, and also carbonate, would already decompose. This suggests that the amounts of carbon that can be present in the sol-gel prepared photocatalysts after calcinations and thorough washing are incorporated in a stable form into titanium dioxide crystal lattice [15].

In order to evaluate the stability of the photocatalysts, every experiment was carried out using at least three times under identical conditions using the same portion of the photocatalyst. The difference between the results of single experiments was even in case of 24-h experiments well within the parallel experiments deviation (under 5%) with no tendencies observed.

The crystallinity of modified titania photocatalysts was analysed using X-ray diffraction (XRD) spectroscopy D5000 Kristalloflex, Siemens (Cu K $\alpha$  irradiation source). Elements content was measured with X-ray photoelectron spectroscopy PHI 5600. The specific area (BET and Langmuir adsorption) and the pore volume of the catalysts were measured by the adsorption of nitrogen using Kelvin 1042 sorptometer.

The decrease of MTBE, TBA, 2-EE and *i*-propanol concentrations was determined from the decrease in chemical oxygen demand (COD), measured by a standard method. This parameter, unlike TOC, was proven to be universal, decreasing with the increased conversion degree in oxidation reactions. Also, with several randomly selected doped catalysts, the decrease of MTBE concentration was measured by gas chromatography, which showed that MTBE was totally degraded in about 1 h time regardless the catalyst used, however, COD decrease, i.e. the degradation of MTBE PCO by-products, proceeded differently; this was another reason for choosing COD decrease to evaluate PCO performance. Concentrations of *p*-toluidine were measured photometrically after diazotization and reaction with phenol at 490 nm, and those of phenol were determined photometrically after reaction with *p*-nitroaniline at 570 nm using Helios  $\beta$  spectrophotometer together with the COD. In case of *p*-toluidine, the evolution of nitrite and nitrate ions was also determined using Metrohm 761 Compact IC ion chromatograph.

The performance of PCO under artificial radiation was characterised by the process efficiency  $E$  defined as the decrease in the amount of pollutants divided by the amount of energy reaching the surface of the treated sample within the treatment time (Eq. (1)).

$$E = \frac{\Delta C \times V \times 1000}{I \times S \times t} \quad (1)$$

where  $E$  – PCO efficiency,  $\text{mg W}^{-1} \text{h}^{-1}$ ;  $\Delta C$  – the decrease in the pollutant's concentration  $\text{mg L}^{-1}$  or  $\text{mg O L}^{-1}$  measured as COD;  $V$  – the volume of the sample to be treated, L;  $I$  – irradiance,  $\text{mW cm}^{-2}$ ;  $S$  – irradiated area,  $\text{cm}^2$ ;  $t$  – treatment time, h.

### 3. Results and discussion

#### 3.1. Photocatalyst characterisation

Table 1 shows the composition and surface properties of S- and B-TiO $_2$ . As one can see, beyond the primary admixtures, i.e. sulphur and boron, there is also some amount of carbon, the presence of which is inevitable in sol-gel synthesis even at high calcinations temperatures (over 1000 °C). The first row of the table shows the reference catalyst synthesised without sulphur or boron precursors. Nitrogen and silica were detected by XPS in small amounts as impurities. Judging from the XRD analysis, anatase prevailed in all doped catalysts.

The specific surface area of both catalyst types shows a tendency to pass a maximum with growing concentration of doping elements. The changes in Millipore area and volume, on the other hand, are far less systematic. It should be also noted that S-TiO $_2$  catalyst samples tended to give acidic and B-TiO $_2$  – alkaline reaction when suspended in water after thorough wash before use, which should be attributed to the functional groups at the catalysts' surface, as the catalysts were thoroughly washed after calcination (see Section 2).

#### 3.2. Photocatalytic oxidation experiments

##### 3.2.1. Sulphur-containing titania

The PCO of MTBE under artificial visible light (Philips TLD 15 W fluorescent lamp) with S-TiO $_2$  proceeds best in acidic media, followed by alkaline and neutral ones (Fig. 2a). This pattern was observed for all S-containing catalysts. For this reason, further experiments with MTBE on the impact of admixture content were conducted in acidic media (pH 3.0). Here the efficiency increased with the increasing sulphur content up to 1.5 at.% and then steadily decreased (see Fig. 3a). The values of MTBE PCO efficiency observed with S-doped catalysts were up to two times higher than with Degussa P25 (350 compared to 170  $\text{mg O W}^{-1} \text{h}^{-1}$ ) [13]. With the photocatalyst containing 1.7 at.% S, COD of the treated solutions reached zero in time, i.e. not only MTBE was oxidized but also its by-products were totally mineralized. Some of the S-containing catalyst specimens under UV-radiation (Sylvania Blacklight lamp) showed activity similar to the one of Degussa P25 (see Fig. 3a).

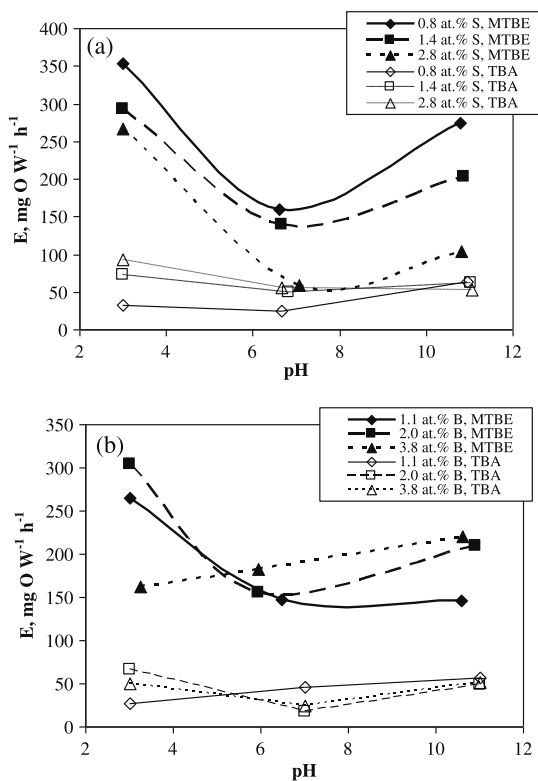


Fig. 2. The dependence of efficiency of PCO of MTBE and TBA on the initial solution pH with the sulphur (a) and boron-modified (b) photocatalysts, pH 3.0, 20 °C, visible light.

The efficiencies achieved with S-containing catalysts in TBA oxidation were also up to three times higher than those with Degussa P25 (90 compared to 33  $\text{mg O W}^{-1} \text{h}^{-1}$  [13]). The dependency of TBA PCO efficiency on pH differed from the pattern of MTBE: under alkaline conditions the catalysts showed similar efficiencies invariant of S-content, although acidic media still seem to be superior, followed by alkaline and neutral media (Fig. 2a). Interestingly, the PCO efficiency of TBA under visible light increased almost linearly with growing sulphur content in the catalysts (Fig. 3a), whereas under UV the dependence of PCO efficiency on dopant concentration was similar to that observed with MTBE, having a maximum at around 1.4 at.% S. The values of PCO efficiency under UV-radiation were similar to the one achieved with Degussa P25.

The degradation of COD of MTBE solutions treated under the solar light proceeded faster with Degussa P25, although the performance of some sulphur-containing photocatalysts was close to that.

Sulphur-containing titania catalysts exhibited poor performance in PCO of phenol: only 3% of phenol in 100-ppm solution was degraded with visible light under experimental conditions in 24 h; under UV-radiation the result was slightly better – 19%. The PCO efficiency in visible light, measured in COD units, was thus only 0.5  $\text{mg O W}^{-1} \text{h}^{-1}$ . The efficiency of Degussa P25 in phenol PCO was 10  $\text{mg O W}^{-1} \text{h}^{-1}$  under similar experimental conditions.

The sulphur-containing catalysts showed poor performance both under artificial and solar radiation in 2-EE PCO. With another aliphatic alcohol *i*-propanol, however, the PCO efficiency with S-TiO<sub>2</sub> under visible light was almost two times higher than the

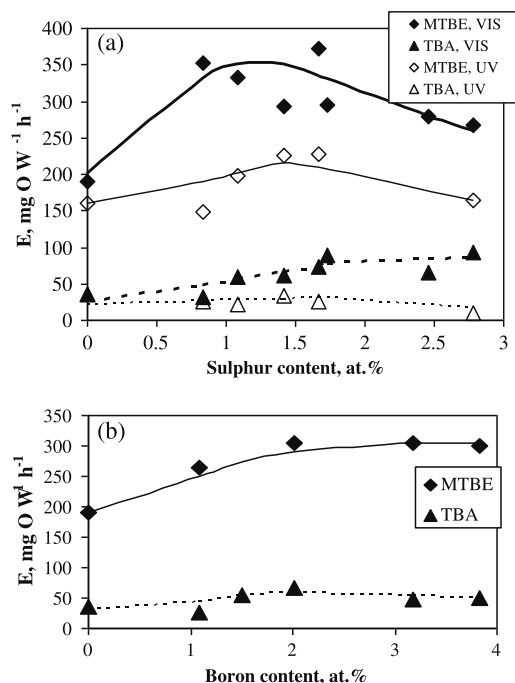


Fig. 3. The dependence of the efficiency of MTBE (a) and TBA (b) PCO on the sulphur content in the photocatalysts, pH 3.0, 20 °C, UV and visible light.

one achieved with Degussa P25 under UV, 69 and 38  $\text{mg O W}^{-1} \text{h}^{-1}$ , respectively.

The best performance in *p*-toluidine PCO with S-TiO<sub>2</sub> was observed under alkaline pH (see Fig. 4a), where the experiments were subsequently carried out. Under acidic and neutral conditions, *p*-toluidine PCO did not proceed with the sulphur-containing photocatalysts. The efficiency of S-TiO<sub>2</sub> catalysts in alkaline media under visible light in PCO of *p*-toluidine was comparable to the one of commercial Degussa's under UV, which was 4  $\text{mg W}^{-1} \text{h}^{-1}$  or 8  $\text{mg O W}^{-1} \text{h}^{-1}$ . However, the variation in sulphur content in the photocatalysts did not affect much the efficiency numbers.

### 3.2.2. Boron-containing titania

With B-TiO<sub>2</sub>, the dependence of the efficiency of MTBE and TBA PCO on pH was similar to that of S-TiO<sub>2</sub> (see Fig. 2b). Under visible radiation at pH 3.0 an increasing trend in PCO efficiency was observed with the boron content increasing to 2 at.%; above that content, the efficiency remained at a constant level (Fig. 3b). Under visible light with B-TiO<sub>2</sub> the efficiency of PCO of both MTBE and TBA exceeded the one achieved with Degussa P25 under UV for about two times (Fig. 3).

Contrary to the S-TiO<sub>2</sub> catalysts, the boron-containing titania exhibited the fastest *p*-toluidine PCO in acidic media followed by neutral and basic ones (Fig. 4b). The PCO efficiency with B-TiO<sub>2</sub> in acidic media under visible light exceeded the one of Degussa's under UV by a factor 1.5 for *p*-toluidine and 2.0 for COD degradation. It is noticeable that in neutral and alkaline media the PCO efficiency decreases slightly with the increase in the boron content in the catalysts (rather similar to the effect observed with S-TiO<sub>2</sub>), however, the trend is quite contrary in case of acidic media, where certain growth can be observed. The reason behind this observation is the different behaviour in acidic media of the catalyst



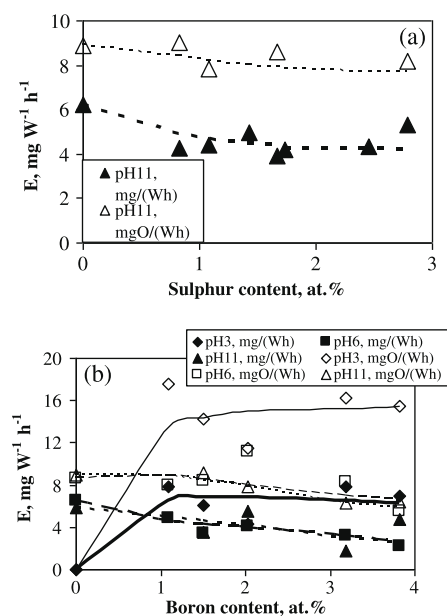


Fig. 4. The dependence of the  $p$ -toluidine PCO efficiency on the initial solution pH with the sulphur (a) and boron-modified (b) photocatalysts: pH 3.0, 20 °C, visible light.

containing only carbon as opposed to those containing boron and carbon.

The adsorption of substances under scope on the surface of both doped catalyst types was found to be insignificantly small, ranging around a few  $\text{mg g}^{-1}$  of titania. This makes the major part of degradation proceeding through hydroxyl radical reactions.

### 3.3. Discussion

The dependence of efficiency of MTBE PCO on the S-admixture concentration passing through the maximum at 1.5–1.7 at.% can be explained by the decrease in catalyst redox potential accompanying the decrease in the band-gap energy with growing dopant concentration [16]. Under visible light, at first, the decrease in the band-gap enhances the PCO performance. With the growing admixture content, however, the decrease in the redox potential overpowers the positive effect of the decreased band-gap, resulting in the PCO efficiency decrease. Slight PCO efficiency growth between 0.8 and 1.5 at.% S may be attributed to the growth of the catalysts' contact surface area. Even though the substances' adsorption does not greatly improve due to this, greater area is illuminated, which may result in a better hydroxyl radical production. The linear growth of PCO efficiency of TBA with growing content of sulphur within the experimental limits could be explained by the turning point laying at higher dopant concentrations.

It may be seen that with aliphatic substances the modified catalysts showed the best performance with MTBE and TBA, followed by *i*-propanol and 2-EE. Since the adsorption of substances under scope on the surface of the catalysts was found to be negligible, the PCO is assumed to proceed here mainly as a nucleophilic attacks of hydroxyl radicals. Nucleophilic attack proceeds upon the carbon atom having the highest partial positive charge. In ethers and alcohols this is a carbon atom located next to oxygen due to oxygen being more electronegative: with 2-EE, the nucleophilic attack proceeds on both C1 and C2 atoms [17], although an attack

on C1 tends to prevail. With *i*-propanol, a secondary carbon atom connected to the hydroxyl group is under attack, in TBA and MTBE molecules hydroxyl radical attacks tertiary carbon atom, connected to the hydroxyl and methoxy groups, respectively, although an attack on the methyl group in MTBE may also take place. Despite obvious geometric obstruction, the nucleophilic attack on tertiary carbon atom is the most effective, followed by secondary and finally by the primary atom, as one can see from the present results. This is to be explained by greater charge localisation on tertiary and secondary carbon atoms: tertiary carbon's electron cloud is pulled to oxygen atom on one hand and to three comparatively electronegative methyl groups on the other hand. The secondary carbon atom is less affected by methyl groups, and the C-atoms in 2-EE are least affected.

The difference observed in the behaviour of S-TiO<sub>2</sub> and B-TiO<sub>2</sub> in PCO of  $p$ -toluidine and phenol may be explained by the different nature of functional groups attached to the aromatic ring: the PCO is known to proceed first through the oxidation of functional groups followed by the ring rupture, which is harder than the first step. In  $p$ -toluidine amino and methyl groups are both less electronegative than hydroxyl group of phenol. Also, it is far easier to oxidize amino or methyl group than the hydroxyl one, as the latter process means in fact breaking the aromatic ring.

The overall performance of S-TiO<sub>2</sub> is slightly better than that of B-TiO<sub>2</sub>, however, when the dependence of PCO efficiency on admixture concentration is examined, the trends observed with oxygenated hydrocarbons are similar. Also, with both catalyst types the best performance was observed in acidic media, despite the fact that PCO of the substances under scope appears to proceed mainly through radical reactions, which should be favoured by basic media. The only exception in terms of pH is  $p$ -toluidine with S-containing titania: the best performance was in alkaline conditions, and the efficiency was higher with B-containing titania. This may be explained by the fact that S-TiO<sub>2</sub> surface had acidic reaction, while B-TiO<sub>2</sub> ones had alkaline; thus, pH of the solutions each time shifted towards neutral reaction during PCO experiments with  $p$ -toluidine.

### 4. Conclusions

Aqueous photocatalytic oxidation (PCO) of methyl-*tert*-butyl ether (MTBE), *tert*-butyl alcohol (TBA), 2-ethoxy ethanol (2-EE), *i*-propanol,  $p$ -toluidine and phenol was undertaken using visible light-sensitive sulphur- and boron-containing titania. Those photocatalysts have proven to be effective against MTBE, TBA and *i*-propanol, with respective PCO efficiencies under visible light exceeding those of commercial photocatalyst Degussa P25 under UV. The performance of S- and B-TiO<sub>2</sub> with  $p$ -toluidine was less efficient but still comparable to that of Degussa P25. In case of 2-EE and phenol, however, the performance of both photocatalyst types was clearly insufficient.

### Acknowledgements

The authors would like to thank the team of Prof. Dr.-Ing. Joachim Deubener, Division of Glass and Glass Technology, Institute of Nonmetallic Materials of the Technical University of Clausthal and especially Dr. Anna Moiseev for providing XRD measurements, Mr. Andrew S. Cavanaugh, the University of Colorado at Boulder, for providing XPS measurements, and Dr. Mai Uibu, the Laboratory of Inorganic Materials of Tallinn University of Technology, for providing specific surface area measurements of the catalysts. The authors would also like to thank Estonian Science Foundation (Grant G7541) and United States Civilian Research and Development

Foundation (Grant US16062) for the financial support of the research.

## References

- [1] C.K. Yeh, J.T. Novak, *Water Environ. Res.* 66 (1994) 744–752.
- [2] P. Johnson, *Environ. Sci. Technol.* 32 (1998) 276–281.
- [3] A. Safarzadeh-Amiri, *Water Res.* 35 (2001) 3706–3714.
- [4] X.R. Xu, Z.X. Zhao, X.Y. Li, J.P. Gu, *Chemosphere* 55 (2004) 73–79.
- [5] K.K. Papok, E.G. Semenidov, *Motor, Jet and Rocket Fuels (Motornye, reaktivnye i raketnye topliva)*, Gostoptehizdat, Moscow, 1962 (in Russian).
- [6] I. Schmeltz, D. Hoffmann, *Chem. Rev.* 77 (1977) 295–311.
- [7] S. Preis, M. Krichevskaya, Y. Terentyeva, A. Moiseev, J. Kallas, *J. Adv. Oxidation Technol.* 5 (2002) 77–84.
- [8] A. Kahru, A. Maloverjan, H. Sillak, L. Pollumaa, *Environ. Sci. Pol. Res.* 1 (2002) 27–33.
- [9] C.D. Church, J.F. Pankow, P.G. Tratnyek, *Environ. Toxicol. Chem.* 18 (1999) 2789–2796.
- [10] D. Klauson, E. Portjanskaja, S. Preis, *Environ. Chem. Lett.* 6 (2008) 35–39.
- [11] S.J. Kirkpatrick, *Dent. Mater.* 21 (2005) 21–26.
- [12] Royal Philips. Available from: <http://www.prismaecat.lighting.philips.com/FredhopperPDFWebServiceInter/docts/f38f1cfb-c971-4d99-87eb-c718c1020c4b/product.pdf>.
- [13] M. Krichevskaya, A. Kachina, T. Malygina, S. Preis, J. Kallas, *Int. J. Photoenergy* 5 (2003) 81–86.
- [14] M. Raileanu, M. Crisan, N. Dragan, D. Crisan, A. Galtayries, A. Braileanu, A. Ianculescu, V.S. Teodorescu, I. Nitoi, M. Anastasescu, *J. Sol–Gel Sci. Technol.* 51 (2009) 315–329.
- [15] S.U.M. Khan, M. Al-shahry, W.B. Ingler Jr., *Science* 297 (2002) 2243–2244.
- [16] Z. Liu, D.D. Sun, P. Guo, J.O. Leckie, *Chem. Eur. J.* 13 (2007) 1851–1855.
- [17] D. Klauson, S. Preis, *Environ. Technol.* 7 (2005) 175–180.

## **Article II:**

Klauson D., Pilnik-Sudareva J. Pronina N, Budarnaja O., Krichevskaya M., Käkinen A., Jugansos K., Preis S., Aqueous photocatalytic oxidation of prednisolone. *Central European Journal of Chemistry*, 2013, 11 (10), pp. 1620-1633, doi: 10.2478/ s11532-013-0290-8



## Aqueous photocatalytic oxidation of prednisolone

## Research Article

Deniss Klauson<sup>1\*</sup>, Jana Pilnik-Sudareva<sup>1</sup>, Natalja Pronina<sup>1</sup>,  
Olga Budarnaja<sup>1</sup>, Marina Krichevskaya<sup>1</sup>, Aleksandr Käkinen<sup>2,3</sup>,  
Katre Juganson<sup>2,4</sup>, Sergei Preis<sup>5</sup>

<sup>1</sup>Department of Chemical Engineering,  
Tallinn University of Technology, 19086 Tallinn, Estonia

<sup>2</sup>Laboratory of Environmental Toxicology,  
National Institute of Chemical Physics and Biophysics,  
12618 Tallinn, Estonia

<sup>3</sup>Department of Chemical and Materials Technology,  
Tallinn University of Technology, 19086 Tallinn, Estonia

<sup>4</sup>Department of Chemistry,  
Tallinn University of Technology, 19086 Tallinn, Estonia

<sup>5</sup>LUT Chemistry, Lappeenranta University of Technology,  
P. O. Box 20, 53851 Lappeenranta, Finland

Received 2 April 2013; Accepted 16 May 2013

**Abstract:** The research into the aqueous photocatalytic oxidation of the anti-inflammatory drug prednisolone was undertaken with P25 titanium dioxide (Evonik) and visible light-sensitive sol-gel synthesized titania-based photocatalysts containing carbon, sulphur, and iron. Possible prednisolone photocatalytic oxidation reaction pathways were proposed based on a number of oxidation by-products determined in the present study. The prednisolone adsorption properties, effects of initial prednisolone concentration, pH, usual wastewater matrix admixtures, like carbamide and sucrose, were studied. The nontoxicity of doped catalysts towards *Tetrahymena thermophila*, a ciliate protozoa present in the activated sludge, indicated their lower oxidative ability compared to P25, but also implied their potential application in pre-treatment of toxic hazardous materials under VIS or solar radiation before the biological degradation stage.

**Keywords:** Photocatalysis • Corticosteroid • Doped titania • Oxidation pathway •  $\text{TiO}_2$   
© Versita Sp. z o.o.

## 1. Introduction

The occurrence of pharmaceuticals as environmental contaminants is reported for ground water, surface water as well as for sludge, soil and sediment samples [1]. Pharmaceuticals get into the environment from disposal of incompletely metabolized and unused drugs, solid waste landfills and wastes of animal feedlots. The wide range of pharmacological properties put hormonal corticosteroids, including prednisolone, among the most used drugs in the world [2]. These are able to affect aquatic organisms in the smallest concentrations [3]. Toxic effects of corticosteroids on aquatic organisms

are exhibited as inhibition of locomotion, aggressive behaviour, immunological responses and altered reproductive cycles [1,4].

Widely present in the influents of the wastewater treatment plants, pharmaceuticals, including steroids, are often incompletely removed by the secondary wastewater and excess sludge treatment, including aerobic oxidation [1], and methane digestion of sediments [4]. As a result, frequent occurrence of pharmaceuticals in the aquatic environment as well as in the drinking water has raised a concern about their potential impact on environmental and public health. Various treatment technologies have been evaluated for pharmaceutical

\* E-mail: deniss.klauson@ttu.ee

removal in recent years, including application of ozone and ozone/hydrogen peroxide, and membrane filtration [5]. Ozonation of pharmaceuticals in low concentrations, however, requires long treatment time and, thus, high doses of expensive ozone are needed doses of expensive ozone are needed [6]. Even more expensive membrane filtration creates retentate with elevated pollutant concentrations requiring further handling [7].

Concentrations of prednisolone present in natural aquifers are reported to be in  $\text{ng L}^{-1}$  scale [5], however, the content in sludges may reach up to  $200 \mu\text{g kg}^{-1}$  [8]. In this study, higher concentrations of prednisolone were used in order to reliably determine its degradability by photocatalytic oxidation, and its degradation by-products. Regularities of prednisolone degradation at elevated concentrations could be extrapolated to lower concentrations, since photocatalytic oxidation has been shown to be kinetically controlled at lower pollutant concentrations [9]. Major physico-chemical properties of prednisolone are summarised in Table 1.

Photocatalytic oxidation is based on the action of positively charged holes on the illuminated surface of semiconductor, most often  $\text{TiO}_2$ . Water molecules decompose on the holes forming hydroxyl radicals [15]; the hole, having even higher oxidation potential than the OH-radical [16], can also directly degrade the pollutants adsorbed on the surface of the photocatalyst, making adsorption often important in photocatalytic oxidation. The ratio of radical to hole oxidation depends on the adsorptive and reactive properties of pollutants [17–19], reflected also in the nature of oxidation products. However, titania photocatalysts can use only UV fraction (4%) of solar radiation due to the high band gap energy [20]. Hence, sensitising  $\text{TiO}_2$  to visible light enables to widen the utilised solar spectrum. The sensitisation could be achieved by doping  $\text{TiO}_2$  with various elements reducing the band-gap [21–23] for excitation of electrons by lower energy photons. However, the authors found earlier that the doped titania photocatalysts may oxidise only selected pollutants, such as methyl-*tert*-butyl ether, *tert*-butyl alcohol, *i*-propanol, *p*-toluidine, amoxicillin, but not phenol, humic substances, 2-ethoxy ethanol and ethylene glycol [9,24,25]. This can be explained by the smaller redox potential and, possibly, faster electron-hole recombination [26]. The reduced redox potential of new catalytic materials may still be high enough to produce hydroxyl radicals, although some substances may escape oxidation due to their susceptibility to hole oxidation only.

The authors failed to find any information in the scientific literature considering photocatalytic oxidation of corticosteroids, including prednisolone. The study on feasibility of prednisolone photocatalytic

**Table 1.** Physico-chemical properties of prednisolone.

IUPAC name	(11 $\beta$ )-11,17,21-trihydroxypregna-1,4-diene-3,20-dione
Molecular mass	360.44
Melting point	235°C, with partial decomposition [10]
Octanol/water partition coefficient	$\log K_{ow} = 1.62$ [11]
Solubility in water	223 mg L <sup>-1</sup> at 25°C [12]
Solubility in organic solvents	1 g / 30 g ethanol, 1 g / 180 mL chloroform, 1 g / 50 mL acetone [13]
Vapour pressure	$1.18 \times 10^{-3}$ mm Hg at 25°C (estimate) [14]
Henry's law constant	$2.71 \times 10^{-9}$ at 25°C (estimate) [14]

oxidation, also in presence of co-pollutants, with the elucidation of its oxidation pathways was one of the objectives of the present research. Another objective was characterisation and study of visible light active photocatalysts testing their performance towards the degradation of prednisolone. The applicability of doped photocatalysts under visible or solar irradiation as the pre-treatment stage before biological oxidation, *i.e.*, the toxicity of the catalysts, not considered before was also studied.

## 2. Materials and methods

### 2.1. Experimental setup and procedures

Two 200-mL thermostated ( $20 \pm 1^\circ\text{C}$ ) batch reactors with inner diameter of 100 mm, irradiated plane surface  $40 \text{ m}^2 \text{ m}^{-3}$ , with magnetic stirrers, were used: the one used for the photocatalytic oxidation further designated as “active” and the other containing no photocatalyst further designated as “reference”, *i.e.*, blank experiments, exposed to the identical conditions. The samples from both reactors were compared to avoid errors caused by water evaporation. A UV-light source, Philips Actinic BL low pressure luminescent mercury UV-lamp (15 W) with maximum emission around 365 nm was positioned horizontally over the reactors, providing the irradiance of  $1.5 \text{ mW cm}^{-2}$  at their surface, measured by the radiometer Micropulse MP100. The illuminance of the daylight fluorescent lamp (Phillips TL-D 15W/33-640) was measured using TES 1332 luxmeter reaching  $3,700 \text{ lx}$  ( $1 \text{ l m m}^{-2}$ ), which corresponds to the irradiance of  $0.6 \text{ mW cm}^{-2}$  [27]. For Philips TLD lamp, the amount of UV-irradiation was measured at 254 and 365 nm using the above mentioned Micropulse radiometer and total amount of UV was measured with Ocean Optics USB2000+UV-VIS-ES spectrometer. Only negligible fraction of UV around 365–400 nm was observed, which is in accordance with the data provided by the Philips TLD manufacturer. Thus, when using Philips TLD lamp,

any noticeable action of the photocatalyst is clearly due to the activity of the catalyst in visible light region. The prednisolone photocatalytic oxidation experiments were additionally conducted outdoors using natural solar radiation; the irradiance was measured by luxmeter approximating  $16 \text{ mW cm}^{-2}$ .

$\text{TiO}_2$  was used as a slurry of  $1 \text{ g L}^{-1}$ . The prednisolone (Sigma-Aldrich) concentration varied from 10 to  $100 \text{ mg L}^{-1}$ . The pH was adjusted with sulphuric acid (4 N) or sodium hydroxide (15%) and the impact of pH was studied in the range from 3 to 10. The pH changes were monitored during the runs, pH was not kept constant, and its changes were monitored. The treatment times chosen according to pre-screening results were 2 h under artificial irradiation, and 1 h under natural solar irradiation. Such treatment conditions were chosen in order to achieve at least 50% reduction of the initial prednisolone concentration, as complete conversion may require greatly increased treatment time, and will not give additional information on the possibility of prednisolone degradation by photocatalysis. Experiments were carried out three times under identical conditions with the average deviations under 5%.

Carbamide and sucrose, used as model co-pollutants in prednisolone photocatalytic oxidation experiment in order to simulate municipal wastewater, were used in the amounts of 75 and  $50 \text{ mg L}^{-1}$ , respectively. These concentrations broadly reflect normal values in domestic sewage [28] and are in agreement with previously conducted experiments [29]. These additives simulated wastewater with chemical oxygen demand (COD) of  $145 \text{ mg O L}^{-1}$  and  $35 \text{ mg L}^{-1}$  of total nitrogen. *tert*-Butyl alcohol (TBA) as a radical scavenger was added to the treated prednisolone solution at molar ratio of [prednisolone]:[TBA] = 1:2 in order to determine the dominance of reactions taking place on titanium dioxide surface vs. reactions in the solution in the vicinity of the surface in prednisolone photocatalytic oxidation. These experiments were carried out at near-neutral pH with the prednisolone concentration of  $10 \text{ mg L}^{-1}$ .

Adsorption experiments were carried out in thermostated flasks with magnetic stirrers at  $20 \pm 1^\circ\text{C}$ . The amount of prednisolone adsorbed on titanium dioxide was derived from the mass balance by determining the concentration of the dissolved substance before adsorption and after the equilibrium was reached in 30 min, determined experimentally. With P25 titanium dioxide (Evonik), the adsorption experiments were performed in the prednisolone concentration range of 10 to  $100 \text{ mg L}^{-1}$ . With doped titania samples, adsorption of prednisolone was studied at  $25 \text{ mg L}^{-1}$ , in order to compare the photocatalysts' adsorption capabilities.

## 2.2. Synthesis of photocatalysts

Specimens of carbon-containing titania were obtained by hydrolysing tetrabutyl orthotitanate at room temperature with unadjusted pH around 5.5 to 6.0, followed by thermal treatment in a range between 200 and  $400^\circ\text{C}$ . Three sulphur-containing photocatalysts used in this study were prepared by hydrolysis of tetrabutyl orthotitanate with addition of a pre-calculated amount of 0.1 N sodium thiosulphate as a sulphur source, followed by calcination at  $400^\circ\text{C}$ . Three iron-containing titania catalysts with calculated iron content from 0.4 to 1.3 at.% were prepared by pulverisation of 75 mL of tetrabutyl orthotitanate into 1 L of pre-sonicated  $\text{Fe}_2\text{O}_3$  suspensions of various concentrations (from 0.1 to  $0.5 \text{ g L}^{-1}$ ). The hydrolysis was followed by sonication, drying and calcination at  $200^\circ\text{C}$ . After 4-h calcination, all the catalysts were washed with hot, 70 to  $80^\circ\text{C}$ , distilled water applied in a sequence of fifteen rinsing rounds, making about 1 L per 1 g of catalyst in total, to clean the catalyst from water-soluble compounds. In order to determine possible leaching of the dopants, the catalysts were dispersed in distilled water and subjected to UV-irradiation for overnight. After the catalyst separation, the possible content of dopants was analysed as follows: carbon species in the water were analysed for chemical oxygen demand (COD, see Section 2.3), the contents of nitrate and sulphate were analysed using Metrohm 761 Compact IC ion chromatograph; ammonia content was analysed photometrically by a modified version of standard phenate method [30]. The iron ions leakage was analysed using modified version of standard phenantrolin method [30]. No leakage of any dopant was detected within the accuracy of the methods used.

## 2.3. Analytical procedures

High-performance liquid chromatography combined with diode array detector and mass-spectrometer, (HPLC-PDA-MS, Shimadzu LC-MS 2020) was used for the determination of prednisolone concentration. Phenomenex Gemini-NX 5u C18 110A  $150 \times 2.0 \text{ mm}$  column, inner diameter  $1.7 \mu\text{m}$ , was used with two eluents, 0.1% acetic acid aqueous solution (eluent A), and acetonitrile (eluent B), with total eluents flow of  $0.3 \text{ mL min}^{-1}$ . The starting concentration of eluent B was 5%, increased to 48.5% by 23 minutes with linear gradient, held at that concentration for two minutes, and then decreased to 9.5% by 30 minutes, out of 30 minute analysis. Mass spectra were acquired in full scan mode, MS operated in positive ionisation mode with interface voltage of 4.5 kV, and detector voltage of 3.3 kV. Diode array detector was set to scan samples at 190 – 800 nm. The instrument was operated and the results obtained with MS and PDA detectors were handled using



Shimadzu LabSolutions software. The by-products of prednisolone photocatalytic oxidation were determined using the described HPLC-MS method, at different initial pH values (3.0, 6.8 and 10.0).

Chemical oxygen demand (COD) was determined by a standard dichromate method [30], using HACH kit LCK 314 (15 to 150 mg O L<sup>-1</sup>). This parameter was used to evaluate the oxidation degree of prednisolone, reflecting, unlike total organic carbon (TOC), not only the prednisolone mineralization, but also the changes in oxygen incorporation to organic matter during photocatalytic oxidation.

The crystallinity of carbon-containing titania was analysed using D5000 Kristalloflex, Siemens X-ray diffraction spectroscopy (XRD), with composition calculated by Topas R software, and sulphur- and iron-containing specimen were analysed with Scintag PAD V XRD (Cu K $\alpha$  irradiation source in both cases). The specific surface area (SSA: BET and Langmuir adsorption) and the pore volume were measured by the adsorption of nitrogen using KELVIN 1042 sorptometer.

The isoelectric points (IEP) of pure and sulfur-, carbon and iron-doped titanium dioxide suspensions were determined by potentiometric titration using a Zetasizer Nano-ZS equipped with an MPT-2 autotitrator and vacuum degasser (Malvern Instruments, UK). The technique (Laser Doppler Micro-electrophoresis) is based on the electrophoretic light-scattering that measures migration rate of dispersed particles under the influence of an electric field. Zeta,  $\zeta$ , potential was calculated by Malvern software using Smoluchowski equation. Suspensions of 1 g L<sup>-1</sup> TiO<sub>2</sub> (P25) and doped TiO<sub>2</sub> were prepared in deionized water, sonicated for 30 min (70 W, 42 kHz, Branson 1510, Branson Ultrasonic Corporation, USA) and diluted to 100 mg L<sup>-1</sup> in deionized water. Automatic titrations were performed in 10 ml as an initial sample volume, from pH 11 to pH 1.5 with 0.25 M NaOH and 0.25 M HCl. pH increment was 0.5 and target pH tolerance was 0.2. Each  $\zeta$ -potential value recorded was the average of 10 measurements.

Protozoan culture (*Tetrahymena thermophila* strain BIII) used for toxicity analysis was cultivated as described previously [31]. The cells were harvested during the exponential growth phase (cell density 5 × 10<sup>5</sup> cells mL<sup>-1</sup>) by centrifugation at 300 g for 5 min at 4°C and washed twice with MilliQ water. In order to evaluate cell density the cells were counted in haemocytometer (Neubauer Improved, bright line; Germany) after immobilising the cells in 5% formalin. To conduct the toxicity test 100  $\mu$ L of the photocatalyst in MilliQ water was pipetted into the wells of 96-well polystyrene plates (Falcon) and 100  $\mu$ L of *T. thermophila* cells in MilliQ water was added to the wells. The final photocatalysts concentrations in the test

were 50, 500 and 1000 mg L<sup>-1</sup>, each concentration was tested in three replicates and the final cell density in the test was 5 × 10<sup>5</sup> cells mL<sup>-1</sup>. The protozoan culture in MilliQ water and photocatalysts in MilliQ water were used as controls. The exposure of the protozoa to photocatalysts was performed comparatively under illumination and dark conditions for 2 and 24 h at 30°C with moderate shaking. The plates were illuminated from below using Philips TL-D 38 W aquarelle fluorescent tubes. The pH of *T. thermophila* control culture in MilliQ water was 6.8 and did not change significantly upon the addition of the photocatalysts. The pH remained unchanged during the 24-hour toxicity test. The viability of the cells was evaluated by measuring the ATP content using the luciferin-luciferase method as described previously [31] with slight modifications. The EC<sub>50</sub> (effective concentration leading to a 50% cell death) values were calculated from concentration-effect curves with REGTOX software for Microsoft Excel™ [32].

## 2.4. Photocatalytic oxidation efficiency

To express the results of prednisolone photocatalytic oxidation, the photocatalytic oxidation efficiency  $E$ , defined as the decrease in the pollutant amount divided by the amount of energy reaching the treated sample, was calculated according to Eq. 1 [33]:

$$E = \frac{\Delta C \times V \times 1000}{I \times s \times t} \quad (1)$$

where  $E$  – photocatalytic oxidation efficiency, mg W<sup>-1</sup> h<sup>-1</sup>;  $\Delta c$  – the decrease in the pollutant's concentration, mg L<sup>-1</sup>, or COD, mg O L<sup>-1</sup>;  $V$  – the volume of the sample to be treated, L;  $I$  – irradiance, mW cm<sup>-2</sup>;  $s$  – irradiated area, cm<sup>2</sup>;  $t$  – treatment time, h.

## 3. Results and discussion

### 3.1. Dark adsorption experiments

The most efficient prednisolone (initial concentration 25 mg L<sup>-1</sup>) adsorption on P25 was observed at near-neutral pH, followed by acidic media and being negligible in basic solutions as shown in Fig. 1a. This may be explained by charging of both TiO<sub>2</sub> surface and prednisolone molecules in acidic (minor positive charging of prednisolone) and alkaline (major negative charging of prednisolone) media, that results in electrostatic repulsion of prednisolone molecules in both cases; however, this is strongly pronounced only in alkaline media. Since no significant charging of TiO<sub>2</sub> occurs in neutral media, prednisolone adsorption improves. A similar trend was observed with all other catalysts studied.



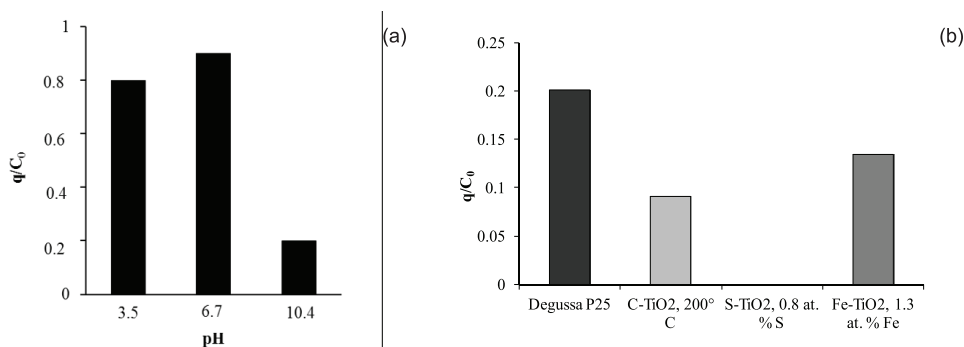


**Figure 1.** Dependence of prednisolone (PNL) adsorption ( $\text{mg PNL g}^{-1} \text{TiO}_2$  divided by  $\text{mg PNL L}^{-1}$ ) on pH for P25 (a) and for  $\text{TiO}_2$ -based catalysts (b) at prednisolone concentration  $25 \text{ mg L}^{-1}$  and photocatalyst concentration  $1 \text{ g L}^{-1}$  at pH 6.7. Sulphur-doped  $\text{TiO}_2$  showed negligible adsorption.

The prednisolone dark adsorption on the P25 in neutral media ranged from  $0.8$  to  $15 \text{ mg g}^{-1}$  at the initial prednisolone concentration from  $10$  to  $100 \text{ mg L}^{-1}$  respectively. The adsorption experimental data fits well to the Freundlich equation (Eq. 2,  $R^2=0.9675$ ):

$$q_{Fr} = A \times C^m, \quad (2)$$

where  $q$  – adsorption,  $\text{mmol g}^{-1}$ ;  $A$  and  $m$  – empirical constants, giving  $A = 0.262$  and  $m = 1.25$ .

Fig. 1b shows the adsorption results for prednisolone in  $25 \text{ mg L}^{-1}$  solution on three synthesized catalysts, carbon-containing and iron- and sulphur-doped  $\text{TiO}_2$ , compared to undoped P25  $\text{TiO}_2$ , as the decrease of prednisolone normalised adsorption at pH 6.7. The adsorption of prednisolone on the doped catalysts showed that over 10% of initial prednisolone was adsorbed on their surface at best, while up to 20% of prednisolone adsorbed on P25 from the solution with prednisolone initial concentration of  $25 \text{ mg L}^{-1}$ . No prednisolone adsorption was detected on S- $\text{TiO}_2$ , indicating that increased specific surface area of the doped photocatalysts does not necessarily lead to an improved adsorption.

### 3.2. Photocatalytic oxidation experiments with P25 (Evonik)

Similarly to the adsorption pattern, the best photocatalytic oxidation performance was observed at pH 6.7, occurring naturally in the prednisolone solutions, followed closely by acidic media (pH 3), with the least effective performance observed in alkaline solutions (pH 10) (data not shown for the sake of brevity). Such pH dependence was earlier observed with e.g. alcohols [34–36] to which prednisolone is expected to exhibit similar behaviour due to its chemical structure. The

decrease in the photocatalytic oxidation efficiency in alkaline media favourable for the reactions of hydroxyl radicals in the vicinity of photocatalyst surface indicates the minor role that mechanism in photocatalytic oxidation of prednisolone. Since photocatalytic oxidation efficiency under acidic and near-neutral conditions is higher, the prevalence of oxidation of adsorbed prednisolone on the photocatalyst surface, as opposed to previously mentioned mechanism, favoured by alkaline media, is assumed. This assumption finds confirmation in the prednisolone adsorption properties on P25 (see Section 3.1). However, the prevalence of oxidation of molecules adsorbed on the photocatalyst surface may concern only the starting point of prednisolone oxidation. The prednisolone molecule that has lost one or more electrons on titanium dioxide surface may subsequently react both there and with hydroxyl radicals in the solution in the vicinity of the photocatalyst surface.

The efficiency of COD reduction has the same trend as efficiency calculated for prednisolone concentration reduction. However, it yields to the efficiency of prednisolone removal demonstrating slower degradation rate of prednisolone photocatalytic oxidation by-products. The significant difference, for almost 40%, in the efficiency of COD reduction between neutral and acidic media indicates lower reactivity of prednisolone photocatalytic oxidation by-products at lower pH. Thus, it could be assumed that since neutral medium is the most favourable for oxidation of prednisolone by-products, photocatalytic oxidation of by-products necessitates utilizing both mechanisms, while low efficiency in alkaline medium points that adsorption remains the prerequisite of photocatalytic oxidation.

Fig. 2 shows the dependence of photocatalytic oxidation efficiency  $E$  on the prednisolone initial concentration:  $E$  increases with the increased initial

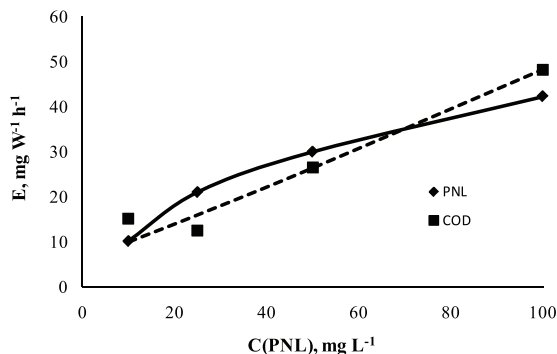


**Figure 2.** The dependence of photocatalytic oxidation efficiency on the prednisolone initial concentration with P25 photocatalyst: pH 6.7, 2 h treatment time, 1 g L<sup>-1</sup> photocatalyst.

prednisolone concentration assuming the description of the photocatalytic oxidation using Langmuir-Hinshelwood (L-H) model of monomolecular surface reaction, followed by the products desorption (Eq. 3). The equation, derived from the experimental data via the  $1/r_0 = f(1/c_0)$  dependence (plot not shown), gives  $k = 0.0044 \text{ mM}^{-1} \text{ min}^{-1}$  and  $K = 11.4 \text{ mM}$  at average square deviation  $R^2 = 0.9999$ , supporting the proposed L-H data fit:

$$r_0 = k \frac{Kc_0}{1 + Kc_0}, \quad (3)$$

where  $r_0$  is the reaction rate,  $\text{mM min}^{-1}$ ;  $k$  – reaction rate constant,  $\text{mM}^{-1} \text{ min}^{-1}$ ;  $K$  – adsorption constant,  $\text{mM}$ ;  $c_0$  – initial prednisolone concentration,  $\text{mM}$ .

The similar efficiencies of prednisolone and COD degradation at neutral pH implies a high degree of mineralization: indeed, at prednisolone concentrations up to  $25 \text{ mg L}^{-1}$ , prednisolone removal was around 90-96% with simultaneous COD decrease over 80% in 2 h of treatment time. At prednisolone concentration of  $100 \text{ mg L}^{-1}$ , the target pollutant and COD removal rates decreased to 57 and 30%, respectively, although the absolute oxidation rates increased. Thus, photocatalytic oxidation is able to degrade both target compound and its degradation by-products reasonably well.

### 3.3. Prednisolone photocatalytic oxidation reaction pathway

A number of organic by-products were determined qualitatively using HPLC coupled with Electrospray Ionization MS (ESI-MS, see Materials and Methods for more detail). The determined products allow to distinguishing four possible prednisolone photocatalytic oxidation pathways (Fig. 3), depending on initial pH of

the treated solution. Two of them (A at pH 3 and B at pH of 6.8 and 10) begin with stepwise oxidation of quinonic ring before finally forming the identified products with  $m/z = 373$  and  $371$ , respectively; from both the product with  $m/z = 359$  is formed. Subsequently, in pathway A the hydroxymethylene group connected to the cyclohexanic ring (leftmost in the scheme) is oxidised stepwise, yielding products with  $m/z = 357$  and  $327$ . In pathway B, the abovementioned cyclohexanic ring undergoes direct cleavage, leading to the formation of product with  $m/z = 345$ . Pathway C, present at natural pH of prednisolone, begins with the oxidation of cyclopentanic part of the molecule, leading to the formation of products with  $m/z = 323$  and  $277$ , depending on whether the cyclohexanic part of the molecule adjacent to cyclopentanic is cleaved or remains intact; subsequent oxidation of both fragments leads to the formation of product with  $m/z = 253$ . In alkaline media, product with  $m/z = 281$  was identified, suggesting a reaction pathway similar to C. Finally, pathway D, occurring at both natural and alkaline pH shows simultaneous oxidation of prednisolone molecule from both sides. The relative abundance of the reaction pathways is explained by the different prednisolone adsorption mechanisms taking place simultaneously: depending on which part of the prednisolone molecule is adsorbed first (*i.e.*, quinonic cycle, or one of hydroxyl groups), the photocatalytic oxidation follows one of the oxidation pathways proposed. At acidic pH prednisolone, being a weak base as an alcohol, may be slightly protonated and thus positively charged, leading to electrostatic repulsion from the likewise positively charged titanium dioxide surface, whereas the quinonic group oxygen should be less affected by this, resulting in the domination of pathway A, which originates from prednisolone adsorption via quinonic group. At natural pH of prednisolone and at alkaline pH, electrostatic

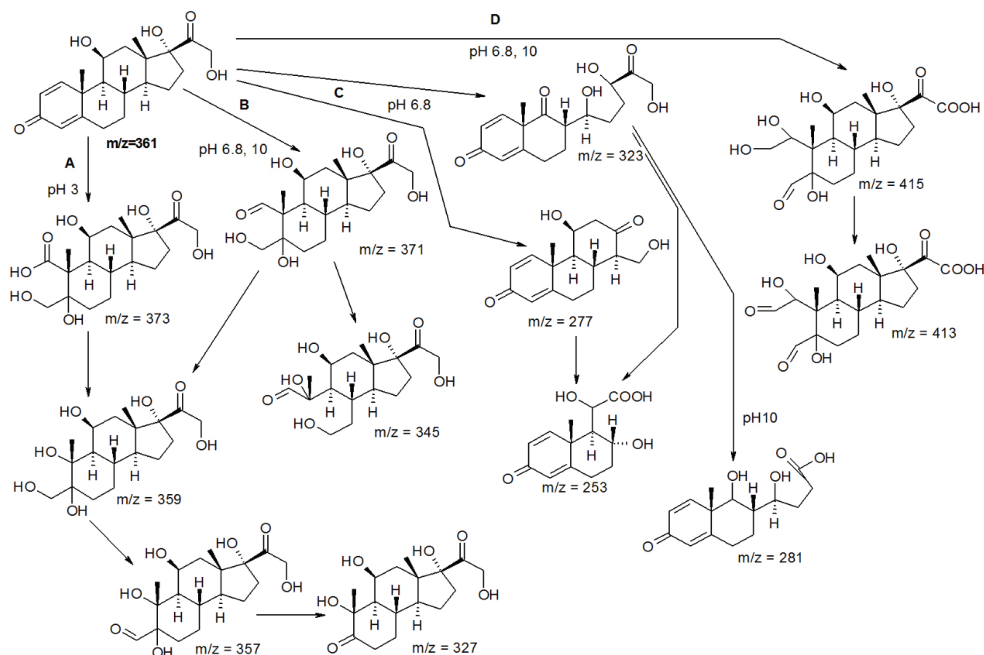


**Figure 3.** Proposed prednisolone photocatalytic oxidation reaction pathway.

effects appear to be far less pronounced, resulting in a greater variety of oxidation products forming pathways B to D.

### 3.4. The influence of admixtures on prednisolone photocatalytic oxidation

The addition of *tert-butyl alcohol* did not exhibit any influence on the efficiency of prednisolone oxidation. This supports the hypothesis of the minor role of radical reactions taking place in the vicinity of the photocatalyst surface played in prednisolone photocatalytic oxidation when compared to oxidation of adsorbed prednisolone molecules on the surface of  $\text{TiO}_2$ .

The addition of *carbamide* showed no negative influence on the photocatalytic oxidation of prednisolone (see Fig. 4). This can be explained by the insignificant carbamide adsorption on the surface of titanium dioxide [29], that, in turn, means practically unhindered prednisolone adsorption, leaving overall photocatalytic oxidation performance largely unaffected. No noticeable carbamide oxidation was observed during the course of the experiments.

The addition of *sucrose* hindered the photocatalytic oxidation of prednisolone noticeably: around 20% of the initial concentration remained unoxidized, as opposed to complete prednisolone elimination without sucrose

under identical experimental conditions (Fig. 4). This can be explained by the competitive adsorption of sucrose and prednisolone on the catalyst surface: adsorbed sucrose molecules hinder prednisolone adsorption, leading to a decrease in prednisolone photocatalytic oxidation rate. When carbamide and sucrose were added to prednisolone solution simultaneously, the decrease of prednisolone degradation rate was identical to that observed upon sucrose admixture (Fig. 4), with no synergism clearly observed.

These results show the ability of prednisolone to successfully undergo oxidation upon the addition of wastewater constituents, establishing the practicability of photocatalysis against corticosteroids.

### 3.5. Characterization of photocatalytic materials

Table 2 shows the characteristics of carbon-containing photocatalysts varying with calcination temperature. Within the calcination temperature range applied, the catalysts were composed of mainly anatase (>70%) and brookite (>20%). X-ray diffraction curves for C- $\text{TiO}_2$  specimen can be seen in Fig. 5a; for anatase, (1 0 1), (0 0 4) and (2 0 0) peaks are the most pronounced, with (1 0 1) being the most distinctive, and for brookite, (1 2 0), (1 2 1), and (2 3 1) peaks were identified. Although no systematic changes in the catalysts' phase

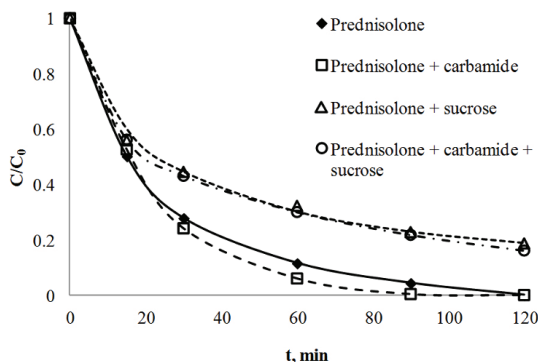


**Figure 4.** The decrease of prednisolone (10 mg L<sup>-1</sup>) concentration in the presence of carbamide (75 mg L<sup>-1</sup>) and sucrose (50 mg L<sup>-1</sup>): pH 6.7, 2 h treatment time, 1 g L<sup>-1</sup> photocatalyst.

**Table 2.** Physical characteristics of carbon-containing photocatalysts dependent on the calcination temperature

T(calcination), °C	Phase composition, %			S(BET), m <sup>2</sup> g <sup>-1</sup>	S(Langmuir), m <sup>2</sup> g <sup>-1</sup>	Micropore area, m <sup>2</sup> g <sup>-1</sup>	Micropore volume, mm <sup>3</sup> g <sup>-1</sup>
	Anatase	Brookite	Rutile				
200	71.9	28.1	-	202	279	0	0
300	74.7	25.3	-	157	216	0.42	0.15
400	78.1	21.9	-	106	145	4.12	1.54

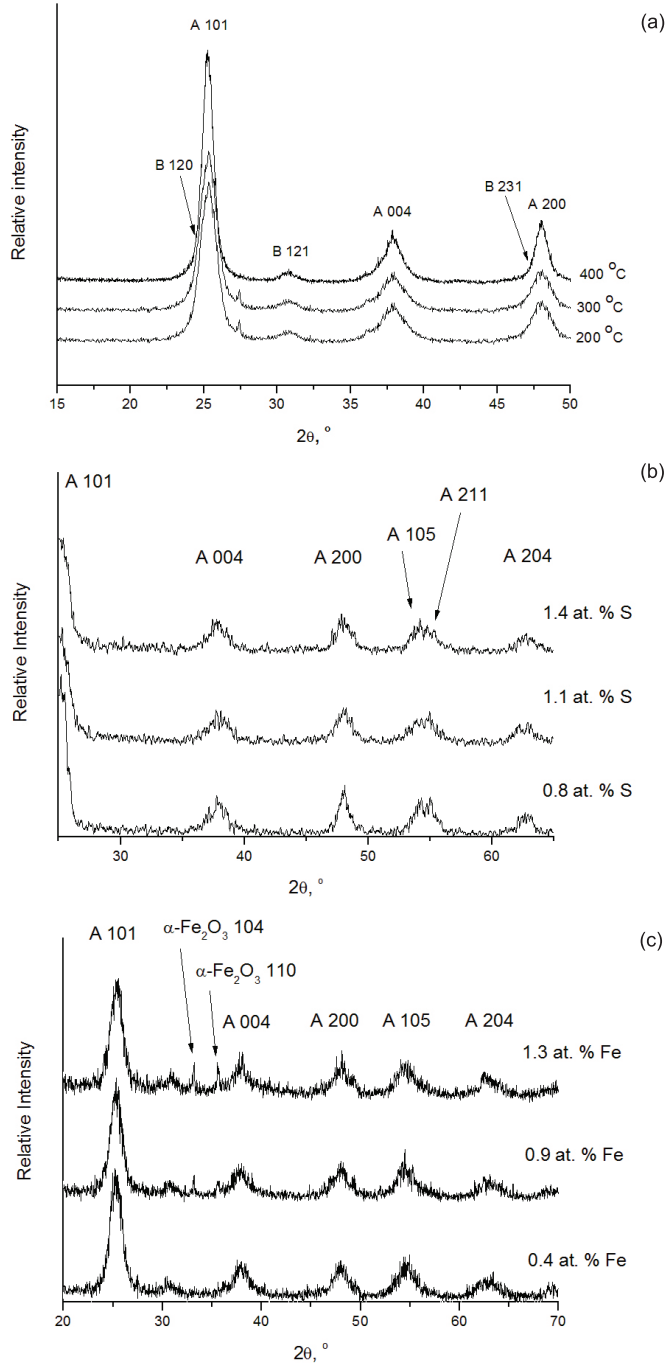
**Table 3.** Main characteristics of sulphur-doped TiO<sub>2</sub> photocatalysts (calcination temperature 400°C).

at.% S	SSA(BET), m <sup>2</sup> g <sup>-1</sup>	SSA(Langmuir), m <sup>2</sup> g <sup>-1</sup>	Micropore area, m <sup>2</sup> g <sup>-1</sup>	Micropore volume, mm <sup>3</sup> g <sup>-1</sup>
0.8	93.8	126.7	1.7	0.6
1.1	129.0	176.0	0	0
1.4	170.7	234.0	0	0

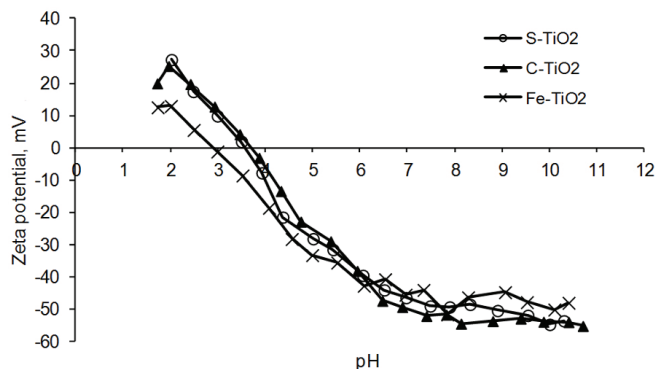
composition were observed, specific surface area (SSA) clearly decreased with the increased C-TiO<sub>2</sub> calcination temperature from 200 to 400°C, whereas micropore area and volume increased. However, the previous results show that the surface area and pore volume of the modified titania photocatalysts do not always correlate with the adsorbed pollutants amount and the photocatalytic oxidation performance [9,24]. Thus, the surface data yield by their importance to the adsorption and photocatalytic oxidation efficiency [9].

Table 3 shows the composition and surface properties of S-TiO<sub>2</sub> photocatalysts after calcinations at 400°C. Judging from the XRD analysis (Fig. 5b), anatase is the main crystallographic form, with (1 0 1), (0 0 4), (2 0 0), (1 0 5), (2 1 1) and (2 0 4) peaks identified; (1 0 1) peak has the highest intensity. Sulphur-containing catalysts are described in more detail in previous paper from the authors [25].

The calculated amount of iron in the Fe-TiO<sub>2</sub> catalysts calcinated at 400°C was 0.4, 0.9 and 1.3 at.%. XRD data for iron-containing titanium dioxide specimen used in this study is provided in Fig. 5c. All specimen exhibited (1 0 1), (0 0 4), (2 0 0), (1 0 5) and (2 0 4) anatase peaks, with (1 0 1) being the most intensive here as well. It can be seen that at 0.4 at.% Fe the catalyst is pure anatase, whereas two other specimen with higher iron content show two well-pronounced α-Fe<sub>2</sub>O<sub>3</sub> peaks – (1 0 4) and (1 1 0), with their relative intensity increasing with increasing iron content. This suggests that at elevated dopant concentrations a portion of iron remains unincorporated into titanium dioxide crystal lattice in these catalysts, as no iron species-associated peaks were observed at 0.4 at.% Fe, where at least partial incorporation is supposed lowering the measurable iron quantities to undetectable limits.



**Figure 5.** X-ray diffraction curves for carbon- (a), sulphur- (b) and iron-containing titanium dioxide (c); A – anatase, B - brookite.



**Figure 6.** Zeta potential values of C- (200°C), S- (0.8 at.%) and Fe- (0.4 at.%) doped titanium dioxide suspensions (100 mg L<sup>-1</sup>) as a function of pH.

Potentiometric titration curves of 100 mg L<sup>-1</sup> P25, S-TiO<sub>2</sub> (0.8 at.%), C-TiO<sub>2</sub> (200°C) and Fe-TiO<sub>2</sub> (0.4 at.%) suspensions are presented in Fig. 6. The doping agents decreased the values of isoelectric point of titanium dioxide suspension: C-TiO<sub>2</sub> IEP = 3.69 ± 0.12, S-TiO<sub>2</sub> IEP = 3.59 ± 0.04 and Fe-TiO<sub>2</sub> IEP = 2.90 ± 0.12; for comparison, IEP of P25 titanium dioxide has been reported to be around 6 [37].

It has been shown previously that P25 was harmful (EC<sub>50</sub> < 100 mg L<sup>-1</sup>) to the “young” and “old” algal cultures [38] and phototoxic to bacteria: concentration of 100 mg TiO<sub>2</sub> L<sup>-1</sup> was lethal to 75% of the *Escherichia coli* population whereas the same concentration of TiO<sub>2</sub> in the dark showed no impact [39]. Thus, biological effects of applied photocatalysts on microorganisms present in the activated sludge process should be considered. Beside bacteria ciliates constitute the second most relevant and abundant community in the activated sludge [40]. *Tetrahymena* are freshwater ciliate protozoa that have been used as model organisms for environmental research for years [41]. Furthermore, *Tetrahymena thermophila* is also present in the activated sludge process [42]. The biological effects of P25 and synthesized TiO<sub>2</sub> photocatalysts on *Tetrahymena thermophila* were evaluated and average calculated EC<sub>50</sub> values are presented in Table 4.

The results indicate that according to the risk phrases for ranking toxicity of chemicals for aquatic organisms (EC Directive 93/67/EEC) the tested photocatalysts could be classified as not harmful to *Tetrahymena thermophila* as all the EC<sub>50</sub> values were above 100 mg L<sup>-1</sup>. Moreover, the EC<sub>50</sub> values of the doped titania photocatalysts exceeded even 1 g L<sup>-1</sup> which is the concentration used in the experiments of photocatalytic degradation of prednisolone. However, the illumination at VIS-range rendered P25 TiO<sub>2</sub> about

two times more toxic compared to the dark conditions. Additionally, compared to P25, doped TiO<sub>2</sub> samples had milder effects on *T. thermophila* viability, indicating the lower redox potential of synthesized catalytic materials evidenced later in the course of photocatalytic oxidation of prednisolone (see Section 3.6).

### 3.6. Photocatalytic oxidation experiments with doped titania

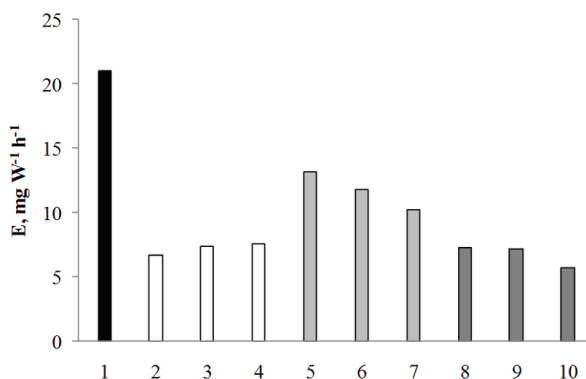
During the course of the experiments the dopants were not washed out of the catalysts, indicate by the sustaining of their catalytic activity in sequential reuse and leaching tests (see Section 2.2). It can be thus clearly stated that the dopants were stably incorporated into the catalysts' crystal lattice.

Negligible quantity of UV emitted by the VIS lamps (see Section 2.1) cannot explain the photocatalytic oxidation performance of the doped catalysts, as it does not correlate with the level of observed photocatalytic efficiency as compared to the results with the UV-irradiated P25. This observation indicates that visible light is responsible for photocatalytic oxidation due to dopant species. The performance of three doped titania catalysts containing carbon, sulphur and iron was tested with prednisolone solutions of 25 mg L<sup>-1</sup> at pH 6.7 under VIS radiation (Fig. 7).

The S-TiO<sub>2</sub> sample with sulphur content of 0.8 at.% showed the best photocatalytic oxidation performance under VIS irradiation reaching 67% of the efficiency of UV-radiated P25 photocatalyst. Iron-doped and carbon-containing TiO<sub>2</sub> had relatively low efficiency. The efficiency of iron-doped TiO<sub>2</sub> increased slightly with iron content achieving the highest value at the iron content 0.3 at.%; nevertheless, the best iron-doped TiO<sub>2</sub> was about three times lower in efficiency than the P25 under UV-light. Similarly, the performance of carbon-containing TiO<sub>2</sub> under VIS light increased slightly with

**Table 4.** Toxicity of the studied photocatalysts to protozoa *Tetrahymena thermophila*. Average  $EC_{50}$  values ( $mg\ L^{-1}$ ) based on the loss of the viability after 2- and 24-h exposure in light and dark are presented.

Photocatalyst	2-h $EC_{50}$ (95% confidence intervals), $mg\ L^{-1}$		24-h $EC_{50}$ (95% confidence intervals), $mg\ L^{-1}$	
	Light	Dark	Light	Dark
<b>P25 (nano-TiO<sub>2</sub>, Evonik)</b>	180 (148-219)	296 (230-430)	294 (220-550)	620 (355-9409)
<b>C-TiO<sub>2</sub> (200°C)</b>	> 1000	> 1000	> 1000	> 1000
<b>S-TiO<sub>2</sub> (0.8 at.%)</b>	> 1000	> 1000	> 1000	> 1000
<b>Fe-TiO<sub>2</sub> (0.4 at.%)</b>	773 (535-1186)	917 (706-2161)	> 1000	> 1000

**Figure 7.** The photocatalytic oxidation efficiency of prednisolone with doped catalysts under VIS irradiation in comparison with the P25 under UV irradiation: 1 – P25 with UV; Fe-TiO<sub>2</sub>: 2 – 0.4 at.% Fe, 3 – 0.9 at.% Fe, 4 – 1.3 at.% Fe; S-TiO<sub>2</sub>: 5 – 0.8 at.% S, 6 – 1.1 at.% S, 7 – 1.4 at.% S; C-TiO<sub>2</sub>: 8 – 200°C, 9 – 300°C, 10 – 400°C; prednisolone concentration 25  $mg\ L^{-1}$  and photocatalyst concentration 1  $g\ L^{-1}$ , initial pH 6.7, treatment time 2 h.

the decrease in catalysts' calcination temperature, the latter is expected to result in higher carbon content.

The differences in behaviour of visible light-sensitive photocatalysts containing different dopants may be explained by different nature of the dopants and the corresponding changes in the catalysts' band gap and redox potential. The comparison of the photocatalytic oxidation and adsorption results obtained with the doped catalysts show a consistence of both photocatalytic oxidation efficiency and adsorption for iron-doped and carbon-containing catalysts. The reason for poor adsorption of prednisolone at S-TiO<sub>2</sub> despite its surface area exceeding the one of P25 remains unknown, especially taking into account the overall similarity of the catalysts' IEP and zeta-potential values at the pH of the experiments. However, sulphur-doped catalysts show the highest photocatalytic oxidation efficiency at no adsorption observed (see Section 3.2). Unlike carbon and iron-containing photocatalysts, S-TiO<sub>2</sub> exhibited strongly acidic properties: solution pH decreased once the catalyst was added to water. Since the catalysts were thoroughly washed upon preparation, and no sulphates leaching was detected, the acidic reaction

should originate from partially bonded sulphate on the catalyst surface and resulting in negative catalyst surface charge due to the sulphates' dissociation. On the other hand, in such conditions the prednisolone molecule may be expected to act as a weak base having its hydroxyl groups partially protonated and the prednisolone molecule or its part charged positively. As a result, the prednisolone molecule may be drawn into close vicinity of the catalyst surface, where it can react with the hydroxyl radicals. Though prednisolone is better adsorbed onto the surface of C- and Fe-TiO<sub>2</sub>, the photocatalytic oxidation efficiency of these catalysts is low. The latter is in agreement with the data reported by Liu *et al.* [26], indicating the redox potential of doped catalysts' holes being lower than that of undoped titania, consequently resulting in reduced photocatalytic oxidation rate.

### 3.7. Solar photocatalytic oxidation experiments

The performance of prednisolone photocatalytic oxidation under solar irradiation was studied with P25 industrial photocatalyst and with sulphur-doped (0.8 at.%) photocatalyst, utilizing the VIS portion of solar



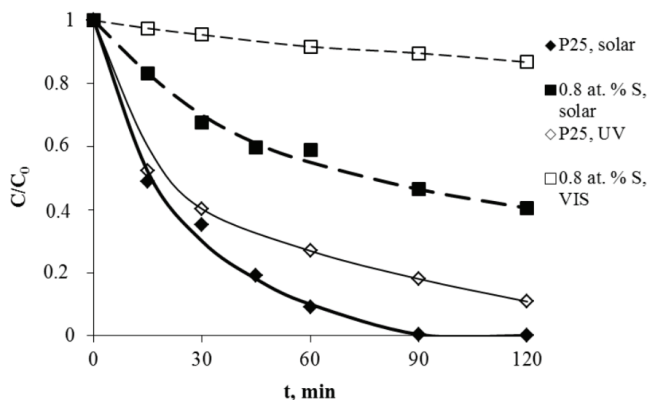


**Figure 8.** The decrease of normalised prednisolone concentration ( $25 \text{ mg L}^{-1}$ ) in solar photocatalytic oxidation experiment compared to the experiments with artificial irradiation,  $1 \text{ g L}^{-1}$  photocatalyst.

light along with UV. The main goal of these experiments was not only convincing that the photocatalysts applied can successfully operate under natural irradiation, but mainly to investigate the changes in their performance under solar light. The results obtained under solar radiation were compared to the ones achieved under artificial UV and VIS (see Section 2.1) (Fig. 8).

Degradation of prednisolone with P25 and sulphur-doped  $\text{TiO}_2$  under solar radiation was expectedly faster than under artificial UV- or VIS-light. However, the improvement of the photocatalytic oxidation rate observed for different catalysts was also different. For example, prednisolone was degraded with P25 for 94% and 73% in 60 min under solar irradiation and artificial UV, respectively. With S- $\text{TiO}_2$  the corresponding numbers were 58% and 15%. Thus the performance of the sulphur-doped catalyst increased to a greater extent than that of P25, even though the latter was still more effective. The reason behind the different response of the catalysts to natural solar radiation lays in the higher intensity of ultraviolet and visible radiation in solar spectrum (see Materials and Methods section).

## 4. Conclusions

Aqueous photocatalytic oxidation of prednisolone was studied using P25 (Evonik) and visible light-sensitive synthetic sol-gel carbon-containing titania catalysts used as is or doped with sulphur and iron. Photocatalytic oxidation was shown to be an effective method for prednisolone degradation with near-complete prednisolone removal at lower concentrations, and the observed oxidation efficiency up to  $40 \text{ mg W}^{-1} \text{ h}^{-1}$ . A number of prednisolone photocatalytic

oxidation by-products determined in the present study allowed the suggestion of possible reaction pathways proceeding simultaneously: the stepwise oxidation of the terminal parts of the prednisolone molecule, quinonic ring or cyclopentanic part, or oxidation from both quinonic and cyclopentanic part at the same time was assumed.

In the presence of major wastewater constituents, carbamide and sucrose, prednisolone photocatalytic oxidation also proceeded well with a minor disturbance from sucrose. The best prednisolone photocatalytic oxidation results were achieved at near-neutral pH, natural to prednisolone solutions.

The efficiency of doped titania of up to  $13 \text{ mg W}^{-1} \text{ h}^{-1}$  under visible light was inferior to the one observed with P25 under UV; higher efficiencies were observed as expected for the solar light application. Sulphur-doped titania (0.8 at.%) showed the best photocatalytic oxidation performance among the doped photocatalysts tested although yielding to the commercial P25 under both artificial and solar radiation conditions. The nontoxicity of doped catalysts towards *Tetrahymena thermophila*, a ciliate protozoa present in the activated sludge, indicates their lower oxidative ability, but also implies their potential application in pre-treatment of toxic hazardous materials under VIS or solar radiation before the biological degradation stage.

## Acknowledgements

The authors would like to thank Dr. Anna Moiseev, TU of Clausthal, and Dr. Paul Boni, University of Colorado, Boulder, for providing assistance with XRD measurements, Dr. Mai Uibu, Tallinn UT, for surface



area measurements, and Dr. Monika Mortimer, NICPB, for fruitful discussions. The support of the Estonian Science Agency (projects IUT1-7 and SF0690063s08), Estonian Science Foundation (grants 8978, 8561 and

GUS10), Archimedes Foundation (project 3.2.0801.11-0009) and the United States Civilian Research and Development Foundation (grant ESC2-2974-TL-09) is greatly appreciated.

## References

- [1] A.Y.C. Lin, T.H. Yu, S.K. Lateef, J. Hazard. Mater. 167, 1163 (2009)
- [2] M. DellaGreca, A. Fiorentino, M. Isidori, M. Lavorgna, L. Previtiera, M. Rubino, F. Temussi, Chemosphere 54, 629 (2004)
- [3] Y. Kitaichi, A. Miyamoto, K. Uchikura, J. Health Sci. 56, 547 (2010)
- [4] H. Chang, J.Y. Hu, B. Shao, Environ. Sci. Technol. 41, 3462 (2007)
- [5] K. Ikehata, N.J. Naghashkar, M.G. Ei-Din, Ozone Sci. Eng. 28, 353 (2006)
- [6] B. Langlais, D. Reckow, D. Brink, Ozone in Water Treatment. Application and engineering (Lewis Publishers, Inc., Chelsea, 1991)
- [7] B.K. Nandi, R. Uppaluri, M.K. Purkait, Appl. Clay Sci. 42, 102 (2008)
- [8] S. Liu, G.-G. Ying, J.-L. Zhao, F. Chen, B. Yang, L.-J. Zhou, H.-j. Lai, J. Chromatography A 1218, 1367 (2011)
- [9] D. Klauson, J. Babkina, K. Stepanova, M. Krichevskaya, S. Preis, Catal. Today 151, 39 (2010)
- [10] R.J.S. Lewis, Hawley's Condensed Chemical Dictionary, 14 edition (John Wiley and Sons, Inc., Chelsea, 2001)
- [11] D. Hansch, A. Leo, D. Hoekman, Exploring QSAR - Hydrophobic, Electronic, and Steric Constants (American Chemical Society, Washington, DC, 1995)
- [12] S.H. Yalkowski, Y. He, Handbook of Aqueous Solubility data: An Extensive Compilation of Aqueous Solubility data for Organic Compounds Extracted from the AQUASOL dATABase (CRC Press LLC, Boca Raton, FL, 2003)
- [13] M.J. O'Neil, The Merck Index - An Encyclopedia of Chemicals, Drugs and Biologicals., 13 edition (Merck and Co., Inc, Whitehouse Station, NJ, 2001)
- [14] US EPA, Estimation Program Interface (EPI) Suite. Ver. 3.12 (US Environmental Protection Agency (EPA), USA, November 30, 2004) <http://www.epa.gov/oppt/exposure/pubs/episuitd.htm>
- [15] B. Sun, M. Sato, J.S. Clements, J. Electrostatics 39, 189 (1997)
- [16] D. Bahnemann, Solar Energy 77, 445 (2004)
- [17] R.W. Matthews, Water Research 20, 569 (1986)
- [18] J. Chen, D.F. Ollis, W.H. Rulkens, H. Bruning, Water Research 33, 669 (1999)
- [19] V. Brezová, Š. Vodný, M. Veselý, M. Čeppan, L. Lapčík, J. Photochem. Photobiol. A 56, 125 (1991)
- [20] Y. Zhang, J.C. Crittenden, D.W. Hand, D.L. Perram, Environ. Sci. Technol. 28, 435 (1994)
- [21] C. Lettmann, K. Hildenbrand, H. Kisch, W. Macyk, W.F. Maier, Appl. Catal. B 32, 215 (2001)
- [22] T. Ihara, M. Miyoshi, Y. Iriyama, O. Matsumoto, S. Sugihara, Appl. Catal. B 42, 403 (2003)
- [23] Z. Wang, W. Cai, X. Hong, X. Zhao, F. Xu, C. Cai, Appl. Catal. B 57, 223 (2005)
- [24] D. Klauson, E. Portjanskaja, S. Preis, Environ. Chem. Lett. 6, 35 (2008)
- [25] D. Klauson, E. Portjanskaya, O. Budarnaja, M. Krichevskaya, S. Preis, Catal. Comm. 11, 715 (2010)
- [26] Z. Liu, D.D. Sun, P. Guo, J.O. Leckie, Chem. Eur. J. 13, 1851 (2007)
- [27] S.J. Kirkpatrick, Dental Mater. 21, 21 (2005)
- [28] G. Boeije, R. Corstjanje, A. Rottiers, D. Schowanek, Chemosphere 38, 699 (1999)
- [29] T. Karpova, S. Preis, J. Kallas, Int. J. Photoenergy 2007, Article ID 53853 (2007)
- [30] L.S. Clesceri, A.E. Greenberg, R.R. Trussel, Standard methods for the examination of water and wastewater (APHA, AWWA, WPCF, Washington, DC, 1989)
- [31] M. Mortimer, K. Kasemets, A. Kahru, Toxicology 269, 182 (2010)
- [32] E. Vindimian, MSeExcel macro REGTOX\_EV7.0.5.xls (Eric Vindimian, France) <http://www.normalesup.org/~vindimian/> 2011
- [33] S. Preis, M. Krichevskaya, Y. Terentyeva, A. Moiseev, J. Kallas, J. Adv. Oxid. Technol. 5, 77 (2002)
- [34] M. Krichevskaya, T. Malygina, S. Preis, J. Kallas, Water Sci. Technol. 44, 1 (2001)
- [35] M. Krichevskaya, A. Kachina, T. Malygina, S. Preis, J. Kallas, Int. J. Photoenergy 5, 81 (2003)
- [36] D. Klauson, S. Preis, Int. J. Photoenergy 2007, Article ID 89359 (2007)
- [37] K. Mogyorósi, N. Balázs, D.F. Srankó, E. Tombácz, I. Dékány, A. Oszkó, P. Sipos, A. Dombi, Appl.

- Catal. B 96, 577 (2010)
- [38] D.M. Metzler, M.H. Li, A. Erdem, C.P. Huang, Chem. Eng. J. 170, 538 (2011)
- [39] L. Brunet, D.Y. Lyon, E.M. Hotze, P.J.J. Alvarez, M.R. Wiesner, Environ. Sci. Technol. 43, 4355 (2009)
- [40] P. Madoni, Water Research 28, 67 (1994)
- [41] M.P. Sauvant, D. Pepin, E. Piccinni, Chemosphere 38, 1631 (1999)
- [42] G. Esteban, C. Tellez, L.M. Bautista, Water Research 25, 967 (1991)

### **Article III:**

Klauson D., Budarnaja O., Stepanova K., Krichevskaya M., Dedova T., Käkinen A., Preis S., Selective performance of sol-gel synthesised titanium dioxide photocatalysts in aqueous oxidation of various-type organic pollutants. *Kinetics and Catalysis*, 2014, 55 (1), pp. 47-55, doi: 10.1134/S0023158414010030



# Selective Performance of Sol–Gel Synthesised Titanium Dioxide Photocatalysts in Aqueous Oxidation of Various-Type Organic Pollutants<sup>1</sup>

Deniss Klauson<sup>a,\*</sup>, Olga Budarnaja<sup>a</sup>, Kristina Stepanova<sup>a</sup>, Marina Krichevskaya<sup>a</sup>,  
Tatjana Dedova<sup>b</sup>, Aleksandr Käkinen<sup>c,d</sup> and Sergei Preis<sup>e</sup>

<sup>a</sup> Department of Chemical Engineering, Tallinn University of Technology,  
Ehitajate tee 5, Tallinn 19086, Estonia

<sup>b</sup> Department of Materials Science, Tallinn University of Technology,  
Ehitajate tee 5, Tallinn 19086, Estonia

<sup>c</sup> Laboratory of Environmental Toxicology, National Institute of Chemical Physics and Biophysics,  
Akadeemia tee 23, Tallinn 12618, Estonia

<sup>d</sup> Department of Chemical and Materials Technology, Tallinn University of Technology,  
Ehitajate tee 5, Tallinn 19086, Estonia

<sup>e</sup> LUT Chemistry, Lappeenranta University of Technology,  
P.O. Box 20, Lappeenranta 53851, Finland

\*e-mail: deniss.klauson@tu.ee

**Abstract**—Photocatalysts synthesized by sol–gel method inevitably incorporate carbon together with dopants. The objective of the research consists in the synthesis and testing of photocatalytic activity of carbon-containing titanium dioxide photocatalysts calcinated at various temperatures. The optical and structural properties of the catalysts were also studied. The activity was tested in visible light in aqueous photocatalytic oxidation of three various-type pollutants, methyl-*tert*-butyl ether, *p*-toluidine and phenol, where the divergent character of the C–TiO<sub>2</sub> catalysts was distinctively observed: methyl-*tert*-butyl ether and *p*-toluidine were oxidized with the efficiency close to or even surpassing that of UV-irradiated P25 (Evonik), whereas phenol was oxidized poorly. The observed photocatalytic activity, where quantum efficiency varied from 0.6 to 2.3 and from 0.1 to 1.2% for *p*-toluidine and phenol degradation respectively, may be explained by the different electrostatic properties of the catalysts' surface and the tested substances, i.e. their interaction. This compromises the widespread usage of phenol as a reference substance for comparison of catalytic activities of catalysts.

**Keywords:** TiO<sub>2</sub>, doping, visible light, photocatalysis, methyl-*tert*-butyl ether, *p*-toluidine, phenol

**DOI:** 10.1134/S0023158414010030

## 1. INTRODUCTION

Heterogeneous photocatalytic oxidation (PCO) of organic pollutants over semiconductor photocatalysts is the result of the action of positively charged holes formed by the displacement of electrons with irradiation, oxidising adsorbed organic pollutant molecules, or forming from water hydroxyl radicals oxidizing the pollutant. Commercially available titanium dioxide photocatalysts with the band-gap energy of 3.2 eV can utilize only ultraviolet radiation photons, i.e. no more than 4% of the solar radiation reaching the Earth surface. Development of visible light sensitive photocatalysts receives attention for the reduced band gap and, thus, widened light spectrum used in photocatalytic reactions.

To widen the solar spectrum useful in photocatalysis, the band-gap can be reduced by introducing additive atoms into titanium dioxide, thus creating a crystalline structure with a misbalance in charge carriers creating a new energetic level inside the band-gap, from which electrons can be displaced with greater wavelength radiation. Various non-metal dopants are used in photocatalyst synthesis widening the active light spectrum, although the results of anion doping are often contradictory: widening the absorption spectrum, the doping weakens the photocatalyst's activity [1, 2]. The authors previously observed the selective character of the PCO with N-, S- and B-doped catalysts showing dramatically dissimilar efficiencies with different substances [3, 4].

The synthesis of doped photocatalysts using hydrolysis of titanium-containing organic substances in presence of doping ingredients is incapable of pro-

<sup>1</sup> The article is published in the original.

ducing catalysts free from carbon admixtures [3–5]. This requires clarification of its dopant role, which was undertaken in the present research. Aqueous PCO of methyl-*tert*-butyl ether (MTBE), *p*-toluidine, and phenol, using carbon-containing titanium dioxide under visible light, was studied for assessment of the photocatalytic activity of the catalysts.

Methyl-*tert*-butyl ether, banned in the USA, is still widely used as an oxygenated component of motor fuels by the rest of the world. This substance is of particular concern because of its poor biodegradability and accumulation in groundwater [6]. Physical removal and chemical oxidation methods have been proven to be ineffective against MTBE [7–9].

*p*-Toluidine is a non-biodegradable chemical with its use ranging from a component of jet and rocket fuels to applications in paint and pharmaceutical industries [10]. It is also a degradation intermediate of *p*-nitrotoluene, thus polluting the soil and groundwater at military installations.

Phenol, a widespread environment pollutant, has a reputation of a standard contaminant that is used to test the efficiency of various oxidation methods, or the activity of different catalysts [11, 12].

The objective of the present research was studying the performance of carbon-containing photocatalyst and providing explanation for the observed PCO activity phenomenon. Although the attempts on the doping of titanium dioxide with carbon were undertaken earlier [13–16], this topic is still of interest [17, 18]; the novelty of the present research consists of the catalysts of different composition tested in PCO of priority pollutants different in their structure and properties giving a more encompassing description of the new catalysts' activity. The works showing high activity of newly synthesised carbon-containing catalysts in PCO of a single pollutant, most often textile dyes, may lead to erroneous conclusions concerning a wider application of the catalysts. In the present research, the authors tested ten carbon-containing titanium dioxide photocatalysts in PCO of the abovementioned pollutants to establish the impact of the catalyst composition and calcination temperature on the PCO efficiency. The results were compared to the ones obtained with P25 titanium dioxide (Evonik) under the UV light. The comparison of the photocatalysts' activity was done as described due to the fact that in both theory and practice P25 is active only in UV, as opposed to visible light; working in UV with specifically synthesised visible light-active photocatalysts is possible, but does not seem proper as efforts were made to move further from UV. Consequently, the performance of both photocatalyst types is undertaken in the conditions that suit them best; also, P25 under UV-irradiation can be considered to be somewhat of a reference system for testing new photocatalytic materials.

## 2. EXPERIMENTAL

Two thermostatted at  $20 \pm 1^\circ\text{C}$  agitated with magnetic stirrers 200-mL simple batch reactors with inner diameter 100 mm (evaporation dishes) with the irradiated contact surface  $40 \text{ m}^2 \text{ m}^{-3}$  were used in PCO experiments: the one used for the PCO was called "active" and the other, called "reference" or "blank," contained no photocatalyst and was not exposed to the light. The samples from the active reactor were compared to the reference samples to avoid complications caused by water evaporation.

A UV-light source, Phillips 365-nm low pressure luminescent mercury UV-lamp (Sylvania Blacklight F15 W 350 BL-T8), was positioned horizontally over the active reactor, providing the irradiance of about  $0.7 \text{ mW cm}^{-2}$  measured at a distance corresponding to the level of the free surface of the reactor by the optical radiometer Micropulse MP100 (Micropulse Technology, UK).

With daylight fluorescent lamp (Philips TL-D 15W/33-640), the irradiance was determined indirectly, being calculated from the illuminance, measured by TES luxmeter (TES, Taiwan), using lumen to watt ratio of 684 [19]. The irradiance of the reactors under visible light was close to the one of the UV used in experiments with P25 (Evonik). With Phillips TL-D visible light lamp, the amount of UV-irradiation was also measured using the abovementioned radiometer for 254 and 365 nm, showing zero radiance, as well as the total amount of UV by using Ocean Optics USB2000+UV-VIS-ES spectrometer: this instrument showed only negligibly small fraction of UV around 365–400 nm, which is in agreement with the data from the lamp manufacturer [20]. Thus, any noticeable action of the photocatalyst when using Phillips TLD visible light lamp may not be attributed to the emitted UV fraction but is clearly due to the activity of the catalysts in visible light.

The experiments were carried out using aqueous solutions of the chemicals (Sigma-Aldrich) at their initial concentrations of  $100 \text{ mg L}^{-1}$ . With MTBE, the experiments were conducted at naturally set pH 6.5 within the maximum treatment time 1 h. *p*-Toluidine solution was used at maximum treatment time 24 h carried out at pH 3, naturally set 6.5 and 11. Phenol solutions were also treated for 24 h at natural pH 6.5. The pollutant concentrations were chosen with reference to those found in real contaminated aquifers used in previous experiments [12, 15, 21]. The treatment time was chosen to provide the concentration of pollutants reduced to about 50%; this was also used in calculations of the process efficiency  $E$  (see Eq. 2). All the experiments were carried out for at least three times under identical experimental conditions to derive the average value of the process efficiency. The average deviation of data in parallel experiments did not exceed 5%. In order to evaluate the stability of the photocatalysts, the repeated experiments were carried

out using the same portion of the photocatalyst. The difference also fitted well to the 5% error with no tendencies observed. This indicates the stable character of the catalysts, i.e. is consistent with the carbon incorporated into titanium dioxide crystal lattice in sol-gel synthesis [5].

The experiments were performed using photocatalyst suspension with the concentration of  $1 \text{ g L}^{-1}$ . Titanium dioxide P25 and carbon-containing catalysts synthesised on course of the research were used. Carbon-containing photocatalysts were prepared by the near-instant hydrolysis of pure titanium tetrabutoxide, followed by calcinations at temperatures from 200 to  $950^\circ\text{C}$  for 4 h. After this, the catalysts were washed with hot distilled water applied in a sequence of 10 to 15 rinsing rounds (ca. 1 L per gram of catalyst) in order to clean the catalyst surface from water-soluble compounds.

The crystallinity, crystal structure and phase composition of carbon-containing titanium dioxide were analysed using D 5000 Kristalloflex, Siemens ( $\text{CuK}_\alpha$  irradiation source) X-ray diffraction spectroscopy (XRD), with the phase composition calculated by Topas R Software. The specific surface area (BET and Langmuir adsorption) and the pore volume of the catalysts were measured by the adsorption of nitrogen using KELVIN 1042 sorptometer. Identified peak positions were compared to the data found in literature [22, 23].

For the optical measurements ethanol-based suspensions ( $1 \text{ g L}^{-1}$ ) of  $\text{TiO}_2$  powders were prepared on microscopic glass substrates and after total ethanol evaporation measurements were carried out with the obtained coatings. Total and diffused reflectance spectra of the coatings were measured in the wavelength range of 250–2500 nm on a Jasco V-670 UV-VIS spectrophotometer equipped with an integrating sphere. Obtained data were used to calculate the absorption coefficient ( $\alpha$ ) and optical band gap values ( $E_g$ ). For the titanium dioxide photocatalysts of various crystalline modifications, evidence supporting both direct electron transition [24, 25] and indirect one [23, 24, 26–30] has been published. It should be pointed out, however, that the majority of the last decade publications report indirect transition for titanium dioxide. Consequently, band gap values of the new photocatalysts were calculated assuming indirect transition type. A standard expression for transitions between two parabolic bands for the calculation of band gap energy is:

$$(\alpha h\nu)^m = A(h\nu - E_g), \quad (1)$$

where  $m = 1/2$  and  $A$  is a constant.

Band gap values were found from the intercept of the linear fitting curve extrapolated to the zero absorption of  $(\alpha h\nu)^m$  vs.  $h\nu$  plot [31, 32]. Haze factor values were calculated as the relationship of diffused reflectance to total reflectance; it shows the extent of light

scattering, and, thus, the relative roughness of the coatings [32].

The decrease in the MTBE concentration was determined by gas chromatography using Finnigan Focus GC chromatograph; MTBE was extracted from pre-salinated aqueous samples by benzyl alcohol using IKA Vortex Genius 3 extractor. Oxidation rate was measured by a standard method from the decrease in chemical oxygen demand (COD). This parameter, unlike TOC, was proven to be decreasing with the increasing conversion degree in oxidation reactions.

Concentrations of *p*-toluidine were measured photometrically after diazotation and reaction with phenol at 490 nm, and concentrations of phenol were determined photometrically after reaction with *p*-nitroaniline at 570 nm using Helios  $\beta$  spectrophotometer [33].

The methods are highly selective without interference from the PCO by-products proven by the PCO reaction rationales for MTBE and phenol given in [34, 35]. Neither ammonia, the predominant PCO by-product of amines, nor PCO intermediates of aromatic amino compounds [36] may interfere with *p*-toluidine measurement [33]. The decrease in COD was also followed. The evolution of nitrite and nitrate ions was monitored using Metrohm 761 Compact IC ion chromatograph.

Adsorption experiments with the pollutants on the photocatalyst surface were carried out at respective pH in closed flasks thermostatted at  $20 \pm 1^\circ\text{C}$  and equipped with magnetic stirrers. The adsorbed amount of substances was derived from the batch mass balance: the concentration of the dissolved substance was determined before and after adsorption.

The performance of PCO with artificial radiation sources was characterised by the process efficiency  $E$ , defined as the pollutants degradation relative to the energy reaching the surface of the treated sample calculated for the treatment time. This makes the PCO efficiency the universal term to compare the results achieved with different catalysts:

$$E = \frac{\Delta c V}{I s t} \times 1000, \quad (2)$$

where  $E$ —PCO efficiency,  $\text{mg W}^{-1} \text{ h}^{-1}$ ;  $\Delta c$ —the decrease in the pollutant's concentration or COD,  $\text{mg L}^{-1}$  or  $\text{mg O L}^{-1}$ ;  $V$ —the volume of the sample to be treated, L;  $I$ —irradiance,  $\text{mW cm}^{-2}$ ;  $s$ —irradiated area,  $\text{cm}^2$ ;  $t$ —treatment time, h.

In order to measure the quantum efficiency of the photocatalysts (expressed as mol of pollutant/COD removed per 1 mol of photons reaching the surface of the treated solution), the irradiance of the corresponding light sources was measured qualitatively and quantitatively by Ocean Optics USB2000+UV-VIS-ES spectrometer, and integrated in the corresponding part of the irradiance spectrum utilised by the photocatalysts, with the latter knowledge provided by band gap measurements.



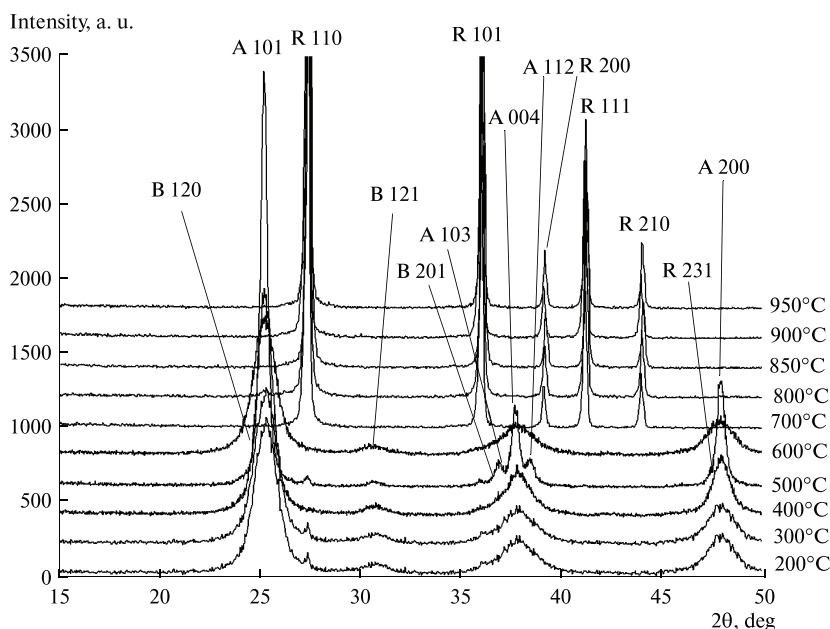


Fig. 1. X-ray diffraction pattern of the C-TiO<sub>2</sub> photocatalysts (A—anatase, B—brookite, R—rutile).

The isoelectric points (IEP) of pure TiO<sub>2</sub> (P25) and carbon-doped titanium dioxide suspensions were determined by potentiometric titration using a Zetasizer Nano-ZS equipped with an MPT-2 autotitrator and vacuum degasser (Malvern Instruments, UK). The technique (Laser Doppler Micro-electrophoresis) is based on the electrophoretic light-scattering that measures migration rate of dispersed particles under the influence of an electric field. Zeta potential was calculated by Malvern software using Smoluchowski equation. Suspensions of 1 g L<sup>-1</sup> were prepared in deionized water, sonicated for 30 min (70 W, 42 kHz, Branson 1510, Branson Ultrasonic Corporation, USA) and diluted to 100 mg L<sup>-1</sup> in deionised water. Automatic titrations were performed in 10 mL as an initial sample volume, from pH 11 to pH 1.5 with 0.25 M NaOH and 0.25 M HCl, pH increment was 0.5 and target pH tolerance was 0.2. Each  $\zeta$ -potential value recorded was the average of 10 measurements.

### 3. RESULTS

#### 3.1. Characterisation of Photocatalysts

Figure 1 shows the X-ray diffraction patterns of carbon-containing titania. With the growth of the calcination temperature, abrupt changes take place in the catalyst crystallographic composition at 600 to 700°C. Judging from the XRD analysis, at temperatures up to 600°C the catalysts are composed of both anatase and

brookite in relatively constant amounts with occasional fluctuations in measurements. For anatase, the (1 0 1) peak was the best pronounced, followed by (1 0 3), (2 0 0), (0 0 4), (1 0 3) and (1 1 2) whereas for brookite, the (1 2 0), (1 2 1), (2 0 1) and (2 3 1) peaks were determined. The catalysts obtained at the temperatures starting from 700°C are pure rutile, as expected for both anatase and brookite transforming directly to rutile at temperatures around 500 to 600°C [37]. For rutile, (1 1 0), (1 0 1), (1 1 1), (2 1 0) and (2 2 0) peaks were identified. The exact composition of the photocatalyst, as calculated from the XRD graphs, is given in Table 1. All the observed peaks belong to titanium dioxide, with no additional peaks that could be attributed to carbon or carbon species. The characteristic peaks of C-TiO<sub>2</sub> materials are shifted relative to those of pure TiO<sub>2</sub> crystalline modifications, by up to ca.  $\sim 0.12^\circ$ , in either direction, which can be explained by distortions in titanium dioxide crystal lattice originating from the inclusion of carbon into TiO<sub>2</sub> structure [17, 24]. The reason behind crystal lattice distortions is the differences in atomic radii during the replacement of oxygen atoms with carbon ones for increased angles [17], and, probably, the replacement of titanium atoms with carbon ones for decreased angles. The peak shifts, along with the absence of any secondary carbon-associated phase peaks, are indirect evidence of stable carbon incorpo-



**Table 1.** Crystallographic and surface properties of carbon-containing photocatalysts dependent on the calcination temperature

<i>T</i> calcination, °C	Crystallographic composition, %			$S_{\text{BET}}$ , $\text{m}^2 \text{g}^{-1}$	$S_{\text{Langmuir}}$ , $\text{m}^2 \text{g}^{-1}$	Micropore area, $\text{m}^2 \text{g}^{-1}$	Micropore volume, $\text{mm}^3 \text{g}^{-1}$
	anatase	brookite	rutile				
200	71.9	28.1	–	202.3	278.9	0	0
300	74.7	25.3	–	157.2	215.8	0.42	0.15
400	78.1	21.9	–	105.7	144.7	4.12	1.54
500	76.9	18.2	5.0	39.45	53.85	3.95	1.39
600	74.4	25.6	–	8.81	12.08	0	0
700	–	–	100	3.52	4.81	0.20	0.07
800	0.8	–	99.2	3.75	5.14	0.13	0.05
850	–	–	100	2.92	4.03	0	0
900	–	–	100	2.94	4.02	0.05	0.02
950	–	–	100	2.62	3.61	0	0

ration into  $\text{TiO}_2$  crystal lattice, i.e. titanium dioxide doping.

The analysis of major XRD characteristic peaks shifts shows that the calcination temperature increased from 200 to 600°C results in anatase peaks (1 0 1), (1 0 3) and (2 0 0) shifted towards smaller angles, suggesting the preference of titanium replacement with carbon in the titania crystal lattice. In rutile, however, the contrary situation was observed: calcination temperature increased from 700 to 950°C resulted in the increased shift of (1 0 1) peak position, which suggests the oxygen preferential replacement by carbon in the crystal lattice. With other peaks, no clear dependence was observed. The difference observed between carbon incorporation mechanisms in anatase and rutile could possibly be explained by the difference in structure and formation mechanism of anatase and rutile grains, along with transformation of anatase to rutile.

The specific surface area of the catalysts decreases with the calcination temperature increased from 200 to 500°C, whereas micropore volume and area somewhat increased at 400–500°C, approximating zero at higher temperatures within accuracy of measurements (Table 1). However, since the adsorption of the pollutants by the catalysts was observed to be negligible, surface structure and characteristics of the catalysts can be considered as being of secondary importance for the purposes of this study.

Diffused reflectance spectra given in Fig. 2a suggest that in general smaller photocatalyst grains dominate over the larger ones since the reflectance decreases with the wavelength, however, the increased calcination temperature results in increased relative size of the particles. With the calcination temperature increased from 200 to 500°C, total reflectance of the photocatalysts at 400 nm increased from 62 to 74%, and then steadily decreases to 22% at 950°C. For com-

parison, total reflectance of P25 at 400 nm was 71%. Thus, with the anatase and brookite phase transformation to rutile, total reflectance of the catalysts abruptly decreased (see Table 2). Haze factor characterizing light scattering decreased with the increased calcination temperature (Fig. 2b), suggesting the surface of the coatings becoming smoother.

Optical band gap values, calculated for indirect transition, as well as corresponding cut-off wavelengths, are given in Table 2. Optical band gap values of the photocatalysts decreased with the increased calcination temperature, with the biggest changes observed between 500 and 700°C, coinciding with the  $\text{TiO}_2$  phase transformation. The changes in the band gap energy should be viewed with the respect to both dopant incorporation into titanium dioxide crystal lattice and the changes in phase composition. Anatase, brookite and rutile as individual phases were reported to have band-gap energies of 3.34, 3.40 and 2.95 eV

**Table 2.** Optical properties of carbon-containing photocatalysts dependent on the calcination temperature

<i>T</i> calcination, °C	Total reflectance at 400 nm, %	$E_g$ , eV	$\lambda_{\text{cut-off}}$ , nm
200	62	2.81	442
300	71	2.89	429
400	73	2.89	429
500	74	2.89	429
600	29	2.74	452
700	30.5	2.77	448
800	33	2.78	446
850	30.5	2.79	444
900	30.5	2.77	448
950	22	2.78	446

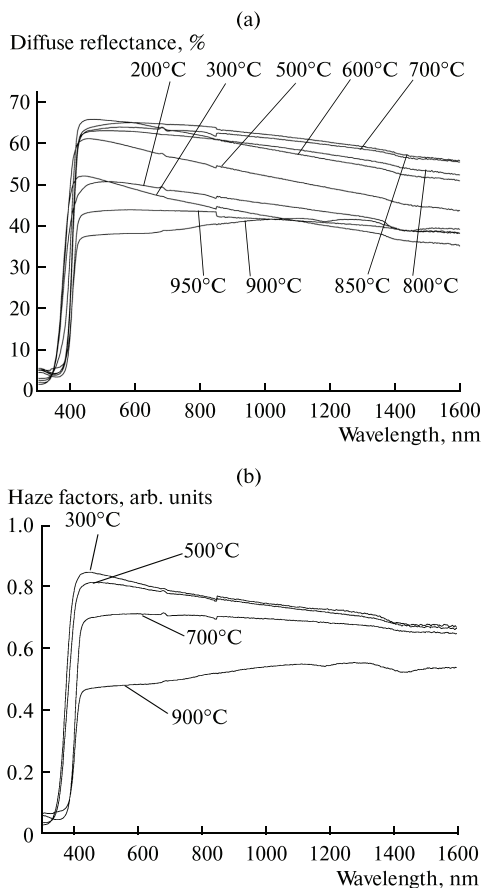


Fig. 2. The dependence of diffuse reflectance (a) and haze factor (b) on the calcination temperature of C-TiO<sub>2</sub>.

respectively [23, 26]. Optical band gap of a multi-phase material gives an average value, which takes into account, although not linearly, the band gaps of each phase and their relative amounts. The decreased band-gap energies, additionally to XRD analysis data (Fig. 2), proves the incorporation of carbon into the titanium dioxide crystal lattice, i.e. TiO<sub>2</sub> doping, especially well observed for rutile photocatalysts.

The zeta-potential determination showed the isoelectric point (IEP) of carbon-doped titanium dioxide decreased in comparison to that of P25: 3.69 and 4.74 for C-TiO<sub>2</sub> calcinated at 200°C and P25 respectively. The reason for the choice of single specific photocatalyst for ZPC measurements is that in general this photocatalyst has shown the highest activity among other C-TiO<sub>2</sub> samples (see below).

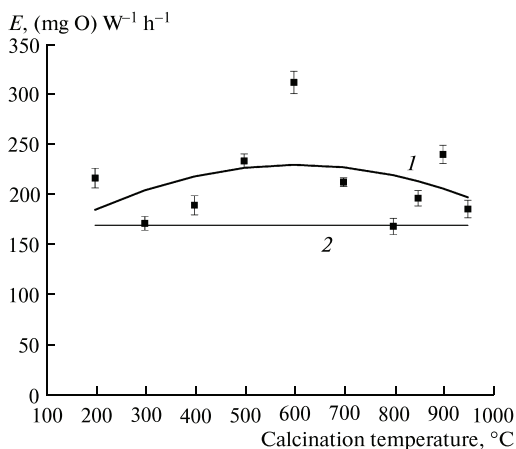


Fig. 3. The PCO efficiency of MTBE vs. the temperature of C-TiO<sub>2</sub> calcination (squares, black bold solid line) compared to P25 under UV (grey solid line): pH 6.5, 2 h.

### 3.2. Adsorption

Under applied experimental conditions, no adsorption of the substances under consideration was observed on the surface of the carbon-containing photocatalysts above the limits of analytical precision. Consequently, radical reactions may be responsible for PCO at C-TiO<sub>2</sub> catalysts with surface hole reactions playing less important role.

### 3.3. Oxidation of MTBE

Under visible light MTBE was totally degraded within 1 h with all tested C-TiO<sub>2</sub> catalysts. Evaluated by the decrease in COD, the PCO efficiency at different catalysts somewhat oscillated showing no visible trend (Fig. 3), although the catalyst calcinated at 600°C appears to give the best result. The values of PCO efficiency observed with C-TiO<sub>2</sub> irradiated with visual light were higher than that with UV-irradiated P25 under similar experimental conditions (170 mg O<sub>2</sub>W<sup>-1</sup> h<sup>-1</sup>) [21]. The efficiency of rutile C-TiO<sub>2</sub> catalysts was also equal to or exceeding the one of P25. For MTBE, classical photonic efficiency calculations were not applicable, as it appears to partly undergo self-catalysis during PCO.

### 3.4. Oxidation of *p*-Toluidine

Similarly to P25 showing the maximum PCO efficiency in acidic media [38], the best performance of C-TiO<sub>2</sub> catalysts with *p*-toluidine was achieved at unregulated natural pH 6.5 shifted on course of PCO to acidic range, at which most of the experiments were consequently carried out. The PCO efficiency observed with C-TiO<sub>2</sub> under artificial daylight was

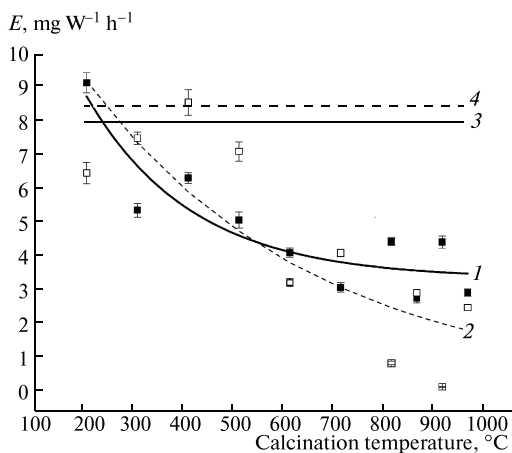


**Fig. 4.** The dependence of *p*-toluidine PCO efficiency on the photocatalysts calcination temperature compared to P25: *p*-toluidine—solid squares and bold solid line, COD—empty squares, dashed line, compared to P25 under UV (*p*-toluidine—solid line, COD—dotted line); pH 6.5, 24 h.

close to that of P25 under UV. In Fig. 4 one can see the PCO efficiency of *p*-toluidine steadily declining with the growth of calcination temperature, i.e. with the decrease in carbon content and contact surface area. For *p*-toluidine, photonic efficiency ranged between 0.6 and 2.3% for the catalysts calcinated at 850 and 400°C, respectively; in general, with the increase of calcination temperatures, photonic efficiency values decreased as did the PCO efficiency values. In general, quantum efficiency photonic efficiency values were quite low, as the reaction system was not specifically optimized for the efficient use of light.

### 3.5. Oxidation of Phenol

With phenol, the PCO efficiency also decreased with growing catalyst calcination temperature (Fig. 5). For comparison, UV-irradiated P25 can degrade phenol at the same initial concentration with the PCO efficiency at pH from 7 to 3 from 5 to 10 mg W<sup>-1</sup> h<sup>-1</sup> [12], i.e. about 3 to 5 times higher than of C-TiO<sub>2</sub>. In case of phenol, photonic efficiency values were even lower, being between 0.1 and 1.2% for catalysts calcinated at 850 and 500°C. The dependence of photonic efficiency on calcination temperature here was also following the trend observed with PCO efficiency.

## 4. DISCUSSION

Negligible amount of UV emitted by the visible radiation sources, coupled with selectively high photocatalytic performance of C-TiO<sub>2</sub> can only suggest visible light activity of the photocatalysts. For indirect

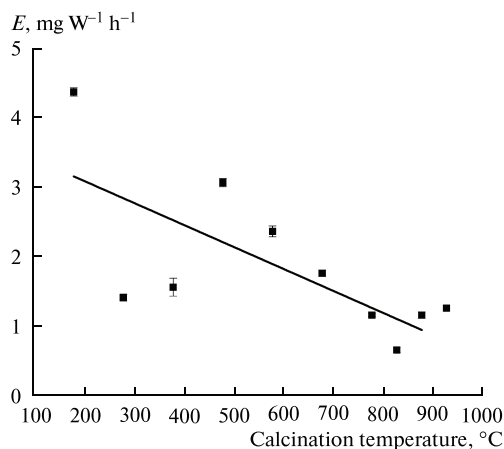


**Fig. 5.** The dependence of phenol PCO efficiency on the photocatalysts calcination temperature: pH 6.5, 24 h.

band gap calculations, the applicability of which is supported by numerous publications (see Introduction), the obtained band gap values, suggesting visible light utilisation, are in good agreement with the observed experimental results.

The divergent PCO performance of carbon-containing titania photocatalysts, observed in oxidation of MTBE and aromatic phenol and *p*-toluidine, may be explained by the different interactions of these substances with the catalysts. No adsorption of the substances was detected beyond the limits of analytical precision, which leaves the radical reactions in the vicinity of the catalyst surface the only PCO mechanism responsible for the pollutants' degradation. Under the experimental conditions, i.e. moderately acidic pH, both TiO<sub>2</sub> and the aromatic substances, are partially protonated and, thus, positively charged. However, according to IEP measurements, C-TiO<sub>2</sub> particles have point zero charge at lower pH, which should give them negative charge at the applied experimental conditions. Thus, if the aromatic substances are electrostatically repelled from the P25 surface with their PCO obstructed, then electrostatic forces attract aromatic compounds to the surface of negatively charged C-TiO<sub>2</sub>. The electrically neutral MTBE molecule, however, can get closer to the surface of a catalyst under the scope with a larger supply of hydroxyl radicals and, thus, a higher probability of the radical impact to the pollutant molecule, resulting in PCO efficiency two orders of magnitude higher. Increased hydroxyl radical production can lead to the increase in PCO efficiency of aromatic substances, which explains the increased PCO efficiency at the decreased catalysts' calcination temperature, i.e. higher content of the most photocatalytically active anatase.

The oxidation potential of positively charged holes formed at the new energetic levels in the semiconductor may be decreased but still sufficient for hydroxyl radicals' production thus improving the oxidation efficiency with increased utilized light flux or irradiated surface. Similar observations were made by the authors with relatively well-adsorbed amoxicillin most likely hole-oxidized at C- and Fe-TiO<sub>2</sub> catalysts [39]. With the growth of the catalysts' calcination temperature, more carbon is burned out from the catalyst, and both anatase and brookite are transformed into less photo-active rutile, thus decreasing the activity of the photocatalysts and also the contact surface. This way the amount of hydroxyl radicals decreases with increasing catalysts' calcination temperature thus having the PCO efficiency of aromatic compounds decreasing.

## 5. CONCLUSIONS

Divergent performance of carbon-containing titanium dioxide photocatalysts was established in aqueous photocatalytic oxidation (PCO) of methyl-*tert*-butyl ether (MTBE), *p*-toluidine and phenol using visible light. With MTBE and *p*-toluidine their performance is similar to or surpasses that of P25 titanium dioxide under UV-irradiation; with phenol, the performance of C-TiO<sub>2</sub> was inferior to that of P25. The observed PCO activity can be explained by the different interactions of these substances with the catalysts due to their electrostatic properties.

The photocatalysts exhibited a pronounced ability to catalyze oxidation reactions of MTBE, *p*-toluidine and phenol under visible light radiation. Variations in the catalysts' crystallographic composition and carbon content, dependent on the calcination temperature, influenced the photocatalytic activity in oxidation of *p*-toluidine and phenol: the lower the anatase and brookite content (higher calcination temperature) the lower the photocatalytic activity. Photocatalytic oxidation of MTBE does not depend on the calcinations temperature even at calcination temperature exceeding 600°C when all anatase and brookite turned to rutile. C-TiO<sub>2</sub> photocatalysts showed stable activity even after repeated applications.

The widespread opinion concerning a phenol used as a single reference substance used for comparison of catalysts is compromised by the dramatically diverse behaviour of tested catalysts in PCO of different-type substances.

## ACKNOWLEDGMENTS

The authors would like to thank the team of Prof. Dr.-Ing. Joachim Deubener, Division of Glass and Glass Technology Institute of Non-Metallic Materials of the Technical University of Clausthal, especially Dr. Anna Moiseev for providing XRD measurements, and Dr. Mai Uibu, Laboratory of Inorganic Materials

of Tallinn University of Technology, for providing specific surface area measurements of the catalysts.

The authors would also like to thank Estonian Science Agency (projects IUT1-7 and SF0690063s08), Estonian Science Foundation (grants GUS10 and ETF8978), United States Civilian Research and Development Foundation (grant ESC2-2974-TL-09) and the European Union through the European Regional Development Fund (Project TK114, 3.2.0101.11-0029) for the financial support of the research.

## REFERENCES

- Liu, Z., Sun, D., Guo, P., and Leckie, J., *Chem. Eur. J.*, 2007, vol. 13, p. 1851.
- Fujishima, A., Zhang, X., and Tryk, D., *Surf. Sci. Rep.*, 2008, vol. 63, p. 515.
- Klauson, D., Portjanskaja, E., and Preis, S., *Environ. Chem. Lett.*, 2008, vol. 6, p. 35.
- Klauson, D., Portjanskaja, E., Budarnaja, O., Krichevskaya, M., and Preis, S., *Catal. Commun.*, 2010, vol. 11, p. 715.
- Park, Y., Kim, W., Park, H., Tachikawa, T., Majima, T., and Choi, W., *Appl. Catal., B*, 2009, vol. 91, p. 355.
- Yeh, C. and Novak, J.T., *Water Environ. Res.*, 1994, vol. 66, p. 744.
- Johnson, P., *Environ. Sci. Technol.*, 1998, vol. 32, p. 276.
- Safarzadeh-Amiri, A., *Water Res.*, 2001, vol. 35, p. 3706.
- Xu, X. and Zhao, Z., Li, X., and Gu, J., *Chemosphere*, 2004, vol. 55, p. 73.
- Papok, K. and Semenid, E., *Motornye, reaktivnye i raketnye topliva* (Motor, Jet, and Rocket Fuels), Moscow: Gostoptekhizdat, 1962.
- Busca, G., Berardinelli, S., Resini, C., and Arrighi, L., *J. Hazard. Mater.*, 2008, vol. 160, p. 265.
- Preis, S., Krichevskaya, M., Terentyeva, Y., Moiseev, A., and Kallas, J., *J. Adv. Oxid. Technol.*, 2002, vol. 5, p. 77.
- Lettmann, C., Hildenbrand, K., Kisch, H., Macyk, W., and Maier, W., *Appl. Catal., B*, 2001, vol. 32, p. 215.
- Shen, M., Wu, Z., Huang, H., Du, Y., Zou, Z., and Yang, P., *Mater. Lett.*, 2006, vol. 60, p. 693.
- Ren, W., Ai, Z., Jia, F., Zhang, L., Fan, X., and Zou, Z., *Appl. Catal., B*, 2007, vol. 69, p. 138.
- Wu, Y., Zhang, J., Xiao, L., and Chen, F., *Appl. Surf. Sci.*, 2010, vol. 13, p. 4260.
- Yun, H., Lee, H., Joo, J., Kim, N., Kang, M., and Yi, J., *Appl. Catal., B*, 2010, vol. 94, p. 241.
- Zhang, Y., Zhang, P., Huo, Y., Zhang, D., Li, G., and Li, H., *Appl. Catal., B*, 2012, vol. 115, p. 236.
- Kirkpatrick, S., *Dent. Mater.*, 2005, vol. 21, p. 21.
- [http://www.ecat.lighting.philips.com/1/catalog/catalog.jsp?userLanguage=en&userCountry=aa&catalog-Type=LP\\_PROF\\_ATG&\\_dyncharset=UTF&categoryid=LP\\_CF\\_TLDSTD\\_EU\\_FA\\_AA\\_LP\\_PROF\\_ATG&productid=928024803347\\_EU\\_AA\\_LP\\_PROF\\_](http://www.ecat.lighting.philips.com/1/catalog/catalog.jsp?userLanguage=en&userCountry=aa&catalog-Type=LP_PROF_ATG&_dyncharset=UTF&categoryid=LP_CF_TLDSTD_EU_FA_AA_LP_PROF_ATG&productid=928024803347_EU_AA_LP_PROF_)

- ATG&title=TL-D%2015W/3340%201SL&ctn=928024803347\_EU
21. Krichevskaya, M., Kachina, A., Malygina, T., Preis, S., and Kallas, J., *Int. J. Photoenergy*, 2003, vol. 5, p. 81.
  22. Sakurai, K. and Mizusawa, M., *Anal. Chem.*, 2010, vol. 82, p. 3519.
  23. Di Paola, A., Cufalo, G., Addamo, M., Ellardita, M., Camprostrini, R., Ischia, M., Ceccato, R., and Palmisano, L., *Colloids Surf. A*, 2008, vol. 317, p. 366.
  24. Reddy, K., Manorama, S., and Reddy, A., *Mater. Chem. Phys.*, 2003, vol. 78, p. 239.
  25. Magne, C., Cassaignon, S., Lancel, G., and Pauporte, T., *ChemPhysChem*, 2011, vol. 12, p. 2461.
  26. Koelsch, M., Cassaignon, S., Guillemoles, J., and Jolivet, J., *Thin Solid Films*, 2002, vol. 403, p. 312.
  27. Tanemura, S., Miao, L., Jin, P., Kaneko, K., Terai, A., and Nabatova-Gabain, N., *Appl. Surf. Sci.*, 2003, vol. 212, p. 654.
  28. Abdel-Aziz, M., Yahia, I., Wahab, L., Fadel, M., and Afifi, M., *Appl. Surf. Sci.*, 2002, vol. 252, p. 8163.
  29. Zallen, R. and Moret, M., *Solid State Commun.*, 2006, vol. 137, p. 154.
  30. Brezova, V., Vreckova, Z., Billik, P., Caplovicova, M., and Plesch, G., *J. Photochem. Photobiol. A: Chem.*, 2009, vol. 206, p. 177.
  31. Hiie, J., Dedova, T., Valdna, V., and Muska, K., *Thin Solid Films*, 2006, vols. 511–512, p. 443.
  32. Dedova, T., Wienke, J., Goris, M., and Krunks, M., *Thin Solid Films*, 2007, vol. 515, p. 6064.
  33. Preis, S., Munter, R., and Siirde, E., *Ozone Sci. Eng.*, 1988, vol. 10, p. 379.
  34. Eaton, A. and Francon, M.A.H., in *Standard Methods for the Examination of Water and Wastewater*, Washington, DC: American Public Health Association, 2005, p. 1200.
  35. Barreto, R., Gray, K., and Anders, K., *Water Res.*, 1995, vol. 29, p. 1243.
  36. Guo, Z., Ma, R., and Li, G., *Chem. Eng. J.*, 2006, vol. 119, p. 55.
  37. Brillas, E., Mur, E., Sauleda, R., Sanchez, L., Peral, J., Domenech, X., and Casado, J., *Appl. Catal., B*, 1998, vol. 16, p. 31.
  38. Preis, S., Terentyeva, Y., and Rozkov, A., *Water Sci. Technol.*, 1997, vol. 35, p. 165.
  39. Klauson, D., Babkina, J., Stepanova, K., Krichevskaya, M., and Preis, S., *Catal. Today*, 2010, vol. 151, p. 39.



#### **Article IV:**

Budarnaja O., Klauson D., Dedova T., Kärber E., Viljus M., Preis S.,  
Template synthesis of titanium dioxide coatings and determination of their  
photocatalytic activity by aqueous oxidation of humic acid. – Kinetics and  
Catalysis 2014, in press.





# Template Synthesis of Titanium Dioxide Coatings and Determination of Their Photocatalytic Activity by Aqueous Oxidation of Humic Acid

Olga Budarnaja<sup>a</sup>, Deniss Klauson<sup>a\*</sup>, Tatjana Dedova<sup>b</sup>, Erki Kärber<sup>b</sup>, Mart Viljus<sup>c</sup>,  
Sergei Preis<sup>d</sup>

<sup>a</sup>*Department of Chemical Engineering, Tallinn University of Technology, Ehitajate tee 5,  
19086 Tallinn, Estonia*

<sup>b</sup>*Department of Material Science, Tallinn University of Technology, Ehitajate tee 5, 19086  
Tallinn, Estonia*

<sup>c</sup>*Materials Research Centre, Tallinn University of Technology, Ehitajate tee 5, 19086 Tallinn,  
Estonia*

<sup>d</sup>*LUT Chemistry, Lappeenranta University of Technology, P.O. Box 20, 53851 Lappeenranta,  
Finland*

\*e-mail: deniss.klauson@ttu.ee

**Abstract**—In this work, aqueous photocatalytic oxidation of humic acid, present in various waters as naturally occurring compound or anthropogenic pollutant, was studied using self-synthesized titanium dioxide coatings. To obtain the latter, template synthesis, widely used for the production of photocatalysts with improved surface properties and activity, was applied with variations in template material, N-cetyl-N,N,N-trimethylammonium bromide content. The catalysts were characterized using XRD, UV-VIS spectroscopy, and SEM. The activity of TiO<sub>2</sub> coatings in the degradation of humic acid proved to be superior to that of commercial photocatalyst P25 (Evonik). The dependence of the photocatalysts' performance on the template content in the synthesis precursors, which was responsible for the various surface features of the coatings, was established and explained.

*Keywords:* titanium dioxide, template synthesis, photocatalysis, humic substances

## 1. INTRODUCTION

Humic substances (**HS**) are the major constituents of various soil types, and, consequently, found in water bodies worldwide. They are the ultimate products of plant matter decomposition. In terms of chemical composition HS are polyaromatic molecules with carboxylic and phenolic groups. Due to their properties, HS are resistant to biological oxidation; being hydroxyl radical scavengers, they are hard to degrade by other chemical means as well. Numerous functional groups enable HS to bond aqueous toxics such as heavy metals and organic pollutants (e.g. pesticides), protecting them against water treatment methods and, thus, conveying them into treated drinking water [1]. In potable water, HS present a hazard as a source of carcinogenic and mutagenic trihalomethanes (**THMs**) formed as a result of water chlorination [2, 3]. Besides natural plant matter decomposition, HS are abundantly formed in landfill leachate due to anaerobic decomposition of lignocellulose [4]. There, HS are a matter of even greater concern because of high heavy metal and organic toxics contents that HS can bond with.

Photocatalytic oxidation (**PCO**) is an advanced oxidation process (**AOP**) that has the highest redox potential, proposing a promising alternative in elimination of toxic non-biodegradable compounds [5, 6]. The use of suspended titanium dioxide, the most widely studied semiconductor photocatalyst, is complicated due to the need to separate powdered  $\text{TiO}_2$  after water treatment. Alternatively, the catalyst may be attached to suitable solid support without the need for separation from the effluent streams [7]. Various techniques are known for the fixation of titanium dioxide onto the support matrix, e.g. dip-coating [8], sol-gel technique [9], electrochemical oxidation [7] and chemical vapour [10] or spray deposition [11]. While the use of photocatalytic films and coatings allows avoiding the slurries' drawbacks, the PCO efficiency of attached catalysts is lower and the problems in the design of reactors arise. However, depending on the reactor setup and the substances to be degraded, the decrease may be not very sharp, especially when taking into account the drastic decrease of photocatalyst dosage and no need for its separation [12].

In order to enhance the performance of photocatalysts, they can be prepared using template synthesis [13]. Meso- $\text{TiO}_2$  can be synthesized not only by sol-gel [14] or precipitation [15] but also by the template-directed approach. Template-directed materials generally possess structural and morphological abundance due to the diversity of employed template precursors [16, 17]. The template-synthesized materials normally exhibit small crystallite size, high

surface area, large surface-to-volume ratio, and favourable structural stability [18]. Surfactants have been employed as structure directing agents to produce a variety of meso-TiO<sub>2</sub> materials.

The first synthesis of a thermally stable hexagonally packed meso-TiO<sub>2</sub> by a modified sol-gel method using an alkyl phosphate surfactant was carried out by Antonelli and Ying in 1995 [19]. Since then, numerous templating agents have been used. Kobayashi and collaborators prepared a fibrous TiO<sub>2</sub> material with “macaroni”- like structure by using their designed amphiphilic compound containing cationic charge moieties [20]. Kavan *et al.* used a polymeric surfactant, poly (alkaline oxide) block copolymer, as templating agent for the formation of anatase TiO<sub>2</sub> and investigated essentially Li<sup>+</sup> insertion [21]. Yang and co-workers used amphiphilic poly (alkaline oxide) block copolymers as structuredirecting agents in non-aqueous solutions for organizing the network forming metal oxide species that include TiO<sub>2</sub> [22]. Byun *et al.* elucidated the beneficial role of cetyl trimethylammoniumbromide as surfactant in the enhancement of photovoltaic properties of mesoporous rutile TiO<sub>2</sub> [23]. Kavan *et al.* synthesized and characterized zirconia-stabilized 2.5 nm TiO<sub>2</sub> anatase crystallites in a mesoporous structure templated by cetyltrimethylammonium chloride [24]. The surfactant assisted templating method was used to fabricate high quality titania nanocrystals by various researchers for different applications (i.e. dye-sensitized solar cells) [25-29]. Sol-gel methods have often been used to prepare sub-micrometre-sized TiO<sub>2</sub> spheres by controlling the hydrolysis and condensation reactions, and their crystallized structure was formed by subsequent calcination at around 500 °C [14]. To conclude, the literature data available shows that the addition of various template substances to photocatalyst precursors during the synthesis can significantly improve the performance of the resulting materials against a range of substrates.

The goal of the present study was the template synthesis of active titanium dioxide coatings capable of efficiently degrading humic substances, with the establishment of optimal template-to-precursor ratio, which results in the highest activity.

## 2. EXPERIMENTAL

Titanium (III) chloride 15 % solution in 10 % HCl, used as titanium precursor, was acquired from Merck, as well as the template, N-cetyl-N,N,N-trimethylammonium bromide (CTAB).

For the photocatalyst coating synthesis, CTAB solutions with the concentrations of 0 to 3  $\mu\text{g mL}^{-1}$  in  $\text{TiCl}_3$  reagent were prepared. The solutions were sprayed with compressed air upon chromic acid-washed Pyrex glass plates (8 to 12  $\text{cm}^2$ ), deposited upon molten tin. The temperature of the glass plate surface was maintained at 220 °C. After ten deposition cycles, the coatings were annealed at 400 °C for 4 h, in order to remove the template, and were further treated under UV (details see below) in distilled water for 24 h. After subsequent drying, the photocatalytic coatings were ready for use. For comparison with Degussa P25 titanium dioxide, P25 was deposited upon identical glass from slurry containing 1  $\text{g L}^{-1}$  titanium dioxide by spraying and drying.

Crystal structure of the photocatalyst coatings were determined by X-ray diffraction (**XRD**). Rigaku Ultima IV diffractometer using  $\text{Cu K}\alpha$  radiation ( $\lambda=1.5406 \text{ \AA}$ , 40 kV at 40 mA) with Bragg–Brentano geometry conditions in the  $\Theta$ - $2\Theta$  regime was used. Joint Committee on Powder Diffraction Standards (**JCPDS**) file no. 01-075-2547 was used as the XRD reference standard. Crystallite size was calculated using the Debye-Scherrer method and the Scherrer constant of 0.94.

The total and diffuse reflectance spectra of the coatings were measured in the wavelength range of 300 – 2500 nm using Jasco V-670 UV–VIS–NIR spectrophotometer equipped with an integrating sphere. Obtained data were used to calculate the absorption coefficient ( $\alpha$ ) and subsequently optical band gap values ( $E_g$ ).

Surface morphology of the photocatalyst coatings was analysed using Zeiss EVO MA-15 scanning electron microscope (**SEM**), working in secondary electron mode. Accelerating voltage was 13 kV, and the working distance was 6.5 to 7 mm.

The activity of the photocatalytic coatings was tested by aqueous PCO of synthetic solutions of humic acid sodium salt (**HA**, Merck) with the concentration of 25  $\text{mg L}^{-1}$ . The experimental setup was similar to the one applied in the authors' previous studies (see e.g. [30]). The experiments were performed at  $20\pm 1$  °C in 200-mL batch glass reactors equipped with magnet stirrers, positioned under reflector-equipped light source. Each experiment involved the use of two reactors, active (with PCO taking place) and blank (to estimate the concentration changes due to water evaporation during the experiment). Photocatalyst-coated plates were positioned on top of Pyrex plates submerged into the solution to the depth of ca. 10 mm. Philips Actinic 15 W lamps were used as the UV source with the maximum energy emission at 365 nm, with irradiance of about 1  $\text{mW cm}^{-2}$  measured at the surface of the

solution (23 cm from the lamp) with Ocean Optics USB 2000+ radiometer. The pH was monitored, but not adjusted; initial pH of HA solution was about 6.5, and changed insignificantly during the treatment. The treatment time was chosen to be 24 h. Parallel experiments were carried out three times under identical conditions, with the average deviation of data being under 5%. For HA concentration, colour was determined with the spectrophotometer HACH Lange DR 2800 at 455 nm. The UV-absorbance of HA samples at 254 nm was measured by Spectronic Unicam spectrophotometer (Helios  $\beta$ ), which was correlated with the content of HA by calibration line. These analytical procedures were used by the authors previously [31], and indicated no interference of HA PCO by-products. Dark adsorption of humic acid was determined in 24 h experiments without irradiation, with adsorbed amount measured from the mass balance: concentration of humic acid was determined before and after contact with photocatalytic coatings. The performance of the coatings synthesised in this work was compared to that of P25 (Evonik), with the latter photocatalyst deposited upon glass plate by spraying.

The results of PCO were described by efficiency  $E$ , showing the rate of HA degradation relative to the amount of energy reaching the photocatalyst coating surface. The PCO efficiency was calculated as follows [32]:

$$E = \frac{\Delta c \cdot V \cdot 1000}{I \cdot S \cdot t} \quad (1)$$

where  $\Delta c$  is the difference in HA concentration before and after PCO,  $\text{mg L}^{-1}$ ,  $V$  – volume of the treated solution, L,  $I$  – irradiance,  $\text{mW cm}^{-2}$ ,  $S$  – photocatalyst-coated plate surface area,  $\text{cm}^2$ , and  $t$  – treatment time, h.

### 3. RESULTS AND DISCUSSION

#### 3.1. Photocatalytic Coatings Characterization

For titanium dioxide photocatalysts, the evidence supporting both direct [33, 34] and indirect [33, 35-40] electron transition for various titanium dioxide crystalline modifications has been published. The majority of the publications published within the last decade report indirect transition for titanium dioxide. The band gap values of the photocatalysts synthesised in the present research were calculated assuming both transition types. A standard expression for transitions between two parabolic bands for the calculation of band gap energy was used [41, 42]:

$$(\alpha h\nu)^m = A(h\nu - E_g) \quad (2)$$

where  $h\nu$  is the quantum energy, eV;  $\alpha$  is the absorption coefficient,  $\text{cm}^{-1}$ ;  $E_g$  is the optical band gap, eV;  $A$  is constant;  $m = 2$  for direct transition, and  $m = 1/2$  for indirect transition.

Band gap values were found from the intercept of the linear fit of  $(\alpha h\nu)^m$  vs  $h\nu$  plot extrapolated to the zero absorption. Haze factor values were calculated as the relationship of diffused reflectance to total reflectance; it shows the extent of light scattering, and, thus, the relative roughness of the photocatalysts' particle surface [43].

The results of the coatings' XRD measurements can be seen in Fig. 1a. In all samples, only anatase phase was identified with (1 0 1) peak being pronounced in all catalysts preferable orientation – 101. It was followed by (0 0 4), (2 0 0), (1 0 5), (2 1 1) and (2 0 4) peaks, indicating the sample containing  $1.0 \mu\text{g mL}^{-1}$  CTAB in synthesis precursors exhibiting also showed (1 1 6) and (2 1 5) peaks. The coatings showed developed crystal orientation, except the sample containing  $2.0 \mu\text{g mL}^{-1}$  CTAB in synthesis precursors, which has rather amorphous structure. Crystallite size, calculated for anatase (1 0 1) peaks according to Scherrer equation, varies between 14 and 19 nm (Fig. 1b), with the minimum observed at  $0.5 \mu\text{g mL}^{-1}$  CTAB content in precursors.

Optical measurements reveal that total (Fig. 2a) and diffused (Fig. 2b) reflectance in general increase with the template addition to the precursors, being in the range of 50 to 60 % of the incident irradiation at the 400 nm wavelength. Reflectance measurements suggest that smaller photocatalyst grains dominate over the larger ones, as the reflectance decreases with the wavelength increase. The lowest reflectance was exhibited by the coating with  $2 \mu\text{g mL}^{-1}$  template in synthesis precursors, which, according to the XRD analysis, has amorphous structure. Both total and diffuse reflectance at 400 nm had the highest and almost identical values of ca. 65 and 45 %, respectively, with the catalysts containing 0.25 to  $1 \mu\text{g mL}^{-1}$  template. Haze factor values (Fig. 2c), indicating surface roughness and light scattering ability, steadily increased with the CTAB concentration increasing from 0.5 to  $1 \mu\text{g mL}^{-1}$ . Higher concentrations of template lead to the decreased haze factor of the specimens. Haze factor values at curtain wavelengths of 500, 1000 and 1500 nm decrease with increasing wavelength, which also indicates that smaller grains dominate over the larger ones.

Optical band gap energy values, calculated for both direct and indirect electron transition (see Table 1), were in good agreement with those expected for pure anatase. The error of Eg

values is mainly connected to the extrapolation procedure of the linear part of the  $(ah\nu)^m$  vs  $h\nu$  plot to the zero absorption and usually does not exceed 0.03 eV. No connection between the template content and the band gap energy was observed.

The coatings' surface structure SEM analysis results are given in Fig. 3a to 3f. One can see that the photocatalyst coating surface has several clearly distinguishable surface features, namely cracks, pores of various size, flake-like crystals, collapsed and unbroken bubbles. Beside these, the structure is fairly homogeneous, although at higher CTAB concentrations the photocatalysts are in the form of coalescent droplets separated by bare glass substrate, as opposed to homogeneous coatings obtained at smaller CTAB concentrations. Cracks should be attributed to annealing process eliminating template, whereas the other surface features can be directly linked with the CTAB concentration. The thickness of the coatings was measured to be generally between 6 and 15  $\mu\text{m}$ , with thicker coatings obtained at higher CTAB concentrations.

The average number of surface features was calculated for five randomly selected  $90 \times 120 \mu\text{m}$  rectangles for every sample with the average values derived. The dependence of the surface feature average numbers on the CTAB concentration in synthesis precursor solution can be seen in Fig. 4. The amount of pores dramatically increased with the addition of the template, reaching the maximum at  $0.25 \mu\text{g mL}^{-1}$  CTAB, and steadily decreasing with further increase of CTAB concentration in the coating precursor. Similar dependence can be seen for unbroken bubbles on the surface, although at the highest CTAB concentration the unbroken bubbles amount somewhat increased.

According to the SEM micrograms (Fig. 3), the pore size steadily increased with the increasing CTAB concentration. The number of collapsed bubbles, on the other hand, increases up to  $0.5 \mu\text{g mL}^{-1}$  CTAB, declining with further increase in template content; this way it is reversely consistent with the observed behaviour of the crystallite size (see Fig. 1b). Also, maximum amount of flake-like structures can be seen on the photocatalyst coating with  $1 \mu\text{g mL}^{-1}$  CTAB content in the precursor solution.

The described surface observations may be explained by the behaviour of CTAB micelles, from which pores, collapsed and unbroken bubbles originate. At smaller CTAB concentrations larger micelles are formed, and with the increased template concentration their diameter decreases at the simultaneously increased number. On the other hand, agglomeration of smaller micelles is expected with increasing CTAB concentration, thus resulting in the



decrease of pores number with their increased dimensions. Bubbles are likely to originate from micelles located deeper within the coating, as opposed to the coating surface: dependent on the micelles' depth, bubbles can either remain intact or collapse. The surface concentration of the unbroken bubbles follows the pattern of pores, indicating similarity in their origin. With collapsed bubbles, however, their maximum surface concentration is shifted towards greater CTAB concentrations; this tendency is similar to the decrease in the crystallite size.

### ***3.2. Humic Acid Adsorption***

No HA adsorption was determined in respective experiments [within the limits of analytical precision \( \$0.5 \text{ mg L}^{-1}\$ \)](#), which suggests oxidation by hydroxyl radicals in the vicinity of the photocatalytic coating surface as the predominant HA PCO mechanism, as opposed to hole-induced oxidation of adsorbed pollutants.

### ***3.3. Photocatalytic Oxidation of Humic Acid***

The dependence of the efficiency of aqueous PCO of HA on the concentration of CTAB in photocatalysts' synthesis precursors can be seen in Fig. 5. One can see its similarity to the dependence of the pores and collapsed bubbles on CTAB concentration, indicating that the porosity and the availability of collapsed bubble feature on the surface of titanium dioxide coatings are mainly responsible for the PCO efficiency of HA. The connection to the crystallite size decrease may also be observable: this similarity can be explained by the possibly greater concentration of  $\text{TiO}_2$  surface defects in pores and on the edges of the collapsed bubbles, acting as traps of positively charged holes as was also observed by [44].

However, since no HA adsorption by the synthesized catalysts was experimentally determined within the limits of analytical precision, the more porous surface is not likely to be responsible for better PCO of HA. The edges of collapsed bubbles, on the other hand, protruding into the treated solutions, can act as "radical volcanoes" producing the oxidants responsible for HA oxidation. The combination of maximum number of collapsed bubbles and the smallest crystallites is able to produce the highest amount of sharp spiked catalyst edges with larger area possessing greater defect concentration, which results in enhanced radical production; [in turn, enhanced radical generation is a key factor in the establishment optimal degradation conditions for organic substrate, allowing treatment of solutions with higher concentration and shorter contact time \[45\]](#).



When comparing the performance of template synthesized photocatalyst coatings with the one of spray-deposited Degussa P25, it was seen that the performance of the coatings was comparable to or superior to that of P25, with the PCO efficiency values being up to around 1.5 times higher.

#### 4. CONCLUSIONS

Template-synthesized photocatalytic TiO<sub>2</sub> coatings deposited on Pyrex glass were characterized using XRD, UV-VIS absorbance, and SEM, and their photocatalytic activity was tested by degradation of humic acid in aqueous solutions. N-cetyl-N,N,N-trimethylammonium bromide was used as the template, with its concentration in synthesis precursor solution ranging from 0 to 3 µg mL<sup>-1</sup>. When comparing the results of the aqueous photocatalytic oxidation with the coatings' surface morphology, the collapsed bubble-like structures appeared to be mainly responsible for the oxidation, as opposed to pores, unbroken bubbles and flake-like crystals. This can be explained by denser localization of surface defects on the edges of collapsed bubbles, acting as hole traps and localized sources of hydroxyl radicals protruding into the treated aqueous solution.

#### ACKNOWLEDGEMENTS

The authors would like to express their gratitude to Estonian Science Agency projects IUT1-7 and IUT19-4, Estonian Science Foundation grant GUS 10, US Civilian Research and Development Foundation grant ESC2-2974-TL-09 and European Regional Development Fund (Centre of Excellence "Mesosystems: Theory and Applications" TK114, 3.2.0101.11-0029) for the financial support of the research.

#### REFERENCES

1. *Manahan, S.E.* Environmental Chemistry. New York: CRC Press/Lewis Publishers 1994.
2. *Eggins, B.R., Palmer, F.L., Byrne, J.A.* // Water Res. 1997, V. 31, P. 1223.
3. *Wang, G.S., Liao, C.H. Wu, F.J.* // Chemosphere 2001, V. 42 P. 379.
4. *Sanchez-Monedero, M.A., Roig, A., Cegarra, J., Bernal, M.P.* // Biores. Technol. 1999, V. 70, P. 193.
5. *Sun, B., Sato, M., Clements, J.S.* // J. Electrostat. 1997. V. 39, P. 189.
6. *Bahnemann, D.* // Solar Energy 2004, V. 77, P. 445.
7. *Byrne, J.A., Eggins, B.R., Brown, N.M.D., McKinney, B., Rouse, M.* // Appl. Catal. B 1998, V. 17, P. 25.

8. Herrmann, J.M., Tahiri, H., Guillard, C., Pichat, P. // *Catal. Today* 1999, V. 54, P. 131.
9. Neppolian, B., Jung, H., Choi, H. // *J. Adv. Oxid. Technol.* 2007, V. 10, P. 369.
10. Bessergenev, V.G., Pereira, R.J.F., Mateus, M.C., Khmelinskii, L., Vasconcelos, D.A., Nicula, R., Burkel, E., do Rego, A.M.B., Saprykin, A.I. // *Thin Solid Films* 2006, V. 503, P. 29.
11. Morozova, M., Kluson, P., Dzik, P., Vesely, M., Baudys, M., Krysa, J., Solcova, O. // *J. Sol-Gel Sci. Technol.* 2013, V. 65, P. 452.
12. Klauson, D., Preis, S., Portianskaja, E., Kachina, A., Krichevskaya, M., Kallas, J. // *Environ. Technol.* 2005, V. 26, P. 653.
13. Lee, A.-C., Lin, R.-H., Yang, C.-Y., Lin, M.-H., Wang, W.-Y. // *Mater. Chem. Phys.* 2008, V. 109, P. 275.
14. Jiang, X.C., Herricks, T., Xia, Y.N. // *Adv. Mater.* 2003, V. 15, P. 1205.
15. Castro, A.L., Nunes, M.R., Carvalho, A.P., Costa, F.M., Florencio, M.H. // *Solid State Sci.* 2008, V. 10, P. 602.
16. Schüth, F., Schmidt, W. // *Adv. Mater.* 2002, V. 14, P. 629.
17. Lee, J., Han, S., Hyeon, T. // *J. Mater. Chem.* 2004, V. 14, P. 478.
18. Gajjala, S.R., Ananthanarayanan, K., Yap, C., Gratzel, M., Balaya, P. // *Energy Environ. Sci.* 2010 V. 3, P. 838.
19. Antonelli, D.M., Ying, J.Y. // *Angew. Chem. Int. Edn. Eng.* 1995, V. 34, P. 2014.
20. Kobayashi, S., Hanabusa, K., Hamasaki, N., Kimura, M., Shirai, H., Shinkai, S. // *Chem. Mater.* 2000, V. 12, P. 1523.
21. Kavan, L., Rathouský, J., Grätzel, M., Shklover, V., Zukal, A. // *Micropor. Mesopor. Mater.* 2001, V. 44–45, P. 653.
22. Yang, P.D., Zhao, D.Y., Margolese, D.I., Chmelka, B.F., Stucky, G.D. // *Nature* 1998, V. 396, P. 152.
23. Byun, H.Y., Vittal, R., Kim, D.Y., Kim, K.J. // *Langmuir* 2004, V. 20, P. 6853.
24. Kavan, L., Attia, A., Lenzmann, F., Elder, S.H., Gratzel, M. // *J. Electrochem. Soc.* 2000, V. 147, P. 2897.
25. Koshitani, N., Sakulphaemaruehai, S., Suzuki, Y., Yoshikawa, S. // *Ceram. Int.* 2006, V. 32, P. 819.
26. Ngamsinlapasathian, S., Sreethawong, T., Suzuki, Y., Yoshikawa, S. // *Solar Energy Mater. Solar Cells* 2006, V. 90, P. 2129.
27. Ngamsinlapasathian, S., Sreethawong, T., Yoshikawa, S. // *Thin Solid Films* 2008, V. 516, P. 7802.
28. Adachi, M., Murata, Y., Harada, M., Yoshikawa, S. // *Chem. Lett.* 2000 V. 8, P. 942.
29. Alexaki, N., Stergiopoulos, T., Kontos, A.G., Tsoukleris, D.S., Katsoulidis, A.P., Pomonis, P.J., LeClere, D.J., Skeldon, P., Thompson, G.E., Falaras, P. // *Micropor. Mesopor. Mater.* 2009, V. 124, P. 52.
30. Klauson, D., Preis, S. // *Int. J. Photoenergy* 2005, V. 7, P. 175.
31. Portjanskaja, E., Stepanova, K., Klauson, D., Preis, S. // *Catal. Today* 2009, V. 144, P. 26.
32. Preis, S., Krichevskaya, M., Terentyeva, Y., Moiseev, A., Kallas, J. // *J. Adv. Oxid. Technol.* 2002, V. 5, P. 77.
33. Reddy, K., Manorama, S., Reddy, A. // *Mater. Chem. Phys.* 2003, V. 78, P. 239.
34. Magne, C., Cassaignon, S., Lancel, G., Pauporte, T. // *Chem. Phys. Chem.* 2011, V. 12, P. 2461.
35. Koelsch, M., Cassaignon, S., Guillemoles, J., Jolivet, J. // *Thin Solid Films* 2002, V. 403, P. 312.
36. Tanemura, S., Miao, L., Jin, P., Kaneko, K., Terai, A., Nabatova-Gabain, N. // *Appl. Surf. Sci.* 2003, V. 212, P. 654.
37. Abdel-Aziz, M., Yahia, I., Wahab, L., Fadel, M., Afifi, M. // *Appl. Surf. Sci.* 2002, V. 252, P. 8163.
38. Zallen, R., Moret, M. // *Solid State Commun.* 2006, V. 137, P. 154.
39. Di Paola, A., Cufalo, G., Addamo, M., Ellardita, M.B., Campostrini, R., Ischia, M., Ceccato, R., Palmisano, L. // *Colloids Surf A* 2008, V. 317, P. 366.

40. Brezova, V., Vreckova, Z., Billik, P., Caplovicova, M., Plesch, G. // J. Photochem. Photobiol. A Chem. 2009, V. 206, P. 177.
41. Dedova, T.; Wienke, J.; Goris, M.; Krunks, M. // Thin Solid Films 2007, V. 515, P. 6064.
42. Hiie, J.; Dedova, T.; Valdna, V.; Muska, K. // Thin Solid Films 2006, V. 511, P. 443.
43. Lin, C., Yu, W., Chien, S. // Appl. Phys. Lett. 2007, V. 91, P. 233120.
44. Serpone, N., Sauve, G., Koch, R., Tahiri, H., Pichat, P., Piccinini, P., Pelizzetti, E., Hidaka, H. // J. Photochem. Photobiol. A 1996, V. 94, P. 191.
45. Jiang, W., Joens, J.A., Dionysiou D.D., O'Shea K.E. // J. Photochem. Photobiol. A. 2013, V. 262, P. 7.

**Fig. 1.** X-ray diffraction pattern of titanium dioxide coatings, dependent on the concentration of CTAB in synthesis precursors from 0 to 3.0  $\mu\text{g mL}^{-1}$ (a) and changes in anatase (1 0 1) crystallite size with the increased CTAB content in synthesis precursors (b).

**Fig. 2** The dependence of total (a) and diffused (b) reflectance, and haze factor (c) on the template content in the coatings' synthesis precursors.

**Table 1.** Optical band gap values of titanium dioxide coatings, calculated for direct and indirect electron transition.

C(CTAB), $\mu\text{g mL}^{-1}$	Direct band gap, eV	Indirect band gap, eV
0	3.19	2.85
0.25	3.21	3.04
0.5	3.19	3.11
1	3.22	3.03
2	3.10	2.85
3	3.20	2.92

**Fig. 3.** SEM microgrammes of  $\text{TiO}_2$  coatings deposited at different CTAB concentrations,  $\mu\text{g mL}^{-1}$ : a) 0; b) 0.25; c) 0.5; d) 1.0; e) 2.0; f) 3.0.

**Fig. 4.** The dependence of average number of surface features of  $\text{TiO}_2$  coatings on the content of template in synthesis precursors.

**Fig. 5.** The dependence of the efficiency of photocatalytic oxidation of humic acid on the content of template in the precursors of coatings' synthesis.

**Fig. 1.** X-ray diffraction pattern of titanium dioxide coatings, dependent on the concentration of CTAB in synthesis precursors from 0 to 3.0  $\mu\text{g mL}^{-1}$ (a) and changes in anatase (1 0 1) crystallite size with the increased CTAB content in synthesis precursors (b).

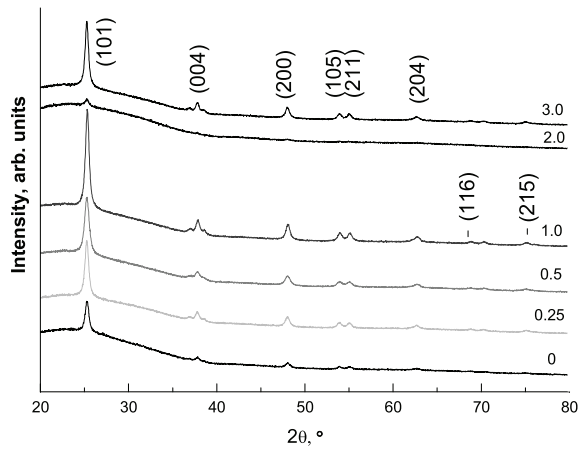
**Fig. 2** The dependence of total (a) and diffused (b) reflectance, and haze factor (c) on the template content in the coatings' synthesis precursors.

**Table 1.** Optical band gap values of titanium dioxide coatings, calculated for direct and indirect electron transition.

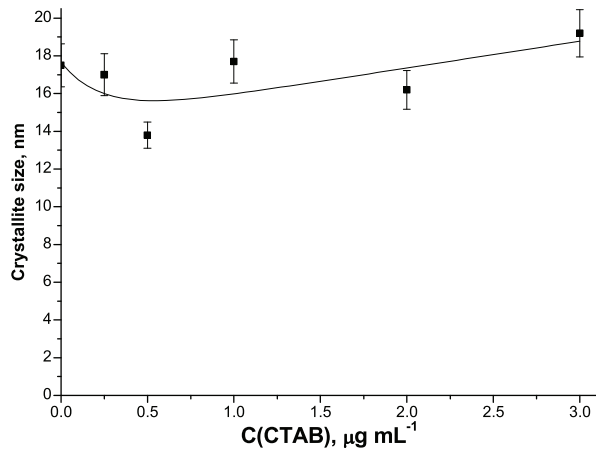
**Fig. 3.** SEM microgrammes of  $\text{TiO}_2$  coatings deposited at different CTAB concentrations,  $\mu\text{g mL}^{-1}$ : a) 0; b) 0.25; c) 0.5; d) 1.0; e) 2.0; f) 3.0.

**Fig. 4.** The dependence of average number of surface features of  $\text{TiO}_2$  coatings on the content of template in synthesis precursors.

**Fig. 5.** The dependence of the efficiency of photocatalytic oxidation of humic acid on the content of template in the precursors of coatings' synthesis.

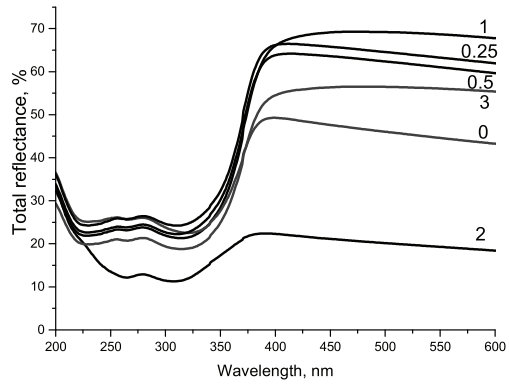


a)

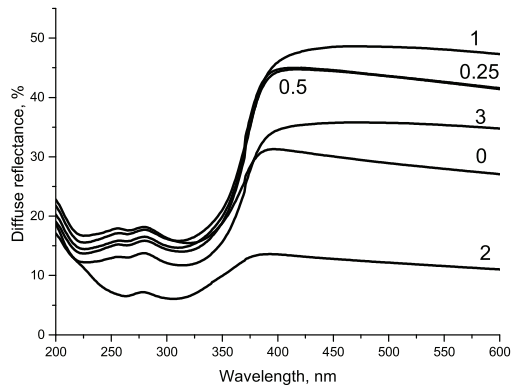


b)

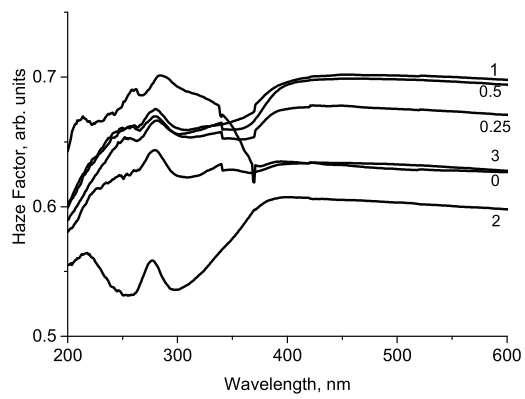
Fig. 1, Budarnaja



a)



b)



c)

Fig. 2, Budarnaja

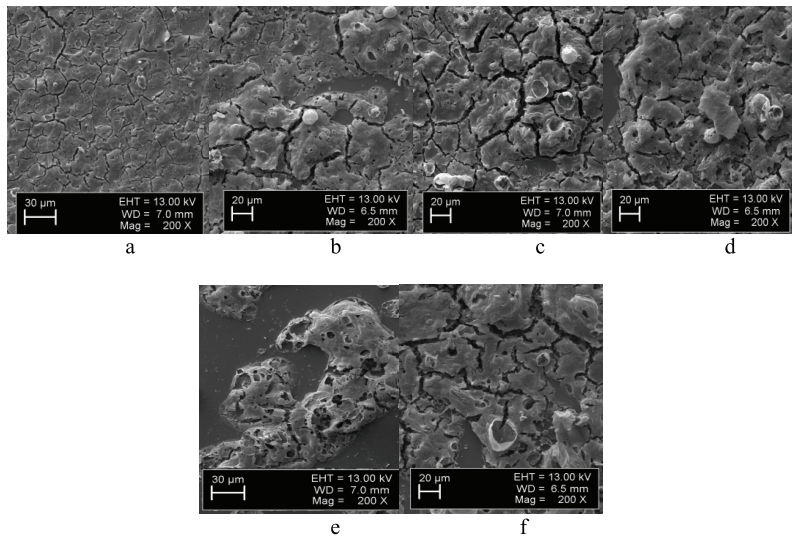


Fig. 3, Budarnaja



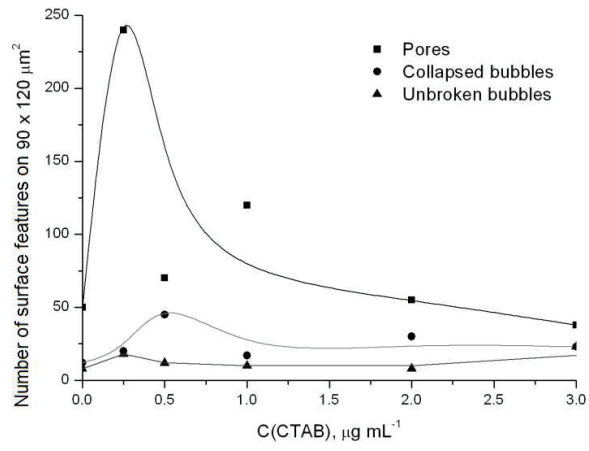


Fig. 4, Budarnaja

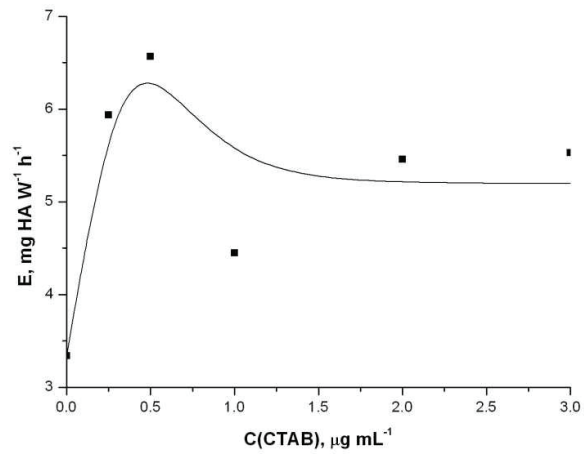


Fig. 5, Budarnaja

#### **Article V:**

Klauson D., Budarnaja O., Castellanos Beltran I., Krichevskaya M., Preis S., Photocatalytic decomposition of humic acids in anoxic aqueous solution producing hydrogen, oxygen and light hydrocarbons. *Environmental Technology*, 2014, in press, doi: 10.1080/09593330.2014.900116.



## Photocatalytic decomposition of humic acids in anoxic aqueous solutions producing hydrogen, oxygen and light hydrocarbons

Deniss Klauson<sup>a\*</sup>, Olga Budarnaja<sup>a</sup>, Ignacio Castellanos Beltran<sup>b</sup>, Marina Krichevskaya<sup>a</sup> and Sergei Preis<sup>c</sup>

<sup>a</sup>Department of Chemical Engineering, Tallinn University of Technology, Ehitajate tee 5, Tallinn 19086, Estonia; <sup>b</sup>Department of Chemical and Biological Engineering, University of Colorado, UCB 596, ECCH 111, 1111 Engineering Drive, Boulder, CO 80309, USA; <sup>c</sup>LUT Chemistry, Lappeenranta University of Technology, P.O. Box 20, 53851 Lappeenranta, Finland

(Received 19 November 2013; accepted 26 February 2014)

Photocatalytic water splitting for hydrogen and oxygen production requires sacrificial electron donors, for example, organic compounds. Titanium dioxide catalysts doped with platinum, cobalt, tungsten, copper and iron were experimentally tested for the production of hydrogen, oxygen and low molecular weight hydrocarbons from aqueous solutions of humic substances (HS). Platinum-doped catalyst showed the best results in hydrogen generation, also producing methane, ethene and ethane, whereas the best oxygen production was exhibited by P25, followed by copper – and cobalt-containing photocatalysts. Iron-containing photocatalyst produced carbon monoxide as a major product. HS undergoing anoxic photocatalytic degradation produce hydrogen with minor hydrocarbons, and/or oxygen. It appears that better hydrogen yield is achieved when direct HS splitting takes place, as opposed to HS acting as electron donors for water splitting.

**Keywords:** humic substances; photocatalysis; hydrogen generation; doped titanium dioxide; template synthesis

### 1. Introduction

The problem of growing energy consumption at the likely shortages in fossil fuels and the environmental degradation has raised the questions of alternative, environmental-friendly sustainable energy sources. One of the ‘green fuels’ hydrogen has a high combustion heat coupled with reduced greenhouse gas emissions when compared with fossil fuels.[1] Among various possibilities in hydrogen production, semiconductor photocatalysis is one of the promising ones being a powerful and relatively inexpensive process: due to the high oxidation potential of the positively charged holes on the surface of semiconductor photocatalysts, especially titanium dioxide,[2,3] it is possible to directly split water into hydrogen and oxygen transforming solar radiation to energy-rich products.

In a semiconductor, the action of electromagnetic radiation with the quantum energy equal to or exceeding the semiconductor’s band gap results in the simultaneous formation of a single-electron oxidant, positively charged hole and the reductant, conductivity electron, which are spatially separated in the electric field at the solid–liquid interface. Following that, the catalytic oxidation of water to free oxygen with the positively charged hole starts simultaneously with the reduction of protons to hydrogen with the conductivity electron. The principal difficulty in this scenario is the fast electron-hole recombination taking place in up to 40 ns.[4] This makes the quantum yield of the

photocatalytic reaction on the plain semiconductors very small, at a centime fraction of percent level.

The success in the water decomposition reaction depends on the spatial separation of the electron-hole pair and the catalytic reactions’ rate in oxidation and reduction of water. Starting from the first publications,[5] photocatalytic water decomposition under UV radiation was extensively studied in 1980s and 1990s.[6,7] Since then, there has been constantly growing interest in the use of various promoters with the function of advancement of certain catalytic reaction stages in reduction of water to hydrogen and oxidation of it to oxygen. For example, the dopants such as Cr, V, Mn, Fe, Co, Ag, Pt, (d-elements), N and Be expand the activity spectrum of titanium dioxide to the visible range.[8–14] However, the light absorbance coefficient of doped semiconductors can be considerably lower than that of the corresponding coefficient of the semiconductor itself.[15] Also, the redox potential of semiconductors was reported to decrease on doping,[16] which may be compensated by the enlarged utilizable wavelengths diapason making the water decomposition efficiency improved.

For the last years, a considerable growth in number and the complexity of the photocatalytic systems for the decomposition of water was observed as a result of increased interest towards hydrogen power. The data on high photoactivity of titanium dioxide doped with, e.g. nitrogen [17,18] and the Au-doped mesoporous titanium dioxide [19] were

\*Corresponding author. Email: deniss.klauson@ttu.ee

published. Various systems based on the In, Sn, Sb and Ge compounds doped with ions of strontium, niobium, tantalum and other metals showed certain activity in water decomposition under the UV radiation.[20–27]

Besides the choice of effective photocatalytic material, two prerequisites must be fulfilled in order for the photocatalytic water splitting to proceed successfully: the solution to be treated must be free of oxygen and to slow down the electron-hole recombination, additional electron donor is needed in excess. It has been reported [28–32] that the availability of electron donors can enhance hydrogen evolution by several orders of magnitude. For this purpose, many inorganic and organic substances can be utilized. It is seen that the electron donors are sacrificial, i.e. they are oxidized on course of the photocatalytic water splitting.[30] When organic substances are added as donors for water splitting, one must also bear in mind the possibility of their direct photocatalytic degradation coupled with hydrogen production.[30,33]

Naturally, when speaking of sacrificial electron donors, putting non-biodegradable recalcitrant water pollutants into that role presents a possibility of two problems, waste decomposition and fuel production, being solved simultaneously. Variable hydrogen yield upon the changes in wastewater composition may still be considered as a better option than straightforward degradation of the pollutants without getting beneficial side-products. Different pollutant classes have been shown yielding to hydrogen-producing photocatalysis, such as aromatics, dyes, organic acids, urea and urine, estrogens, chemical warfare agents, etc. [1,28–30,34,35]. Photocatalysis could effectively serve as pre- or especially after-treatment stage in combination with conventional treatment methods for the removal of recalcitrant pollutants.[36]

Humic substances (HS) are the coloured ultimate products of plant tissue decomposition of a polyaromatic character with carboxylic and phenolic groups. Being objectionable to water end users, HS are resistant to biological oxidation and HS present a hazard as a source of carcinogenic and mutagenic trihalomethanes formed as a result of water chlorination.[37,38] Abundantly formed in landfill leachate due to anaerobic decomposition of lignocellulose,[39] HS are of great concern due to bonding aqueous toxics such as heavy metals and organic pollutants, e.g. pesticides.[40] Bonding makes the toxics soluble in complex form and thus difficult to remove by conventional water treatment methods.[41]

Waste streams, such as landfill leachates, or natural surface waters containing sufficient quantities of HS, may be of great interest for the production of clean non-fossil fuel, hydrogen, with HS serving as a sacrificial electron donor in photocatalytic water splitting: non-biodegradable waste decomposition and fuel production by a cost-efficient method are achieved simultaneously. Since photocatalysis is powerful, but slow process, in this work the authors were interested in testing the abilities of several selected

photocatalysts for the establishment of maximal hydrogen and oxygen production within a relatively short treatment time.

The goal of the present study is the comparison of several visible light-utilizing titanium-dioxide-based photocatalysts in terms of producing hydrogen from humic acid sodium salt (taken as a representative of HS) solutions under simulated solar irradiation, combining organic pollutant removal with fuel gas production.

## 2. Materials and methods

The experiments were conducted using 5 ml of the synthetic solutions of humic acid sodium salt (HA, CAS 68131-04-4, Arcos Organics), with the initial concentration of  $100 \text{ mg L}^{-1}$ ; photocatalysts were used as  $1 \text{ g L}^{-1}$  slurries stirred at 350 rpm. Schematic outline of the experimental setup can be seen in Figure 1. The reactor was a glass vial equipped with magnet stirrer; the vial was placed in a hermetically sealed metal reactor (interior volume 48.2 ml) with a window on top for the solution illumination. Solar simulator (Abet Technologies) with the equivalent of 1 SUN ( $\approx 100 \text{ mW cm}^{-2}$ ) was used as the radiation source; a Petri dish with water layer was placed between the reactor and solar simulator to cut off IR part of the radiation spectrum. The solution was purged with nitrogen ( $0.15 \text{ L min}^{-1}$ ) for 0.5 h before the experiment to eliminate oxygen, and then the reaction system was purged for another 0.5 h with argon ( $0.1 \text{ L min}^{-1}$ ), which was used as the carrier for the gas chromatography system in subsequent reaction gaseous products analysis. At the start of the experiment, oxygen was present neither in the solution nor in the reaction system. The treatment time 4 h was chosen to obtain at least 50% HA removal by P25 Evonik, often applied as a reference photocatalyst, and enable comparison of the photocatalysts' potentials in water splitting in terms of gaseous products amounts. For the HA concentration measurement, the analytical procedure

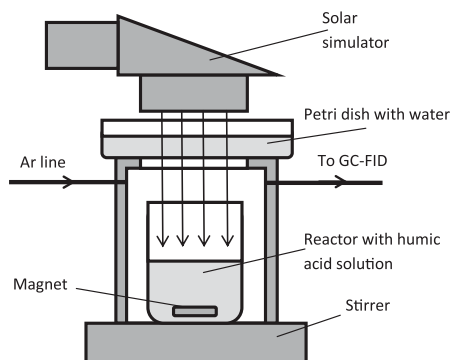


Figure 1. Schematic outline of the photocatalytic experimental setup.

used previously was applied:[42] after filtration, colour at 455 nm was determined with the Thermo Scientific Evaluation 300 UV-Vis dual-wavelength spectrophotometer with the results interpreted using VisionPro software. In the end of each experimental run, the gaseous products in 1-ml sample were analysed using the Hewlett Packard Gas Chromatograph, model #61540A with the thermal conductive detector and the flame ionizer detector, with the concentrations expressed as parts per million (ppm). A combination of the mentioned detectors allows measuring both combustible and non-combustible (i.e. CO<sub>2</sub>) gaseous products of HA degradation. The experiments were performed at pH around 6.5, which was monitored along the experiment together with the temperature, but not adjusted. During the experimental runs, the pH changes were small, mostly an increase of 0.2–0.3. Adsorption of HA, which may be an important step preceding the immediate degradation reactions,[43] was investigated at the same temperature conditions in the dark, with the amount of adsorbed HA calculated from batch mass balance using initial and final HA concentrations on the solution.

Copper-containing hydrogen-treated titanium dioxide sample was synthesized by sol-gel method, as described by Chen et al.,[44] loaded with pre-calculated amount of copper (I) acetate to achieve 0.5% of copper in the catalyst, dried under vacuum and then calcinated at 400°C for 3 h. This was followed by the drying period at 200°C with H<sub>2</sub> gas introduced to the pressurized compartment at 200°C and 25 bar. The sample was left in the reactor for 3 days and then cooled down to ambient temperature. Platinum-containing photocatalyst was produced by Vorontsov et al.,[45] referred in their publication as the specimen C. Cobalt- and tungsten-containing photocatalysts were obtained by the hydrolysis of TiCl<sub>3</sub> (15% solution in 10% HCl, Merck) in the presence of cetyl trimethylammonium bromide (0.005 μg ml<sup>-1</sup>, Merck) as the template with dopant sources, Co(OOCCH<sub>3</sub>)<sub>2</sub> (9.4 μg ml<sup>-1</sup> solution) and Na<sub>2</sub>WO<sub>4</sub> (1.17 μg ml<sup>-1</sup> solution), respectively, added to the solution. The precipitate was dried at room temperature and calcinated at 400°C to remove template. Iron-containing titanium dioxide sample was prepared by a variation of sol-gel method: 75 ml of Ti(OBu)<sub>4</sub> (25% solution in *t*-butyl alcohol, Merck) was sprayed into 1 L of pre-sonicated Fe<sub>2</sub>O<sub>3</sub> suspension (0.5 g L<sup>-1</sup>). Hydrolysis was followed by sonication, and after drying at room temperature the product was calcinated at 200°C. After calcinations, all the last three catalysts were washed with hot, 70–80°C, distilled water applied in a sequence of 15 rounds, making about 1 L of rinsing water per 1 g of catalyst, to clean them from any possible water-soluble compounds.

The crystallinity, crystal structure and phase composition of cobalt, tungsten, iron and nickel-containing titanium dioxide were analysed using Scintag Pad V Siemens (Cu Kα irradiation source) X-ray diffraction (XRD) spectroscopy. Surface morphology was examined by scanning electronic spectroscopy (SEM) JEOL JSM-6480 LV equipped with

energy-dispersive spectroscopy. The crystal structure of copper-containing catalyst was determined with XRD measurements using a Scintag XDS 2000 X-ray diffractometer. Quantitative measurements of the samples' composition were performed with an ARL 3410 + inductively coupled optical emission spectrometer.

### 3. Results and discussion

#### 3.1. Photocatalysts characterization

Figure 2 shows the XRD spectra of the doped titanium dioxide photocatalysts. It can be seen that platinum-, iron- and tungsten-containing photocatalysts are composed of anatase: peaks (1 0 1), (0 0 4), (2 0 0), (1 0 5) and (2 0 4) were clearly visible, with (1 0 1) peak having the highest intensity. Tungsten-containing titania sample showed the less pronounced peaks, indicating relatively amorphous structure in comparison with other catalysts. Iron-containing photocatalyst showed two peaks of α-Fe<sub>2</sub>O<sub>3</sub>, (1 0 4) and (1 1 0).

On the other hand, CuO- and Co-TiO<sub>2</sub> samples exhibit both anatase and rutile phase; for rutile, (1 1 0) and (1 0 1) peaks were the most pronounced, with (1 1 0) possessing the highest intensity. The anatase phase percentage was determined according to the following equation:

$$[A]\% = \frac{100 \times I_A}{I_A + 1.265 \times I_R}, \quad (1)$$

where  $I_A$  and  $I_R$  are the anatase phase plane (1 0 1) and rutile phase plane (1 1 0), respectively. The Co-TiO<sub>2</sub> photocatalyst contains anatase in the amount of 71% and Cu<sub>x</sub>O-TiO<sub>2</sub> 80%.

According to optical emission spectroscopy measurements, the dopants content is shown in Table 1. It shows the general dopant to titanium ratio between 0.15% and 0.53%.

#### 3.2. Adsorption experiments

At the applied experimental conditions, ca. 16% of the initial HA amount was adsorbed on the surface of Pt-TiO<sub>2</sub>, whereas in the case of other photocatalysts it was negligible (well below 1%). Accordingly, surface reactions play important role in HA removal at platinumized titania, while their role in case of other photocatalysts applied is negligible (minor).

#### 3.3. Photocatalytic degradation experiments

The experimental results of the HA aqueous solution photocatalytic treatment can be seen in Table 2. One can see that the best humic acid removal was obtained with P25, which also gave the best oxygen production. With hydrogen production, however, platinum-doped photocatalyst showed unsurpassed results, producing 94 ppm of hydrogen gas in 4 h; ca. 29% of humic acid was removed with this catalyst. Taking into account the estimated mass of HA of 226 Da and the volumes of solution and gas (see

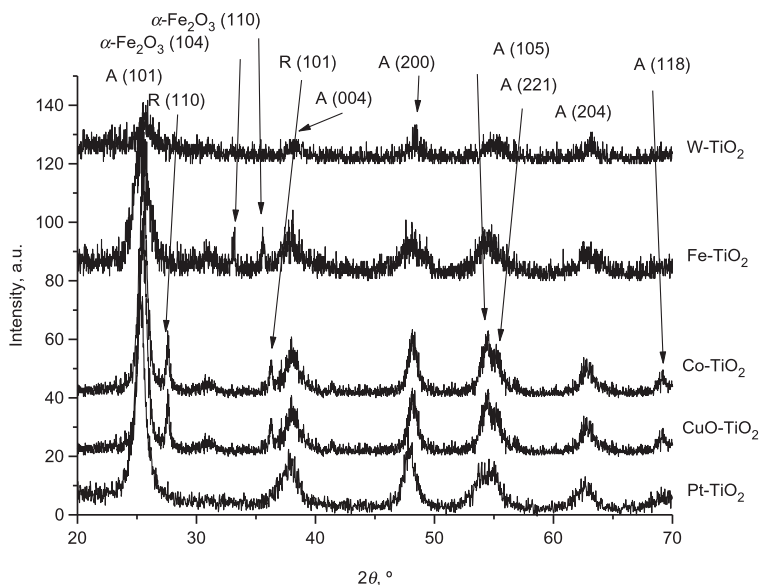


Figure 2. X-ray diffraction patterns of the photocatalysts.

Table 1. The dopant content measured by optical emission spectroscopy.

Catalyst	Co (ppm)	W (ppm)	Fe (ppm)	Pt (ppm)	Cu (ppm)	Ti (ppm)
Pt-TiO <sub>2</sub>	—	—	—	1619	—	518,989
Cu <sub>x</sub> O/H <sub>2</sub> -TiO <sub>2</sub>	—	—	—	—	4200	560,600
Co-TiO <sub>2</sub>	842	—	—	—	—	569,353
Fe-TiO <sub>2</sub>	85	—	3011	—	—	566,856
W-TiO <sub>2</sub>	228	1280	—	—	—	561,701

Section 2), 0.25  $\mu\text{mol}$  H<sub>2</sub> was produced per 1  $\mu\text{mol}$  of HA removed. Platinized photocatalyst was able to produce 24 ppm of oxygen, with up to 4 ppm of each methane, ethane and ethene. Hydrogen-treated copper-doped titanium dioxide was also capable of producing hydrogen: 15 ppm H<sub>2</sub> was produced, together with over 280 ppm of oxygen, and traces of methane and ethene with ca. 6% of the initial humic acid removed. Cobalt-doped titanium dioxide, similar to P25, showed good oxygen production with some trace amounts of light hydrocarbons; although the oxygen production rate is inferior to that of P25, the amount of humic acid consumed to obtain this result is dramatically smaller, about 9% of the initial concentration. Oxygen yields for P25-, cobalt- and copper oxide-doped titania are 0.45, 2 and 3.5  $\mu\text{mol O}_2 \mu\text{mol}^{-1}$  HA, respectively, i.e. the best oxygen production is achieved by Cu<sub>x</sub>O/H<sub>2</sub>-TiO<sub>2</sub>. Iron-doped photocatalyst was not able to split water into hydrogen and oxygen, but succeeded in producing significant amounts of CO together with traces of low molecular

weight (LMW) hydrocarbons degrading modest amount of humic acid. Finally, tungsten-doped sample, although being able to remove up to 12% of humic acid, was able to produce only trace amounts of methane. This suggests only partial HA degradation to aqueous by-products taking place: the combination of practical lack of gaseous degradation products and noticeable HA removal detected spectrophotometrically implies primarily to the damaging of chromatophore parts of HA molecule, producing the noted solution discoloration.

Before explaining the observed differences in various photocatalysts' performance, one should look into the differences in their behaviour originating from composition, i.e. different dopants. According to Matsuoka et al.,[46] elementary platinum particles, deposited on titania, can serve as electron traps, which prolongs the lifetime of positively charged holes and also ease the formation of hydrogen from protons; formed hydrogen atoms are adsorbed on the surface of platinum particles, combining there into molecules. Platinum also reduces the overpotential for hydrogen evolution.[47] It has also been reported [33] that hydroxyl groups may dissociate on palladium particles, producing hydrogen, whereas platinum and palladium are similar in their properties. Doping with transition metal ions (in this case, Co, Fe and W) was shown in the literature not only to increase the wavelengths diapason for titanium dioxide excitation, producing red shift, but also to serve as electron and hole traps,[28] effectively promoting charge separation and preventing recombination. Metal oxide-doping (Cu<sub>x</sub>O, Fe<sub>2</sub>O<sub>3</sub>) of titanium dioxide can promote



Table 2. The results of anoxic photocatalytic treatment of humic acid aqueous solution (100 mg L<sup>-1</sup>, pH 6.5, treatment time 4 h).

Catalyst	HA removal (%)	H <sub>2</sub> (ppm)	O <sub>2</sub> (ppm)	CH <sub>4</sub> (ppm)	C <sub>2</sub> H <sub>6</sub> (ppm)	C <sub>2</sub> H <sub>4</sub> (ppm)	CO (ppm)
P25	52.5	0	309.5	0.3	0	0	0
Pt-TiO <sub>2</sub>	29.1	94.3	24.2	4	1.6	4.1	0
W-TiO <sub>2</sub>	11.7	0	0	0.2	0	0	0
Co-TiO <sub>2</sub>	8.9	0	232	0.3	0	0.5	0
Cu <sub>x</sub> O/H <sub>2</sub> -TiO <sub>2</sub>	5.8	15.3	282.3	0.2	0	0.1	0
Fe-TiO <sub>2</sub>	5.5	0	0	0.4	0	0.1	90.5

electron-hole separation due to the differences in two semiconductor oxides' band-gap energy values.[28] Hydrogen treatment of semiconductor photocatalysts increases the overall amount of surface defects, mainly oxygen vacancies, that can also serve as hole traps for efficient charge separation. From the other side,[33] treatment of oxygen-free organics-containing solutions results in hydrogen originating both from water splitting and from the cleavage of organic molecules; the latter process also produces CO and CO<sub>2</sub>, together with LMW alkanes and alkenes, as it was actually observed in the current study.

Summarizing, in relatively short-time experiments the catalysts seem to be clearly differentiated in terms of gaseous products yield. Hydrogen production with HA appears to be directly tied to LMW hydrocarbons production: both seem to proceed simultaneously and they appear to be interdependent. The majority of hydrogen thus originates not only from water splitting but also from HA molecule cleavage, where the shortest pathway for hydrogen production is hydroxyl groups' dissociation on platinum particles, which also serve as electron traps. This is in complete accordance with the available literature data [30] and is further supported by adsorption results. Oxygen production, on the other hand, in the amounts actually observed is more likely the result of water splitting: indeed, in case of oxygen-producing photocatalysts, the amount of HA removed by them differed by an order of magnitude, whereas their results in oxygen production were comparable. As a result, it can be seen that under anoxic conditions, HA can successfully undergo photocatalytic splitting, producing hydrogen.

#### 4. Conclusions

Short-time aqueous photocatalytic treatment of humic acid solutions was undertaken in anoxic conditions using several titanium dioxide-based photocatalysts. Notable hydrogen and oxygen production was observed, whereas the performance of the photocatalysts could be clearly differentiated in terms of gaseous products composition. The difference in the photocatalysts' performance can be explained by different mechanisms responsible for hydrogen production, i.e. direct humic acid molecule splitting versus humic acid serving as sacrificial electron donor for water splitting, whereas

the relative prevalence of one mechanism over another depends on the way of catalysts' synthesis and composition. The direct humic acid splitting results in higher hydrogen yield; oxygen production, on the other hand, could be attributed to water-splitting reactions.

#### Acknowledgements

The authors thank Dr. Paul Boni and Mr. Frederic Luiszer (University of Colorado, Boulder) for the training and assistance in XRD and ICP-OES measurements, respectively.

#### Funding

The financial aid of Estonian Science Agency [Project IUT1-7], Estonian Science Foundation [grant GUS10] and US Civilian Research and Development Foundation [grant ESC2-2974-TL-09] is also greatly appreciated.

#### References

- [1] Zhang W, Li Y, Wang C, Wang P, Wang Q. Energy recovery during advanced wastewater treatment: simultaneous estrogenic activity removal and hydrogen production through solar photocatalysis. *Water Res.* 2013;47:1480–1490.
- [2] Bahnemann D. Photocatalytic water treatment: solar energy applications. *Solar Energy.* 2004;77:445–459.
- [3] Sun B, Sato M, Clements JS. Optical study of active species produced by a pulsed streamer corona discharge in water. *J Electrostat.* 1997;39:189–202.
- [4] Kolen'ko YV, Churagulov BR, Kunst M, Mazerolles L, Colbeau-Justin C. Photocatalytic properties of titania powders prepared by hydrothermal method. *Appl Catal.* 2004;B54:51–58.
- [5] Fujishima A, Honda K. Electrochemical photolysis of water at a semiconductor electrode. *Nature.* 1972;238:37–38.
- [6] Bamwenda GR, Tsubota S, Nakamura T, Haruta M. Photoassisted hydrogen production from a water-ethanol solution: a comparison of activities of Au-TiO<sub>2</sub> and Pt-TiO<sub>2</sub>. *J Photochem Photobiol.* 1995;A89:177–189.
- [7] Kudo A, Domen K, Maruya K, Onishi T. Photocatalytic activities of TiO<sub>2</sub> loaded with NiO. *Chem Phys Lett.* 1987;133:517–519.
- [8] Anpo M, Takeuchi M. The design and development of highly reactive titanium oxide photocatalysts operating under visible light irradiation. *J Catal.* 2003;216:505–516.
- [9] Zhu J, Zheng W, He B, Zhang J, Anpo M. Characterization of Fe-TiO<sub>2</sub> photocatalysts synthesized by hydrothermal method and their photocatalytic reactivity for photodegradation of XRG dye diluted in water. *J Mol Catal.* 2004;A216:35–43.

- [10] Xie Y, Yuan C. Photocatalysis of neodymium ion modified TiO<sub>2</sub> sol under visible light irradiation. *Appl Surf Sci.* 2004;221:17–24.
- [11] Yamashita H, Harada M, Misaka J, Takeuchi M, Ikeue K, Anpo M. Degradation of propanol diluted in water under visible light irradiation using metal ion-implanted titanium dioxide photocatalysts. *J Photochem Photobiol.* 2002;A148:257–261.
- [12] Shie JL, Lee CH, Chiou CS, Chen YH, Chang CY. Photocatalytic characteristic and photodegradation kinetics of toluene using N-doped TiO<sub>2</sub> modified by radio frequency plasma. *Environ Technol.* 2014;35:653–660.
- [13] Shokri M, Jodat A, Modirshahla N, Behnajady MA. Photocatalytic degradation of chloramphenicol in an aqueous suspension of silver-doped TiO<sub>2</sub> nanoparticles. *Environ Technol.* 2013;34:1161–1166.
- [14] Barakat MA, Al-Hutailah RI, Qayyum E, Rashid J, Kuhn JN. Pt nanoparticles/TiO<sub>2</sub> for photocatalytic degradation of phenols in wastewater. *Environ Technol.* 2013;35:137–144.
- [15] Ezema FI, Osuji RU. Band gap shift and optical characterization of chemical bath deposited CdSSe thin films on annealing. *Chalcogen Lett.* 2008;4:69–75.
- [16] Lin CJ, Yu WY, Chien SH. Effect of anodic TiO<sub>2</sub> powder as additive on electron transport properties in nanocrystalline TiO<sub>2</sub> dye-sensitized solar cells. *Appl Phys Lett.* 2007;91:233120.
- [17] In S, Orlov A, Garcia F, Tikhov M, Wright DS, Lambert RM. Efficient visible light-active N-doped TiO<sub>2</sub> photocatalysts by a reproducible and controllable synthetic route. *Chem Commun.* 2006;4236–4238. Available from: <http://pubs.rsc.org/en/Content/ArticleLanding/2006/CC/b610316b#divAbstract>
- [18] Livraghi S, Paganini MC, Giamello E, Selloni A, Di Valentin C, Pacchioni G. Origin of photoactivity of nitrogen-doped titanium dioxide under visible light. *JACS.* 2006;128:15666–15671.
- [19] Sreethawong T, Yoshikawa S. Comparative investigation on photocatalytic hydrogen evolution over Cu-, Pd-, and Au-loaded mesoporous TiO<sub>2</sub> photocatalysts. *Catal Commun.* 2005;6:661–668.
- [20] Sato J, Saito N, Nishiyama H, Inoue Y. Photocatalytic activity for water decomposition of RuO<sub>2</sub>-loaded SrIn<sub>2</sub>O<sub>4</sub> with d(10) configuration. *Chem Lett.* 2001;30:868–869.
- [21] Sato J, Saito N, Nishiyama H, Inoue Y. New photocatalyst group for water decomposition of RuO<sub>2</sub>-loaded p-block metal (In, Sn, and Sb) oxides with d(10) configuration. *J Phys Chem.* 2001;B105:6061–6063.
- [22] Ikarashi K, Sato J, Kobayashi H, Saito N, Nishiyama H, Inoue Y. Photocatalysis for water decomposition by RuO<sub>2</sub>-dispersed ZnGa<sub>2</sub>O<sub>4</sub> with d(10) configuration. *J Phys Chem.* 2002;B106:9048–9053.
- [23] Sato J, Saito N, Nishiyama H, Inoue Y. Photocatalytic water decomposition by RuO<sub>2</sub>-loaded antimonates M<sub>2</sub>Sb<sub>2</sub>O<sub>7</sub> (M = Ca, Sr), CaSb<sub>2</sub>O<sub>6</sub> and NaSbO<sub>3</sub>, with d10 configuration. *J Photochem Photobiol.* 2002;A148:85–89.
- [24] Sato J, Kobayashi H, Saito N, Nishiyama H, Inoue Y. Photocatalytic activities for water decomposition of RuO<sub>2</sub>-loaded AlInO<sub>2</sub> (A = Li, Na) with d10 configuration. *J Photochem Photobiol.* 2003;A158:139–144.
- [25] Sato J, Saito N, Nishiyama H, Inoue Y. Photocatalytic activity for water decomposition of indates with octahedrally coordinated d(10) configuration. I Influences of preparation conditions on activity. *J Phys Chem.* 2003;B107:7965–7969.
- [26] Sato J, Kobayashi H, Ikarashi K, Saito N, Nishiyama H, Inoue Y. Photocatalytic activity for water decomposition of RuO<sub>2</sub>-dispersed Zn<sub>2</sub>GeO<sub>4</sub> with d(10) configuration. *J Phys Chem.* 2004;B108:4369–4375.
- [27] Kadowaki H, Sato J, Kobayashi H, Saito N, Nishiyama H, Simodaira Y, Inoue Y. Photocatalytic activity of the RuO<sub>2</sub>-dispersed composite p-block metal oxide LiInGeO<sub>4</sub> with d(10)-d(10) configuration for water decomposition. *J Phys Chem.* 2005;B109:2995–3000.
- [28] Ni M, Leung MKH, Leung DYC, Sumathy K. A review and recent developments in photocatalytic water-splitting using for hydrogen production. *Renew Sust Energy Rev.* 2007;11:401–425.
- [29] Kim J, Choi W. Hydrogen producing water treatment through solar photocatalysis. *Energy Environ Sci.* 2010;3:1042–1045.
- [30] Kozlova EA, Vorontsov AV. Photocatalytic hydrogen evolution from aqueous solutions of organophosphorous compounds. *Int J Hydrogen Energy.* 2010;35:7337–7343.
- [31] Li Y, Lu G, Li S. Photocatalytic hydrogen generation and decomposition of oxalic acid over platinumized TiO<sub>2</sub>. *Appl Catal.* 2001;A214:179–185.
- [32] Priya R, Kanmani S. Design of pilot-scale solar photocatalytic reactor for the generation of hydrogen from alkaline sulfide wastewater of sewage treatment plant. *Environ Technol.* 2013;34:2817–2823.
- [33] Bahruji H, Bowker M, Davies PR, Al-Mazroai LS, Dickinson A, Greaves J, James D, Millard L, Pedrono F. Sustainable H<sub>2</sub> gas production by photocatalysis. *J Photochem Photobiol.* 2010;A216:115–118.
- [34] Kim J, Monllor-Satoca D, Choi W. Simultaneous production of hydrogen with the degradation of organic pollutants using TiO<sub>2</sub> photocatalyst modified with dual surface components. *Energy Environ Sci.* 2012;5:7647–7656.
- [35] Daskalaki VM, Antoniadou M, Li Puma G, Kondarides DI, Lianos P. Solar light-responsive Pt/CdS/TiO<sub>2</sub> photocatalysts for hydrogen production and simultaneous degradation of inorganic or organic sacrificial agents in wastewater. *Environ Sci Technol.* 2010;44:7200–7205.
- [36] Zhang W, Li Y, Wang C, Wang P, Wang Q. Energy recovery during advanced wastewater treatment: simultaneous estrogenic activity removal and hydrogen production through solar photocatalysis. *Water Res.* 2013;47:1031–1037.
- [37] Eggins BR, Palmer FL, Byrne JA. Photocatalytic treatment of humic substances in drinking water. *Water Res.* 1997;31:1223–1226.
- [38] Wang GS, Liao CH, Wu FJ. Photodegradation of humic acids in the presence of hydrogen peroxide. *Chemosphere.* 2001;42:379–387.
- [39] Sanchez-Monedero MA, Roig A, Cegarra J, Bernal MP. Relationships between water-soluble carbohydrate and phenol fractions and the humification indices of different organic wastes during composting. *Biores Technol.* 1999;70:193–201.
- [40] Rocha LS, Lopes CB, Henriques B, Tavares DS, Borges JA, Duarte AC, Pereira E. Competitive effects on mercury removal by an agricultural waste: application to synthetic and natural spiked waters. *Environ Technol.* 2013;35:661–673.
- [41] Manahan SE. *Environmental Chemistry*. 6th ed. New York: CRC Press/Lewis Publishers; 1994.
- [42] Portjanskaja E, Stepanova K, Klauson D, Preis S. The influence of titanium dioxide modifications on photocatalytic oxidation of lignin and humic acids. *Catal Today.* 2009;144:26–30.
- [43] Wiszniewski J, Robert D, Surmacz-Gorska J, Miksch K, Weber J-V. Photocatalytic decomposition of humic acids on TiO<sub>2</sub>: Part I: discussion of adsorption and mechanism. *J Photochem Photobiol.* 2002;A152:267–273.

- [44] Chen XB, Liu L, Yu PY, Mao SS. Increasing solar absorption for photocatalysis with black hydrogenated titanium dioxide nanocrystals. *Science*. 2011;331:746–750.
- [45] Vorontsov AV, Savinov EN, Jin ZS. Influence of the form of photodeposited platinum on titania upon its photocatalytic activity in CO and acetone oxidation. *J Photochem Photobiol*. 1999;A125:113–117.
- [46] Matsuoka M, Kitano M, Takeuchi M, Tsujimaru K, Anpo M, Thomas JM. Photocatalysis for new energy production: recent advances in photocatalytic water splitting reactions for hydrogen production. *Catal Today*. 2007;122:51–61.
- [47] Linsebigler AL, Lu G, Yates JT. Photocatalysis on TiO<sub>2</sub> surfaces: principles, mechanisms and selected results. *Chem Rev*. 1995;95:735–758.



**APPENDIX II**  
**CURRICULUM VITAE**



## ELULOOKIRJELDUS

### 1. Isikuandmed

Ees- ja perekonnanimi: Olga Budarnaja  
Sünniaeg ja -koht: 22. veebruar 1986. a., Kaliningrad,  
Venemaa  
Kodakondsus: Eesti  
E-posti aadress: olgabudarnaja@gmail.com

### 2. Hariduskäik

Õppeasutus (nimetus lõpetamise ajal)	Lõpetamise aeg	Haridus (eriala/kraad)
Tallinna Tehnikaülikool	2010	Tehnikateaduste magistrikraad
Tallinna Tehnikaülikool	2008	Tehnikateaduste bakalaureusekraad
Tallinna Linnamäe Vene Lütseum	2005	Keskharidus

### 3. Keelteoskus (alg-, kesk- või kõrgtase)

Keel	Tase
Eesti	Kõrgtase
Vene	Kõrgtase
Inglise	Kõrgtase
Saksa	Algtase

### 4. Teenistuskäik

Töötamise aeg	Tööandja nimetus	Ametikoht
2010-k.a.	AS Elcogen	tootmisassistent

### 5. Kaitstud lõputööd

Tehnikateaduste magistrikraad (2010): *p*-Toluidiini fotokatalüütiline oksüdatsioon vesifaasis legeeritud titaandioksiidiga. Juhendajad: Keemiatehnika instituudi vanemteadur Marina Kritševskaja ja insener Deniss Klauson.

### 6. Teadustöö põhisuunad

Bioloogiliselt lagunematute saasteainete fotokatalüütiline oksüdatsioon vesifaasis, nähtavas valguses aktiivsete fotokatalüsaatorite süntees, omaduste ja töö uurimine. Reaktsioonimehhanismide uurimine. Katalüsaatorite rakendusviiside uurimine.

## 7. Uurimisprojektid

Projekt SF0142719s06 (2006-2011): Tehnoloogiliste protsesside intensiivistamine aktuaalsete keskkonnaprobleemide lahendamiseks

Projekt ETF7541 (2008-2010): Nähtavas valguses aktiivsete fotokatalüsaatorite süntees ja nende kinnitamine pindadele saasteainete mineraliseerimiseks

Projekt GUS10 (2010-2012): Fotokatalüüsi kombinatsioon fermentatsiooniga vesilahustest vesiniku ja hapniku tootmiseks

Projekt ETF8978 (2012-k.a.): Toksiliste keskkonnaohtlike ainete lagundamine vees fotokatalüüsi ja bioloogilise oksüdatsiooni kombineerimisel ning õhus fotokatalüüsiga

Projekt IUT1-7 (2013-k.a.): Keemiatehnikapõhine lähenemisviis prioriteetsete saasteainete ja uute esilekerkivate mikrosasteainete kõrvaldamisele veest/reoveest ja pinnasest: täiustatud oksüdatsioonitehnoloogiate kasutamine ja optimeerimine



## CURRICULUM VITAE

### 1. Personal data

Name: Olga Budarnaja  
Date and place of birth: 22<sup>nd</sup> February 1986, Kaliningrad, Russia  
E-mail address: olgabudarnaja@gmail.com

### 2. Education

Educational institution	Graduation year	Education (field of study/degree)
Tallinn University of Technology	2010	Master of Science
Tallinn University of Technology	2008	Master of Bachelor
Tallinna Linnamäe Vene Lütseum	2005	High school education

### 3. Language competence/skills (fluent, average, basic skills)

Language	Level
Estonian	Fluent
Russian	Fluent
English	Fluent
German	Basic skills

### 4. Professional employment

Period	Organisation	Position
2010-onwards	AS Elcogen	Production assistant

### 5. Defended thesis

Master of Science (2010): Photocatalytic oxidation of *p*-toluidine in a aqueous phase with doped titanium dioxide. Supervisor – Senior Researcher Marina Krichevskaya, engineer Deniss Klauson, Department of Chemical Engineering, TUT

### 6. Main areas of scientific work

Aqueous photocatalytic oxidation of non-biodegradable pollutants. The synthesis of visible light-sensitive titania-based photocatalysts and the evaluation of their

properties and performance. The research of reaction mechanisms. Engineering solutions for photocatalysts applications.

## 7. Research projects

Project SF0142719s06 (2006-2011): Intensification of technological processes for the solution of actual environmental problems

Project ETF7541 (2008-2010): Synthesis of photocatalysts active under visible light and their immobilization on surfaces for mineralisation of environmental pollutants

Project GUS10 (2010-2012): Photocatalysis combination with dark fermentation for hydrogen and oxygen production from aqueous solutions

Project ETF8978 (2012-onwards): Degradation of environmentally toxic refractory compounds in water by combination of photocatalysis and biological treatment and in air by photocatalysis

Project IUT1-7 (2013-onwards): Chemical engineering approach to removal of priority pollutants and emerging micropollutants from water/wastewater and soil: implementation and optimization of advanced oxidation technologies

**DISSERTATIONS DEFENDED AT  
TALLINN UNIVERSITY OF TECHNOLOGY ON  
*CHEMISTRY AND CHEMICAL ENGINEERING***

1. **Endel Piiraja**. Oxidation and Destruction of Polyethylene. 1993.
2. **Meili Rei**. Lihatehnoloogia teaduslikud alused. Fundamentals of Food Technology. 1995.
3. **Meeme Põldme**. Phase Transformations in Hydrothermal Sintering Processing of Phosphate Rock. 1995.
4. **Kaia Tõnsuaadu**. Thermophosphates from Kovdor and Siilinjärvi Apatites. 1995.
5. **Anu Hamburg**. The Influence of Food Processing and Storage on the N-Nitrosamines Formation and Content in Some Estonian Foodstuffs. 1995.
6. **Ruth Kuldvee**. Computerized Sampling in Ion Chromatography and in Capillary Electrophoresis. 1999.
7. **Külliki Varvas**. Enzymatic Oxidation of Arachidonic Acid in the Coral *Gersemia fruticosa*. 1999.
8. **Marina Kudrjašova**. Application of Factor Analysis to Thermochromatography and Promotion Studies. 2000.
9. **Viia Lepane**. Characterization of Aquatic Humic Substances by Size Exclusion Chromatography and Capillary Electrophoresis. 2001.
10. **Andres Trikkel**. Estonian Calcareous Rocks and Oil Shale Ash as Sorbents for SO<sub>2</sub>. 2001.
11. **Marina Kritševskaja**. Photocatalytic Oxidation of Organic Pollutants in Aqueous and Gaseous Phases. 2003.
12. **Inna Kamenev**. Aerobic Bio-Oxidation with Ozonation in Recalcitrant Wastewater Treatment. 2003.
13. **Janek Reinik**. Methods for Purification of Xylidine-Polluted Water. 2003.
14. **Andres Krumme**. Crystallisation Behaviour of High Density Polyethylene Blends with Bimodal Molar Mass Distribution. 2003.
15. **Anna Goi**. Advanced Oxidation Processes for Water Purification and Soil Remediation. 2005.
16. **Pille Meier**. Influence of Aqueous Solutions of Organic Substances on Structure and Properties of Pinewood (*Pinus sylvestris*). 2007.
17. **Kristjan Kruusement**. Water Conversion of Oil Shales and Biomass. 2007.
18. **Niina Kulik**. The Application of Fenton-Based Processes for Wastewater and Soil Treatment. 2008.

19. **Raul Järviste**. The Study of the Changes of Diesel Fuel Properties a its Long Term Storage. 2008.
20. **Mai Uibu**. Abatement of CO<sub>2</sub> Emissions in Estonian Oil Shale-Based Power Production. 2008.
21. **Valeri Gorkunov**. Calcium-Aluminothermal Production of Niobium and Utilization of Wastes. 2008.
22. **Elina Portjanskaja**. Photocatalytic Oxidation of Natural Polymers in Aqueous Solutions. 2009.
23. **Karin Reinhold**. Workplace Assessment: Determination of Hazards Profile using a Flexible Risk Assessment Method. 2009.
24. **Natalja Savest**. Solvent Swelling of Estonian Oil Shales: Low Temperature Thermochemical Conversion Caused Changes in Swelling. 2010.
25. **Triin Märtson**. Methodology and Equipment for Optical Studies of Fast Crystallizing Polymers. 2010.
26. **Deniss Klauson**. Aqueous Photocatalytic Oxidation of Non-Biodegradable Pollutants. 2010.
27. **Oliver Järvik**. Intensification of Activated Sludge Process – the Impact of Ozone and Activated Carbon. 2011.
28. **Triinu Poltimäe**. Thermal Analysis of Crystallization Behaviour of Polyethylene Copolymers and Their Blends. 2011.
29. **Mariliis Sihtmäe**. (Eco)toxicological Information on REACH-Relevant Chemicals: Contribution of Alternative Methods to *in vivo* Approaches. 2011.
30. **Olga Velts**. Oil Shale Ash as a Source of Calcium for Calcium Carbonate: Process Feasibility, Mechanism and Modeling. 2011.
31. **Svetlana Jõks**. Gas-Phase Photocatalytic Oxidation of Organic Air Pollutants. 2012.
32. **Aleksandr Dulov**. Advanced Oxidation Processes for the Treatment of Water and Wastewater Contaminated with Refractory Organic Compounds. 2012.
33. **Aleksei Zaidentsal**. Investigation of Estonian Oil Shale Thermo-bituminization in Open and Closed System. 2012.
34. **Dmitri Šumigin**. Composites of Low-Density Polyethylene and Poly(Lactic Acid) With Cellulose and Its Derivatives. 2014.
35. **Aleksandr Käkinen**. The Role of Physico-chemical Properties and Test Environment on Biological Effects of Copper and Silver Nanoparticles. 2014.
36. **Ada Traumann**. Improvement of Work Environment through Modelling the Prevention of Health Risks Focusing on Indoor Pollutants. 2014.